Development and application of analytical tools to study the origin, fate and impact of the oncometabolite 2-hydroxyglutarate and its lactone

DISSERTATION ZUR ERLANGUNG DES DOKTORGRADES DER NATURWISSENSCHAFTEN (DR. RER. NAT.) DER FAKULTÄT CHEMIE UND PHARMAZIE DER UNIVERSITÄT REGENSBURG

vorgelegt von

Raffaela Sarah Berger

aus Rotthalmünster

im Jahr 2019

Promotionsgesuch eingereicht am: 19.09.2019

Die Arbeit wurde angeleitet von: Prof. Dr. Peter J. Oefner

„Der sicherste Weg zum Erfolg ist immer,

es doch noch einmal zu versuchen. „

(Thomas Alva Edison)

1 Table of Content

1 Table of Content ... 1
2 Abbreviations ... 3
3 Objectives ... 5
3.1 Elucidate the mechanism of 2-HG-lactone formation ... 5
3.2 Investigate the metabolic fate of 2-HG and 2-HG-lactone ... 7
3.3 Analytical objectives ... 7
4 Background ... 9
4.1 IDH1/2 mutation and 2-hydroxyglutarate ... 9
4.2 Aspects of enzymology ... 13
4.3 Metabolomics by hyphenated MS-techniques ... 16
4.3.1 Overview ... 16
4.3.2 Quantitative targeted MS-analysis ... 19
4.3.3 Analysis of 2-HG in biological samples ... 21
4.3.4 Flux/tracing analysis ... 25
5 Methods and Material ... 28
5.1 Materials ... 28
5.2 Biological samples ... 28
5.2.1 Cell culture ... 28
5.2.2 Serum samples ... 29
5.2.3 Glioma tissue samples ... 30
5.3 Enzyme assays ... 30
5.4 MS-sample preparation ... 31
5.4.1 Methanol precipitation and sample extraction ... 31
5.4.2 Derivatization for GC-analysis ... 32
5.4.3 PCF-derivatization for amino acid analysis ... 32
5.5 MS methods ... 33
5.5.1 2-HG/-lactone quantification by HPLC-MS/MS ... 33
5.5.2 Amino acid quantification and tracer analysis by HPLC-MS/MS ... 33
5.5.3 Organic acid quantification by GC-EI-MS ... 34

5.5.4 Organic acid tracer analysis 35
5.5.5 Enantioselective analysis of D-/L-2-HG 36
5.6 LysoTracker staining 37
5.7 Miscellaneous 37
5.8 Statistics 38
6 Quantitative analysis of 2-HG/-lactone 39
6.1 Development and validation of a quantitative LC-MS/MS method 39
6.2 Enzymatic assay to measure degradation of D-2-HG 41
7 Strategies for chiral analysis of 2-HG/-lactone 47
8 Investigating metabolism in mutIDH1/2 cells by tracer analysis 53
8.1.1 GC-APCI-TOF-MS for tracer analysis 53
8.1.2 2-HG is the endogenous precursor of its lactone 58
8.1.3 Tracer analysis in HCT116 cell panel 60
8.1.4 Mutant IDH1/2-related effects on cellular metabolism 65
9 Origin and fate of 2-hydroxyglutarate-lactone 72
9.1 2-HG and -lactone in various biological specimens 72
9.2 2-HG-lactone formation is independent of IDH1/2 mutation 75
9.3 Impact of pH on 2-HG-lactone formation 77
9.4 Investigations on lysosomes in context of 2-HG-lactone formation 79
9.5 Does 2-HG-lactone formation involve an enzyme? 81
9.6 2-HG-lactone formation in cell homogenates 85
9.7 2-HG and its lactone are two distinct metabolites 86
10 Conclusions and Perspectives 90
11 References 92
12 Supplement 104
12.1 Supplemental Figures 104
12.2 Supplemental Tables 107
13 Publications and Presentations 115
14 Summary 116
15 Zusammenfassung 117

2 Abbreviations

2-HG	2-Hydroxyglutarate
α-KG	α-Ketoglutarate
Ala	Alanine
AML	Acute myeloid leukemia
APCI	Atmospheric pressure chemical ionization
Arg	Arginine
Asn	Asparagine
Asp	Aspartate
CE	Capillary electrophoresis
D-/L-2-HGA	D-/L-2-Hydroxyglutaric aciduria
D2HGDH; D2HDH	D-2-Hydroxyglutarate dehydrogenase
Da	Dalton
EI	Electron ionization
EIC	Extracted ion chromatogram
ESI	Electrospray ionization
FCS	Fetal calf serum
GC	Gas chromatography
Glc	Glucose
Gln	Glutamine
His	Histidine
IDH1/2, IDH1/2	Isocitrate dehydrogenase 1/2
IS	internal standard
LC	Liquid chromatography
LOD	Limit of detection
(L/U-)LOQ	(Lower/ upper) limit of quantification
m/z	Mass-to-charge ratio

MCT1/4; MCT1/4	Monocarboxylate transporter 1/4
MID	Mass isotopomer distribution vector
MeOH	Methanol
MeOx	Methoximation
mutIDH1/2	Mutated IDH1/2
MRM	Multiple reaction monitoring
MS	Mass spectrometry
MS/MS	Tandem mass spectrometry
$NADP^+$/NADPH	Nicotinamide adenine dinucleotide phosphate (oxidized and reduced form)
(1H-)NMR(-spectroscopy)	(Proton-)nuclear magnetic resonance (-spectroscopy)
PBS	Phosphate buffered saline
PC	Pyruvate carboxylase
PFPP	Pentafluorophenyl propyl
PPP	Pentose phoshphate pathway
Pro	Proline
QqQ	Triple quadupole
Ser	Serine
TCA	Tricarboxylic acid cycle
TIC	Total ion current
TOF	Time-of-flight
TMS	Trimethylsilyl-moiety
WT	Wild type

3 Objectives

3.1 Elucidate the mechanism of 2-HG-lactone formation

This thesis was conducted within the framework of the KFO 262 “Tumor metabolism meets Immunology”, with special focus on the oncometabolite D-2-hydroxyglutarate (D-2-HG), which is produced by mutated isocitrate dehydrogenase IDH1/2 resulting in significantly increased concentrations of this metabolite.

At the Institute of Functional Genomics preliminary work was performed to measure 2-HG in different biological matrices. *IDH1/2* mutations are frequently identified in gliomas and in AML (acute myeloid leukemia), accompanied by increased D-2-HG levels in tissue and serum, respectively. Interestingly, in serum from AML patients not only D-2-HG was detected, but also a closely related metabolite, which had not been described so far. The novel metabolite is the intramolecular ester of D-2-HG and therefore named D-2-HG-lactone (IUPAC: R-5-oxotetrahydrofuran-2-carboxylic acid) (Figure 1).

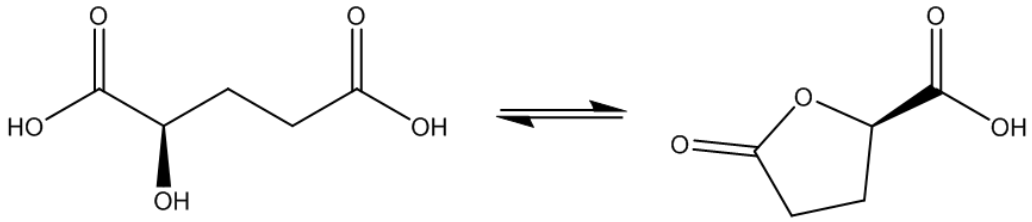

Figure 1. Molecular structure of (R)-2-hydroxyglutarate and its lactone, (R)-5-oxotetrahydrofuran-2-carboxylic acid.

Initially, 2-HG-lactone was detected by chiral GC-MS as a product of the derivatization of 2-HG with methyl chloroformate (MCF)[1]. The presence of multiple 2-HG-derivatives has already been described by others, *e.g.*, by Duran *et al.* (1980) upon esterification of 2-HG with S-2-butanol and acylation with acetic anhydride[2]. However, while the ratio of the two derivatization products remained stable in the case of standard samples, it varied in AML serum samples (Figure 2). This led to the hypothesis that the lactone was an endogenous metabolite. This was confirmed by LC-MS/MS and NMR analysis of an underivatized serum extract.

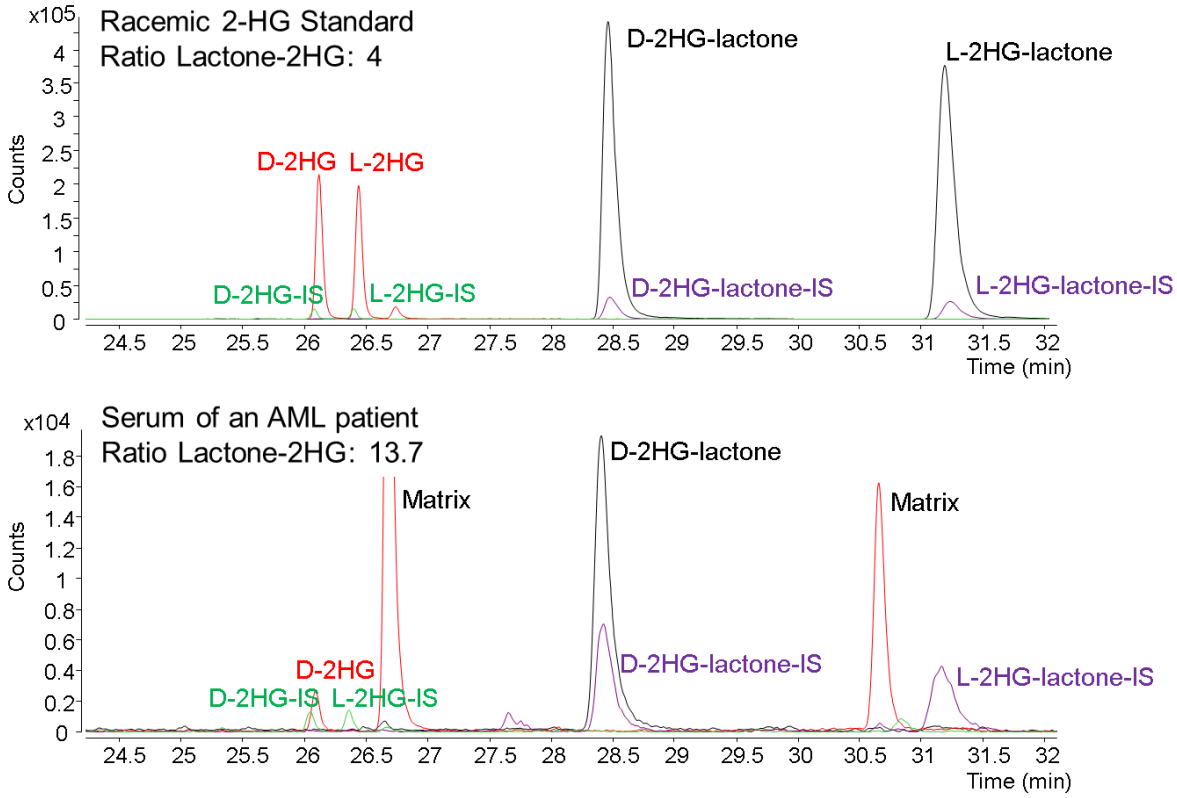

Figure 2. Chiral GC-MS analysis of a racemic D/L-2-HG standard (upper panel) and a serum sample of an AML patient carrying an IDH1/2 mutation (lower panel). For the standard sample, the area ratio of each enantiomer dervative of 2-HG-lactone (shown in black) to 2-HG (shown in red) was constant (4:1) across several measurements. In green and purple the respective stable isotope labeled internal standard is shown. For the exemplary AML serum sample, the ratio of D-2-HG-lactone/D-2-HG(-derivatives) was found to be increased (13.7:1) for the unlabeled, endogenous analyte. Besides, both L-forms are hardly detectable. (Capillary column was a Rt-gDEXsa, connected to an APCI-TOF-MS. Figure is based on data generated by C. Wachsmuth.)

However, the lactone form is not observed in all tumor entities analyzed, raising the question about the origin of 2-HG-lactone. In general, ester formation is favored under acidic conditions, but a pH of ~5-6 seems insufficient to cause the detected 2-HG-lactone concentrations. This thesis aims at finding the conditions and prerequisites for lactonization of 2-HG. For instance, it is investigated whether 2-HG-lactone is a product of a so far unknown enzyme (activity). This includes the analysis of cell culture samples and several biological specimens by LC-MS/MS. Therefore, a HPLC system coupled to a triple-quadrupole mass spectrometer in MRM (multiple reaction monitoring) mode is used for quantification of 2-HG&-lactone.

Cell culture experiments are performed using several cell lines. There are cells with WT-IDH and cell with mutation of IDH, e.g. HT1080 and a panel of HCT116 cells (consisting of cells with mutations in *IDH1* or *IDH2*, respectively, and the WT-IDH parental cell line).

3.2 Investigate the metabolic fate of 2-HG and 2-HG-lactone

It is further hypothesized that D-2-HG is metabolized by its dehydrogenase D2HDH and that this enzyme is upregulated in response to accumulation of the substrate. Therefore, enzyme activity in cell homogenates is determined in an enzyme assay to investigate potential regulation of enzyme kinetics. This LC-MS/MS-based assay has to be established to measure the decline of 2-HG. Regulation on the protein expression level is analyzed by Western Blot.

Moreover, as a valuable technique for investigating the metabolic fate of 2-HG and its lactone in cell culture models, metabolic tracing is performed. Typical stable isotope labeled substrates ([U-^{13}C]glutamine, [U-^{13}C]glucose) are added to cell culture medium with subsequent tracing of the label into metabolic products. For analysis of those cell extracts, new derivatization strategies need to be found as established methods are unsuitable. Finally, this experiment provides data on metabolic effects of *IDH1/2* mutation.

3.3 Analytical objectives

For some of the aforementioned investigations, it is possible to use the already established LC-ESI-MS/MS method for quantification of 2-HG and 2-HG-lactone, but a thorough method validation has to be performed. However, this method is not applicable to enantioselective investigations. A method for chiral analysis of 2-HG is available, but cannot be extended to the analysis of 2-HG-lactone. Moreover, for analysis of labeling patterns, the LC-MS/MS method has to be extended by the respective transitions for 2-HG and 2-HG-lactone. In order to gain more information on cellular metabolism in the context of *IDH1/2* mutation and elevated 2-HG levels, a more widespread method for tracer analysis is established. A GC-APCI-TOF-MS method gives valuable results. But here, like for other (GC-)MS-strategies involving

derivatization, work is hampered by the fact that 2-HG and 2-HG-lactone are closely related and are easily transformed into each other by harsh derivatization conditions. Consequently, various derivatization protocols are tested, especially for the attempt to perform chiral analysis.

4 Background

4.1 IDH1/2 mutation and 2-hydroxyglutarate

Cellular metabolism in cancer is known to be altered to meet the increased energy demand and biomolecule turnover. In this context, several mutations were identified facilitating cellular transformation, which included mutation of isocitrate dehydrogenase[3]. This enzyme has three isoforms in eukaryotic cells, cytosolic IDH1 and mitochondrial IDH2/3, which all catalyze oxidative decarboxylation of isocitrate to α-ketoglutarate using redox equivalents as co-substrates[4]. To date, several non-synonymous mutations have been found in the $NADP^+$-dependent IDH1/2 that seem to be mutually exclusive[5]. *IDH1/2* mutations have been found initially in colorectal cancer[6], and are frequently identified in tumors of the central nervous system, like glioblastoma, and in patients with acute myeloid leukemia (AML)[5,7]. The most frequent mutation type in glial tumors is IDH1-R132H, which is found in 91.5% of patients with *IDH1* mutation[8]. Other substitutions include R132C, R132G, R132S, and R132L. Mutations in *IDH2* in gliomas are rare (<3%) and in most cases of the R172K type[9], with R172 being the analogous residue to R132 in IDH1. In AML patients, the IDH2 mutations R140Q and R172K are typically observed and these two mutations occur at a frequency of 15.4%, which is twice as much as *mutIDH1* in AML[10]. Interestingly, all of the mutated residues are located in the active site of IDH1/2 and contribute to substrate binding via hydrogen bonds[11]. Accordingly, the mutations result in a neo-enzymatic activity, *i.e.*, the production of D-2-HG from α-ketoglutarate and its subsequent accumulation[11]. This corresponds to the almost reverse reaction compared to the WT-IDH1/2, only lacking the carboxylation step.

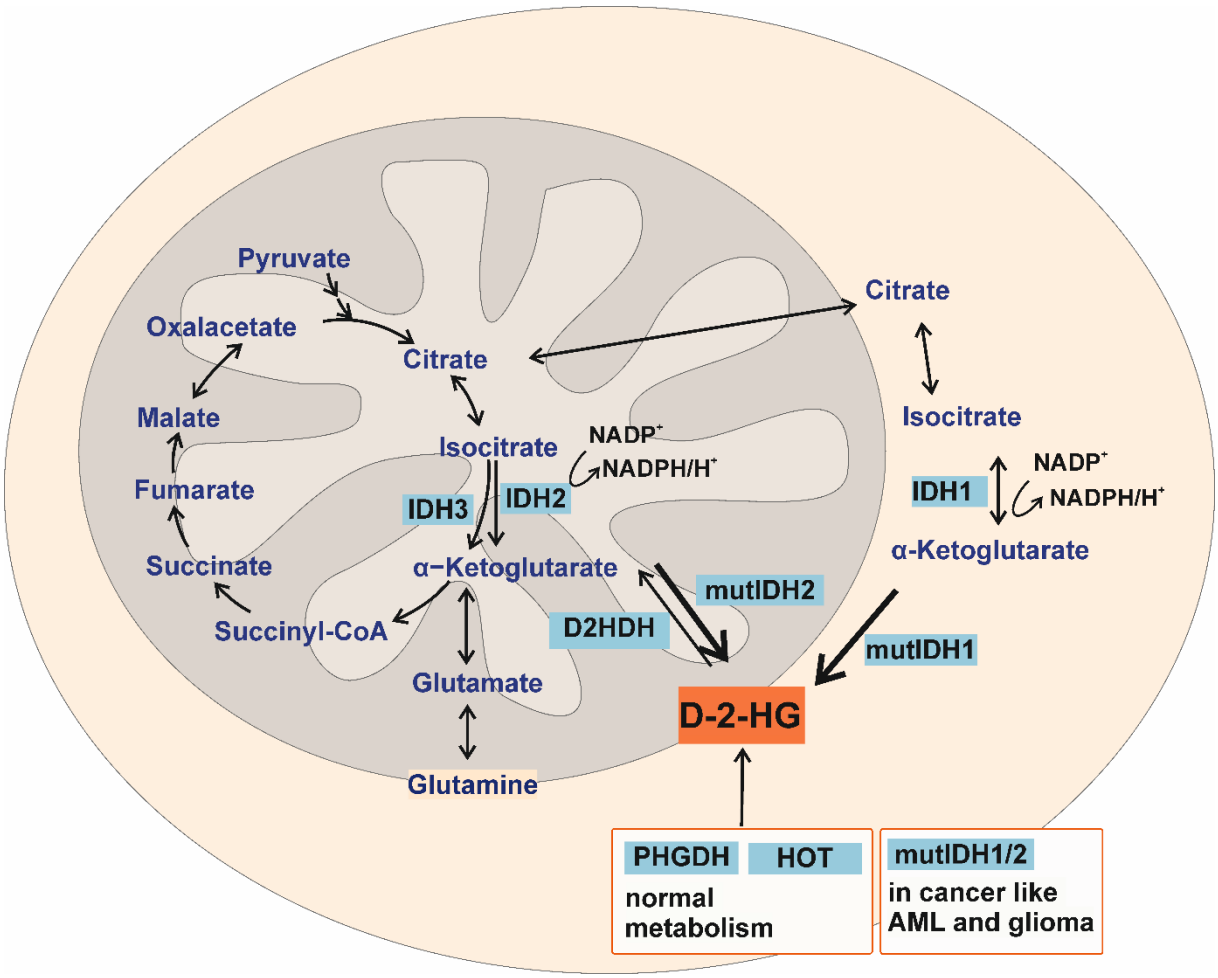

Figure 3. Scheme depicting the formation of D-2-HG in cell metabolism under both, physiological conditions and due to somatic mutations in IDH1/2 in cancer.

Some authors described that *IDH2* mutations result in higher concentrations of 2-HG compared to *IDH1* mutations[12-14]. This seems to be due to the dependency of the latter isoform on metabolic flux through a WT-IDH1 to supply α-KG[13]. Therefore, *IDH1* mutations are generally heterozygous, with only one allele being mutated, whereas for *IDH2* rare cases of biallelic mutations have been reported[15] . MutIDH1/2 generate exclusively the D-enantiomer of 2-HG. The concentrations detected, for instance, in gliomas typically range from 5 to 35 mM, *i.e.*, they are 10-100-fold higher compared to control samples without *IDH1/2* mutations[16]. In healthy cells, 2-HG is produced only in low amounts (intracellular levels <0.1 mM)[17] as side products of enzymes like HOT (hydroxyl acid-oxoacid-transhydrogenase)[18] and PHGDH (phosphoglycerate dehydrogenase)[19] (Figure 3). Enantiospecific dehydrogenases, named D-/L-2-hydroxyglutarate dehydrogenase (D-/L-2HGDH), assure the oxidation back to α-ketoglutarate. Deficiency of these enzymes due to germline mutations result in D-/L-2-hydroxyglutarate aciduria (D-/L-2-HGA) with similarly elevated 2-HG-levels in

urine, plasma and also in cerebrospinal fluid[20,2,21]. Clinical symptoms caused by pathological accumulation of 2-HG differ for the two enantiomers. L2HDH deficient patients suffer from encephalopathy and their risk of brain tumors like gliomas is increased[22]. Deficiency of D2HDH results in a neurometabolic disorder, which is associated with encephalopathy and cardiomyopathy, but not with cancer[23]. Additionally, there is D-2-HGA type II, which is caused by a germline mutation or mosaicism in *IDH2*, also resulting in elevated D-2-HG levels[24,25]. It is suggested that even functional D2HDH cannot cope with the extremely elevated 2-HG levels obtained when *IDH1/2* is mutated due to a huge difference in the catalytic rate for 2-HG production and degradation[11,26].

D-2-HG is regarded as an oncometabolite, contributing to and in cooperation with other oncogenes even initiating oncogenesis[27]. The underlying mechanism(s) are currently still discussed. Its structural similarity to α-KG is known to exert inhibitory effects on α-KG-dependent enzymes and depicts possible ways of mediating transformation. An example is the competitive inhibition of α-KG-dependent TET2 and histone demethylase KDM4C (also known as JMJD2C) resulting in DNA hypermethylation and an altered histone methylation pattern, respectively, which in turn block cell differentiation and change gene expression[28,29].

The L-enantiomer of 2-HG, in contrast, is increasingly produced under hypoxic conditions by promiscuous enzyme activity of lactate dehydrogenase (LDH) and malate dehydrogenase (MDH), which is further enhanced by acidic conditions[30]. The biological function in this context was found to be HIF1a-stabilization in adaptation to acidosis and hypoxia. These interactions again involve inhibition of α-KG-dependent-dioxygenases, which was found to be stronger by L-2-HG than D-2-HG[28,31,32]. Thus, for 2-HG there are shared, as well as enantiospecific effects.

Interestingly, mutations in other TCA enzymes, like fumarate hydratase (FH) and succinate dehydrogenase (SDH), also lead to elevated metabolite levels, which share the common feature of inhibiting α-KG-dependent enzymes[31,33,34]. This indicates, that metabolites like D-2-HG, as well as fumarate and succinate, are implicated in the dysregulation of cellular processes and have comparable roles in cellular transformation and oncogenesis.

Additionally, *IDH1/2* mutant status or elevated D-2-HG concentrations, respectively, were associated with increased ROS-production. This is a consequence of mutant *IDH1/2* consuming rather than producing NADPH[11,35,36], which is used to regenerate the antioxidant glutathione. Therefore, mutIDH1/2 impacts the redox status of the cell, which is important with regard to possible DNA-damage by radicals[37]. Moreover, it was reported that elevated 2-HG concentrations cause a homologous recombination (HR) defect[38], conferring chemosensitivity and radiosensitivity to patients with *mutIDH1* gliomas[38].

Further studies showed that treatment of the erythroblast cell line TF-1 with 200 µM trifluoromethyl benzyl (TFMB)-esterified D-2-HG caused growth factor independence and impaired differentiation[39]. Additionally, overexpression of *D2HGDH* was found to inhibit tumor growth in cells harboring *mutIDH1*[40]. In contrast to slightly elevated D-2-HG levels from *IDH1/2* mutation, which enhance proliferation in some cell line[8], high D-2-HG concentrations are toxic. For example, the LD_{50} for D-2-HG in HEK293T embryonic kidney cells was determined to be 10 mM, while it was approximately 50 mM in LN229 glioblastoma cells. Therefore, it is assumed that toxicity at high concentrations and an increased chemosensitivity are the reasons for a better prognosis of glioma patients with *mutIDH1* compared to *WT-IDH1*[3,41]. Regarding the prognostic impact of D-2-HG/ *IDH1/2* mutation in AML patients, findings are contradictory so far[42,43,44,45].

A growing number of studies investigates the effects of D-2-HG on the tumor environment, for instance in promoting immune escape. I contributed to a study investigating the impact of D-2-HG on T-cells[46]. First of all, it was confirmed by analyzing cell extracts by LC-MS/MS, that T-cells take up D-2-HG produced by *mutIDH1/2* myeloblasts of AML patients. Furthermore, it was shown that D-2-HG altered T-cell metabolism towards oxidative phosphorylation. On a functional level, a higher frequency of regulatory T-cells and a reduced polarization of Th17-cells was observed. A similar study found that D-2-HG impairs differentiation of monocytes into dendritic cells with impaired capacity for T-cell stimulation *(*Hammon *et al,* manuscript in preparation*)*.

For gliomas, which have a different microenvironment, 2-HG also seems to have an impact on immune cells. *MutIDH1/2* gliomas were found to have less immune

infiltration, namely lower accumulation of $CD3^+CD8^+$ T-cell in tumor sites, as a consequence of reduced chemokine production by glioma cells[47]. Additionally, it was reported that *mutIDH1* glioma cells showed translational silencing of NK receptors (NKG2D), which activate NK- and $CD8^+$ T-cells and mediate cytotoxicity. Consequently, those cells acquired resistance to NK cells[48]. In conclusion, these reports provide evidence that D-2-HG might be an immune-modifying factor.

4.2 Aspects of enzymology

In investigations on accumulation of 2-HG in different diseases, enzymes play an important role. There is on the one hand IDH1/2 which - by single amino acid substitutions - undergoes changes in its affinity towards its actual product (α-KG) resulting in the almost reverse reaction now using α-KG as a substrate[11]. Additionally, type and position of the amino acid substitution affect the amount of 2-HG formed[8]. On the other hand, *D2HGDH* mutation like in 2-HG-aciduria cause a decreased enzyme activity with subsequent reduced degradation of D-2-HG. Even intact D2HDH is a low capacity enzyme and is described as a metabolic repair enzyme characterized by high affinity towards its typically low concentrated substrate[49].

These findings were made by investigating enzyme kinetics, hence analyzing and comparing reaction rates, for instance in dependence on changed experimental parameters. A frequently used method here is an enzyme assay, where the velocity of an enzymatic reaction is calculated from the decrease in substrate or increase in product per time, respectively. This is based on the assumption that, under experimental conditions, the reaction is in a steady state according to the theory of Michaelis and Menten, which can be applied to many, but not all enzymes[50,51] (see Figure 4). This state is given, when formation and breakdown of the enzyme-substrate-complex is equal, but not limited by any compound involved in the reaction. Drawing such a curve must give a linear relationship, otherwise the curve does not reflect the initial reaction velocity v_0 and a steady state[52]. If the total amount of enzyme is known, the turnover number of every single enzyme molecule at saturating conditions (called k_{cat}) can be calculated. Likewise, turnover in catalyzing α-KG formation from isocitrate for WT-IDH1 ($4.4x10^4$ 1/s) was found to be 1000 fold higher than for IDH1-R132H (37.5 1/s)[11]. Another characteristic value describing enzyme kinetics is the maximum

velocity v_{max}, which is also required for determination of k_{cat}. Additionally, K_m is the substrate concentration at half maximum velocity and often regarded as a measure for the enzymes´ affinity towards its substrate. However, this is only true in the case of rapid equilibrium for the substrate-enzyme-complex with product formation being the rate limiting step. For applying saturating conditions in assays, a concentration of 10-100 fold K_m is suggested[52].

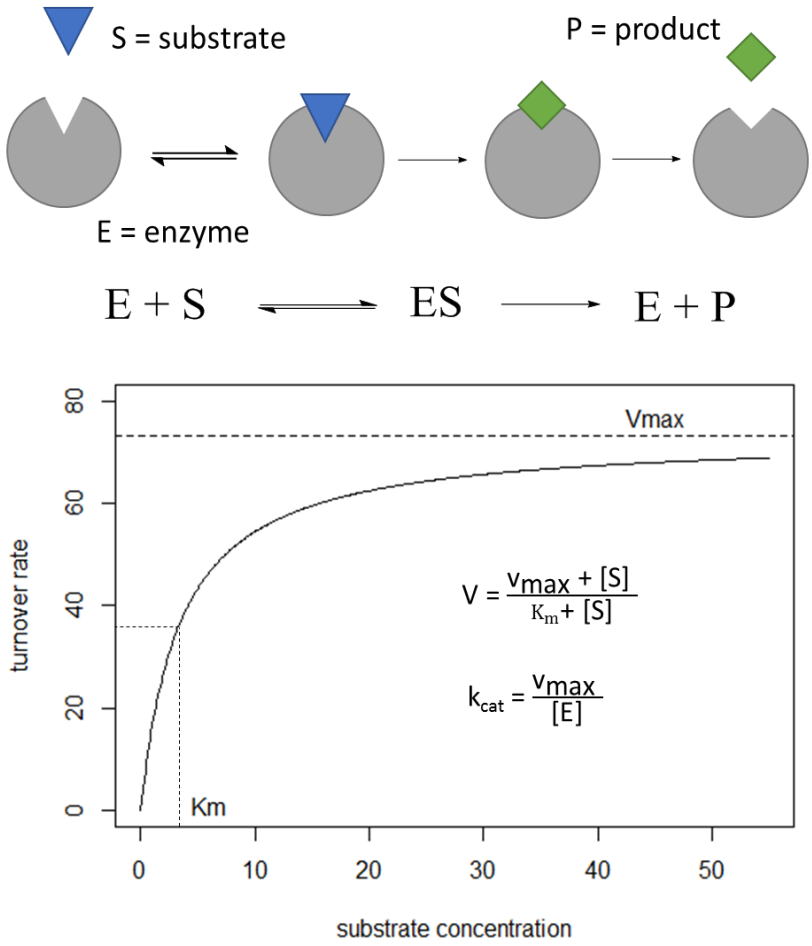

Figure 4. Kinetics of an enzyme-catalysed reaction according to Michaelis and Menten. This theory says that the turnover rate can be determined when formation and breakdown of the enzyme-substrate-complex (ES) are in steady state. K_{cat} can only be calculated when the enzyme concentration [E] is known.

In establishing an enzyme assay, conditions should resemble physiological conditions as closely as possible to obtain sensitive and reliable data on kinetics. Several factors impact enzyme activity. For human enzymes, the optimum temperature usually is 37 °C and reaction rates decrease at higher and lower temperatures. Another important factor is pH, where the optimum often reflects the typical pH of the cell compartment the enzyme is located in[53,54]. The pH as well as ionic strength of the assay buffer are essential for proper conformation and stabilization of the enzyme. Finally, reactions are often dependent on cofactors and counter-ions, which need to

be included into the assay buffer in non-limiting concentrations. Both reactions investigated in this thesis are redox reactions: the formation of 2-HG is a reduction, while its degradation is an oxidation. Consequently, enzyme assays include a redox equivalent. The endogenous co-factors are NADPH for IDH1/2 and FAD for D2HDH. In assay buffers, however, often artificial redox agents are included, which allow for higher reaction rates and, therefore, enhanced sensitivity, especially for low substrate concentrations. Once the optimal assay conditions have been identified, they need to be kept constant. The only compound, the concentration of which may be varied, is the substrate in order to create a Michaelis-Menten plot. The assay is usually started by the addition of substrate to the reaction mixture or any other compound obligatory for the reaction. A blank sample, which lacks one component, can provide information about unspecific noise or spontaneous degradation in the absence of enzyme[52].

The measurement of substrate decrease or product increase, respectively, can be accomplished by different methods. One way is to perform a colorimetric assay, which is especially appropriate for the detection of colored products. A technical variant of this approach is a fluorometric assay, which is more sensitive. One prominent example is detection of the fluorescent signal from NADH, which is also used for determining 2-HG in different biological specimens (explained in detail in 4.3.3)[55]. Fluorescence plate readers can automatically and continuously measure over a defined time range, providing data for kinetic analysis. Like used for this thesis, the substrate/product concentration can also be determined by (hyphenated) MS analysis. This is a so-called stopped assay, as aliquots at different time points are taken and the enzymatic reaction needs to be stopped, *e.g.*, by enzyme precipitation. The advantages of such an assay are higher sensitivity and specificity.

The results of enzyme assays do not only provide information on enzyme characteristics but also on enzyme regulation. Non-competitive inhibition can be seen from reduced v_{max}, while a higher K_m is indicative of competitive inhibition. Furthermore, there is allosteric inhibition, which is a more complex inhibition type and does not necessarily give a Michaelis-Menten kinetic. Allosteric enzymes typically have a low-affinity and a high-affinity state, with an inhibitor or activator, respectively, changing the state by interacting with the enzyme. Feedback inhibition is one example for that regulation; here the end product of a metabolic pathway can downregulate the key enzyme to prevent product accumulation. Compounds interacting in that way, can only

be identified when included in the assay mixture. Besides, regulation can also take part via posttranslational modifications (PTM). These include covalent attachment of a functional group, most commonly phosphorylation. Conformational changes, introduced in this way, can for instance alter substrate binding and, therefore, catalytic activity. For detection of PTMs, further methods are necessary like isoelectric focusing (IEF), which unravels changes in the isoelectric point of proteins. In addition, MS-based proteomics of PTMs has shown the large extent of protein modifications. More detailed information is gained from modification-specific enrichment techniques, like phospho-peptide enrichment, combined with advanced MS/MS methods[56,57]. Finally, many enzymes can be upregulated at the protein level to adapt catalytic capacity. This can be detected via western blot using an antibody specifically raised against the enzyme. For some proteins, there are also antibodies targeting the phospho-site, which can again be helpful in the analysis of modifications.

4.3 Metabolomics by hyphenated MS-techniques

4.3.1 Overview

The analysis of metabolites comprising a systems´ metabolome[58] is called metabolomics[59]. This term was coined based on the nomenclature of other “omics”-techniques such as genomics, transcriptomics and proteomics. Together those techniques reveal the “omics cascade” with the metabolome being the closest to phenotype. The metabolome can be subdivided into further classes, such as amino acids, organic acids, lipids, which all have distinct chemical properties. Thus, no instrument platform is suitable to analyze all metabolites[60] but metabolomics still relies on combining several instruments and analytical methods. Nuclear magnetic resonance (mainly 1H-NMR) is also being used in metabolomics[61-63]. Although 1H-NMR comes close to being a universal detector, it does not allow for complete coverage of a metabolome due to its low sensitivity. In the early years of MS in metabolomics, often direct infusion was favored because of short run time. However, this entails several problems like high background especially when injecting complex samples, severe ion suppression and lack of isomer separation. Coupling of chromatography and MS can overcome many of these problems and often is able to

distinguish between isomers by chromatographic separation. Therefore, in metabolomics hyphenated mass spectrometry is more commonly used, but there are still some rare applications with direct infusion.

The classical metabolomics approach is called fingerprinting or untargeted metabolomics, which entails the analysis of all detectable compounds preferably with high resolution mass spectrometers. From these complex data, metabolites differentially regulated between groups are identified. However, this approach only gives rise to semi-quantitative data. To confirm findings of metabolites differing in abundance between different conditions or specimens, an alternative metabolomics approach has to be applied, namely metabolic profiling also called targeted metabolomics (see below).

Depending on the separation technique coupled to mass spectrometry, one can distinguish three main platforms: GC-MS, LC-MS and CE (capillary electrophoresis)-MS. In GC-analysis the mobile phase is gaseous and, therefore, highly suited for volatile compounds. For polar compounds with insufficient vapor pressure, derivatization is necessary to rise volatility, increase thermal stability, and enhance detection. Derivatization commonly reduces polarity by performing alkylation, silylation or acetylation on polar functional groups. (Some derivatization strategies are explained in chapter 7). For ionization, classically EI (electron ionization) is the first choice, which is regarded as a hard ionization technique commonly causing extensive fragmentation. Hence, the molecular ion is often low abundant or not detectable. However, this can be helpful for identification and structure determination of unknown compounds. The most frequent GC-MS instrument is a GC-EI-qMS, with a quadrupole as mass analyzer. In general, GC-MS is a robust bioanalytical technique providing a high chromatographic resolution.

In liquid chromatography the mobile phase is a liquid; for isocratic elution a solvent is used. Mostly, however, two solvents are employed for gradient elution to facilitate elution and to shorten run times. The stationary phase consists of silica-based or polymer particles, which can be modified to change polarity. Based on the type of stationary phase, one can distinguish between normal phase (NP)-LC, reversed phase (RP)-LC, and HILIC (hydrophilic interaction liquid)-chromatography. Polarity of the mobile phase is adapted to the stationary phase and the type of LC application. The

most frequently used method is RP-LC, which combines a non-polar stationary phase with polar mobile phases (*e.g.*, water, methanol, acetonitrile) for analysis of less polar compounds. By derivatization of bare silica, like in normal phase, the polarity is reversed giving the name to this LC-subtype. The most frequently employed stationary phase consists of C_{18}-alkane modified silica. Finally, HILIC is a valuable separation technique to analyze polar and even ionic compounds, using columns like in NP-LC in combination with rather polar RP like mobile phases (more details see chapter 4.3.3). The choice of technique is driven by the chemical properties (defining solubility/retention) of the metabolites of interest.

The typical ionization technique used in coupling of LC to MS is electrospray ionization (ESI). Ionization procedure starts with formation of charged droplets at the end of a capillary electrode, which are reduced by evaporation of the solvent until a bare charged analyte remains in the gas phase. This type of ionization takes place at atmospheric pressure. It is regarded a soft ionization technique forming primarily quasi-molecular ions, but also for example adducts. Positive and negative mode ionization can be carried out by applying voltage of the respective polarity. Certainly, ESI also has some drawbacks, *e.g.*, matrix effects, which have an irreproducible impact on signal intensity. These interferences arise from coeluting (matrix) components, which are assumed to compete with the analyte during ion formation causing ion suppression or even enhancement[64,65]. However, proper sample extraction and clean-up as well as chromatographic separation can reduce those interferences and, thereby, enhance signal intensity[65]. Furthermore, mobile phase additives can also influence the formation of ions in the source. In this context more problematic modifiers like the ion pairing reagent trifluoroacetic acid might be exchanged by, *e.g.*, formic acid, which causes usually less ion suppression[66]. Finally, internal standards can be used to control for matrix dependent variation in ion yield (see below).

4.3.2 Quantitative targeted MS-analysis

Quantitative analysis means experimental determination of the absolute concentration/ amount of a set of pre-defined compounds. The set of analytes is usually limited to a certain compound class or metabolites and intermediates of an explicit pathway. This targeted analysis is called metabolic profiling and is often used to verify a hypothesis, generated on other preliminary data[67].

One instrument that is highly qualified for this targeted analysis is a LC-ESI-QqQ-MS. As the colloquial name, TripleQuad-MS, already implies this instrument has three quadrupoles (QqQ), which are arranged in line with the second quadrupole Q2 being the collision cell. The other two quadrupoles (Q1 and Q3) can be operated in different scan modes with Q1 and/or Q3 set to a fixed mass or used to scan a certain mass range, respectively. MRM-mode (multiple reaction monitoring) is the most prominent mode for quantification analysis due to its high sensitivity and a broad dynamic range (of three to five orders of magnitude)[68]. Figure 5 shows a scheme of the principle of MRM:

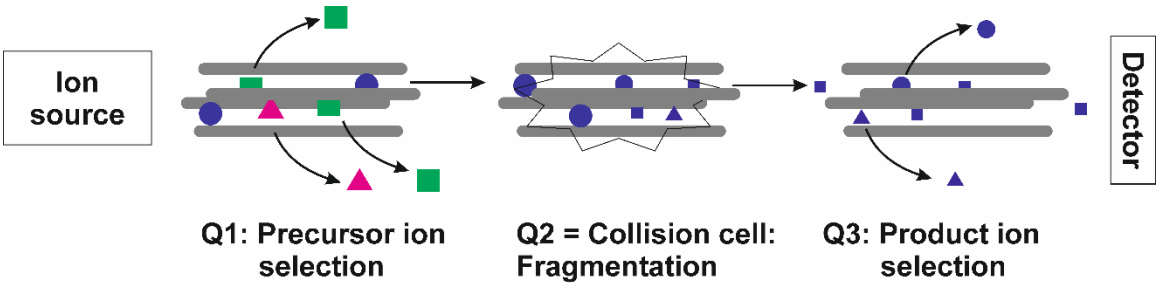

Figure 5. Scheme of a Triple Quad-instrument operated in MRM-mode. The charged analytes, produced by the ion source, are focused to form a narrow ion beam entering the first quadrupole Q1. The voltage applied here is set to isolate the parent ion. Ions of other m/z-values are deflected and leave the ion path. The parent ion is accelerated to Q2, where it is fragmented by collision with a collision gas (N_2 or argon). Q3 is operated identical to Q1, now selecting for the product ion, which hits the detector. The mass range isolated in Q1 and Q3 is usually a window of 1 Da around the m/z-value of the target compound. The pair of precursor and fragment ions is called a transition.

MRM mode benefits from a low signal-to-noise-ratio and increased selectivity. The scheme shows the process for one analyte. For a set of analytes, the process needs to be repeated iteratively. Such a cycle gives one data point for each analyte, which are summed up to re-build a chromatogram. For a reliable peak reconstruction, a

minimal number of 15-20 data points across the peak is necessary[69]. Therefore, the time spent on scanning one analyte (called dwell time) is limited. On the other hand, when the dwell time is too short signal quality will be impaired. To circumvent this issue, it is possible to divide the LC-run into windows/periods, where only transitions of analytes are measured that are expected to elute from the column in this time range. Depending on the instrument options scheduled MRM´s can be programmed with a specific window for each analyte. All acquisition parameters for each compound are optimized by measuring analyte standards during method development.

Linear range of TripleQuad instruments (like with other LC-ESI-MS instruments) is limited at the ULOQ (upper limit of quantification) either by saturation at the detector or due to e.g. charge limitations in the ion source[70]. The LLOQ (lower limit of quantification) is mainly dependent on ionization efficiency. As mentioned before, matrix effects can drastically affect ionization and therefore cause an increase of LOQ in comparison to standard samples or a different biological matrix.

This is one explanation, why response, hence the peak intensity in arbitrary units, does not allow for absolute quantification. Another issue is, for instance, analyte loss during sample preparation. These problems can be overcome by including an internal standard (IS). The internal standard can be a compound of similar chemical nature or a structural analogue. The best option, however, is a stable isotope labeled analogue, where the analyte and its corresponding isotopologue elute from the column at the same retention time and are only distinguished by their mass. Thus, the IS corrects for matrix effects and ensures high specificity. In practice, a known concentration of IS is spiked into the sample at the earliest possible stage during sample preparation. The ratio of the analyte area and the IS area ($A_{analyte} / A_{IS}$; also called response) is used to calculate the sample´s absolute concentration. Two approaches are distinguished: on the one hand, the stable-isotope dilution (SID) methodology[71-73], where the ratio ($A_{analyte} / A_{IS}$) is multiplied with the IS-concentration to calculate the analyte´s concentration. On the other hand, a multipoint calibration curve can be constructed based on the response (y axis) and the ratio of analyte concentration and IS concentration (x axis)[74,75]. The disadvantage of the addition of stable isotope labeled standard is the high expense, especially for methods containing a high number of analytes, and the limited availability.

Furthermore, quantitative approaches exist also for GC-MS. A comparable way to MRM is SIM (selected-ion-monitoring-) mode, where the quadrupole of a GC-EI-qMS instrument is set to iteratively isolate ions of preselected m/z-values[76,77]. Here, again sensitivity is increased in comparison to a full-scan approach. Nevertheless, inclusion of an internal standard and a calibration curve are recommended for absolute quantifications.

The FDA (U.S. Department of Health and Human Services, Food and Drug Administration) has provided a guide for method development and validation of bioanalytical, quantitative assays for the analysis of metabolites and drugs in biological matrices such as blood, serum, plasma, or urine[78]. This guide should ensure high data quality by monitoring accuracy, precision, selectivity, sensitivity, reproducibility, and analyte stability.

4.3.3 Analysis of 2-HG in biological samples

Quantification of 2-HG in biological samples can be achieved by enzymatic assays, on the one hand. As mentioned earlier, Balss *et al.* (2012) developed an assay where degradation of D-2-HG is coupled to a fluorescence reaction via a two-step reaction[55]. Purified 2-hydroxyglutarate dehydrogenase from *A. fermentans* expressed in *E. coli* converts D-2-HG into α-KG using NAD^+ as a hydride acceptor. The produced NADH is used by diaphorase to produce the fluorescent Resorufin from its non-fluorescent precursor Resazurin. To perform this assay, a reaction solution containing all enzymes and cofactors is mixed with the sample and incubated for 30 minutes at room temperature. Fluorescence signal intensity is used to calculate D-2-HG concentrations from a standard curve acquired in parallel with standard samples of known D-2-HG concentration. This assay is applicable to the analysis of several specimens like cell culture supernatant, urine, or serum. Even deparaffinized and deproteinized FFPE-material can be subjected to this assay. According to the authors, the LLOQ for this assay is 0.44 µM D-2-HG in tumor tissue and 2.77 µM in serum. The assay shows results comparable to determination by GC-MS up to a concentration of about 500 µM.

Beyond this enzymatic assay, several (quantitative) methods using GC-MS or LC-MS/MS were published. Quite a few publications apply one of two frequently cited

enantioselective methods: Gibson *et al*.[79] (1993, butylated diastereomers via GC-MS) and Struys *et al*.[80] (2004, DATAN-derivatives via LC-MS). Both methods are enantioselective, as they were developed in context of 2-HG-aciduria, where it is necessary to distinguish between D- and L-2-HG for diagnosis of D-2-HGA or L-2-HGA, respectively. Gibson *et al.* reported a derivatization regimen using D-2-butanol for esterification of carboxyl groups (under acidic conditions) and acetic anhydride for acetylation of hydroxyl groups. By addition of enantiomeric pure D-2-butanol diastereomers are formed, which can be separated on polar, non-chiral GC-columns. In this method GC is coupled to MS via chemical ionization and data are acquired in SIM-mode. This derivatization strategy was already applied by the Wadman group to determine the absolute configuration of urinary 2-hydroxydicarboxylic acids including 2-HG[2,81]. However, Gibson *et al.* further established this approach as a quantitative method including isotope dilution using D,L-[3,3,4,4-D_4]-2-hydroxyglutaric acid (prepared from D_4-α-KG) as internal standard. Similarly, Janin *et al.* in 2014 used [1,2,3,4-$^{13}C_4$]-labeled 2-HG (prepared from [$^{13}C_4$]-α-KG) in a GC-QqQ-MS/MS method[82]. Here the linear range is from ~ 50 pmol to 400 nmol (which equals to 0.5 µM and 4 mM, respectively, in a 100 µL sample) with the LOD determined at 20 pmol.

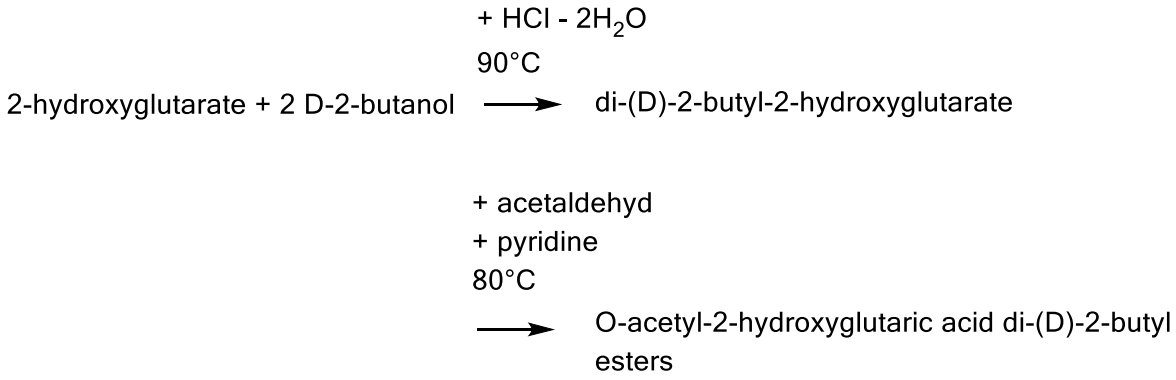

Figure 6. Derivatization of 2-hydroxyglutarate using D-2-butanol and acetaldehyde for enantioselective analysis. For the structure of the derivatization product see Figure 14.

Struys *et al.* used DATAN (diacetyl-L-tartaric anhydride) for derivatization again yielding diastereomers of 2-HG, which could be separated within five minutes on a C18-HPLC column (Xterra, Waters)[80]. Acquisition of MS-data was performed in MRM-mode. Once more, D,L-[3,3,4,4-D_4]-2-hydroxyglutaric acid (prepared from [D_4]-α-KG) is included as stable-isotope labeled standard. This method is stated to be less time-consuming and less expensive than the aforementioned method reported by Gibson

et al. Poinsignon *et al.* (2016) similarly used derivatization with DATAN in the context of *IDH1/2* mutation to analyze AML-patient samples in a clinical setting, as well as in preclinical applications using cellular and tissue samples[83]. Here the linear calibration curve ranged from 0.34 µM to 135.04 µM. Moreover, this method was used in the 2-HG analysis of mutIDH1/2 samples in the context of intrahepatic cholangiocarcinoma (ICC) with a comparable LLOQ of ~0.2 µM[84]. Those recent publications have made use of now commercially available deuterated 2-HG ([2,3,3- D_3]-(RS)-2-hydroxyglutaric acid).

Additionally, Ward *et al.* (2010) reported a GC-EI-MS method based on the silylation of cell extracts with MTBSTFA (N-methyl-N-tert-butyldimethylsilyltrifluoroacetamide)[10]. Derivatized samples were then injected onto a HP-5MS capillary column for non-chiral analysis. Here, no internal standard was included, and peak areas were normalized to glutamate as relative measure of metabolite abundances. Therefore, this publication did not yield absolute quantitative values. It was rather used to check for drastically increased 2-HG levels in AML samples as marker for a mutation in *IDH1/2*.

Many methods developed to detect elevated 2-HG levels due to *mutIDH1/2* are not enantioselective, because the neo-enzymatic activity of IDH1/2 is specific for the production of D-2-HG. Thus, analysis of 2-HG may be accomplished directly by LC-MS without derivatization. However, the hydrophilic nature of 2-HG impedes retention on classical, non-polar RP-LC-columns (*e.g.*, C18). In addition, highly aqueous mobile phase conditions are required for solubilization and loading of 2-HG, which can cause phase collapse of traditional C18 columns. Modern C18 columns (*e.g.*, Agilent, ZORBAX SB-Aq) can be operated with 100% water. Juratli *et al*. (2013) used such a column for the simultaneous quantification of TCA intermediates and 2-HG in low-grade gliomas[85]. Detection was performed in MRM-mode and stable isotope-labeled internal standards were included for absolute quantification.

Besides, methods using other types of LC-columns were developed, which regularly comprise several other metabolites. Fluorinated silica-based columns are an attractive alternative due to their effectiveness in retaining small polar molecules. Navis *et al*. (2013) used a Luna PFP column for analysis of D-2-HG by LC-MS/MS in MRM mode in specimens obtained from an IDH1-R132H mutation carrying xenograft model[86]. For absolute quantification, a $^{13}C_5$-2-HG stable isotope solution was added to the sample before filtration to remove proteins.

Another means for increasing retention of charged analytes on reversed phase columns is the addition of an ion-pairing agent. Those agents are often non-volatile and, therefore, not compatible with online LC-ESI-MS. However, there are also volatile ion pair modifiers like tributylammonium acetate (TBAA), which was introduced into 2-HG (and TCA) analysis by Dang 2009[11]. Thus, a C18-column (Synergi Hydro-RP, Phenomenex) could be used in a LC-MS/MS approach, run on a TripleQuad instrument in MRM-mode. Quantification was achieved by comparison of peak areas with metabolite standards. However, experience in our laboratory showed that TBA is quite "sticky" and tends to remain in the chromatographic system causing serve interferences for methods using positive mode ionization and extensive flushing is required (K. Dettmer, personal communication).

Finally, ion-exchange chromatography can be used for separation of charged compounds. However, high salt concentration is typically applied for elution. Therefore, this is not compatible for detection via MS, as most salts are non-volatile and impede ionization. Still, Borger *et al*. (2014) used a multiple-mode column (BioRad Fast Acid analysis) and isocratic elution with 0.1% formic acid in water[87]. Total run time was only four minutes. In this LC-MS/MS approach, the column was connected to a TripleQuad instrument operated in MRM-mode to quantify 2-HG in serum samples. Internal standard was again $^{13}C_5$-2-HG, which was added before sample precipitation.

Besides, hydrophilic interaction liquid chromatography (HILIC) is highly suitable for separation of polar and even ionic compounds like 2-HG. HILIC is a hybrid LC-method making use of polar stationary phases. Mobile phase - similar like in RP-LC - consists of a high percentage of an organic water-miscible solvent. But the gradient profile for HILIC is inverse to that of RP chromatography, *i.e.*, the highest water content (maximal ~50%) is reached at the end of the run. Separation is achieved by partitioning of the analytes between the water-rich layer, which is formed on the surface of the polar stationary phase, and the water-deficient mobile phase[88]. Consequently, HILIC offers retention to hydrophilic compounds in contrast to classical RP-LC methods. Gelman *et al.* (2015) reported the use of HILIC for the analysis of 2-HG and glutamine[89]. The column used was an Acquity UPLC BEH Amide column (Waters) coupled to a QqQ-MS, again in MRM-mode. Becker-Kettern *et al*. (2016) also set up a HILIC method investigating total 2-HG, together with several organic and amino acids[90]. A

ZicHILIC SeQuant column was connected to a Q-Orbitrap-HRMS. External calibration curves ranged from 0.01 µM to 50 µM for each metabolite.

In addition to mass spectrometric bioanalytical methods, various NMR-based investigations were performed to analyze 2-HG[14,91]. For glioma patients it is even possible to perform *in vivo* measurements via MRT instruments. However, these investigations suffer from low sensitivity and a high background signal. Information on spatial metabolite distribution is also gained from analysis of tissue sections. Volexen *et al*. (2016)[92] developed a bioluminescence assay for this purpose, Longuespee *et al*. (2018)[93] used MALDI-TOF to examine tissue sections.

In conclusion, it can be stated that numerous methods were published for 2-HG analysis, none of which is universally applicable. Each has its strengths but also shortcomings, which determine the usability of the method in the respective context.

4.3.4 Flux/tracing analysis

The metabolic flux of a cell is regarded as the metabolite amount that is converted in a certain time, *i.e.*, the intracellular metabolic rate[94]. Flux or tracer analysis are two methods aiming to answer questions about cellular metabolic pathway (activity) and nutrient contribution. In contrast, quantitative data provide only a snapshot of metabolism at a given time point, but together with uptake and secretion rates it can be used to generate knowledge about a biochemical network. Metabolic flux data are generated by feeding a stable isotope labeled compound, named tracer, to the model system and samples are subsequently analyzed via hyphenated MS or NMR. All metabolites that are produced from the tracer, show an altered mass distribution due to the incorporated label, which can be made visible by MS-measurements. However, metabolic flux data are very complex and require computational data interpretation to calculate absolute pathway activity. Furthermore, the biological system, e.g. a cell, needs to be in a state without changes in flux and metabolite concentrations (metabolic steady state[95]) and in isotopic steady state, which means that the label enrichment in the metabolite of interest (=tracee) is stable[96]. These conditions require continuous cell culture to avoid limitations in nutrients, increasing cell density and therefore changes in proliferation rate. Furthermore, incubation times until isotopic steady state is

reached, differ based on the intermediates/pathways as well as the cell type and are dependent on the tracer used[97].

A much easier, though less informative approach, is tracer analysis, where the labeling patterns of cellular metabolites after incubation with a labeled precursor are interpreted directly[97]. Yet, change in flux should be minimal within the experimental time (ideally metabolic steady state, practically pseudo-steady state). This can be assumed for most pathways (e.g. glycolysis) in monolayer cell culture or suspension cells, when performing the tracer study as long as the cells are in the exponential growth phase[98]. Interpretation of such labeling pattern can give insights into relative pathway activity and contributions, in context of mutations or changes, which were evoked by administration of a metabolically active drug.

Tracer analysis provides labeling patterns in all compounds involved in the metabolism of a labeled nutrient. The mass isotopomer distribution vector (MID) contains all fractional abundances of each isotopologue (M+0 to M+n; n is the analytes´ maximal labeled isotope number, introduced by the tracer, e.g. M+6 for $^{13}C_6$-citrate) normalized to the sum of all possible isotopologues[99]. Therefore, these labeling patterns are independent of pool size and can unravel increased flux while absolute concentrations stay the same. Metabolites with identical patterns are in complete exchange. MIDs do not contain information on the position of label within the molecule. This can be determined by further experiments using NMR or by interpreting specific fragments from MS/MS-analysis.

Another important measure in ^{13}C-tracer analysis is mean isotopic enrichment (also called fractional contribution), which determines the fraction of a metabolite's carbon that is produced from a certain nutrient. The mean isotopic enrichment is calculated as follows:

$$ME = \frac{\sum_{i=0}^{n} i*s}{n},$$

where *n* is the number of carbon atoms in the metabolite, *i* denotes the isotopologues and *s* the relative fraction of the isotopologues as calculated in the MID[100]. Prerequisite is, that the tracer is fully ^{13}C-labeled. Especially glucose and glutamine as the main carbon sources are well suited for tracer analysis. Summing up, the mean isotopic enrichment for those two (calculated from two independent experiments) is often close to 100%. If not, another substrate contributes to the formation of the tracee. For

instance, it was reported for different cells that under hypoxic conditions acetate contributes to fatty acid synthesis[101].

With focus on glycolysis and TCA cycle, commonly fully labeled compounds are used. Lactate can be formed from glycolysis and via pentose phosphate pathway. These two alternative routes can be distinguished by using 1,2-$^{13}C_2$-glucose as tracer[102]. This example shows that the choice of the tracer is dependent on the pathway of interest. Besides ^{13}C-labeled nutrients, also tracers containing further stable isotopes like ^{15}N or ^{2}H are sometimes supplemented to cell culture media[103,104]. Nevertheless, ^{13}C-labeled compounds are the most frequently used.

Cellular compartmentalization can influence the labeling pattern too. An established example here is pyruvate, which is found in both cytosol and mitochondria. A cell´s average labeling pattern cannot resolve the cellular distribution of pyruvate. However, it was found that the labeling pattern of alanine reflects mitochondrial pyruvate, while lactate is a cytosolic product of pyruvate[97].

Once the tracing data has been acquired, it needs to be subjected to correction for natural abundance of heavy isotopes introduced by the tracer. For instance, ^{13}C has a natural abundance of 1.07 % contributing mainly to the M+1, but to a lower extent also to all other isotopologues. This correction is complex, nevertheless can be accomplished by using tools available from different sources (e.g. IsoCor[105], IsocorrectoR[106]). Additionally, some bias is potentially introduced by derivatization, *e.g.*, silylation (^{28}Si 92.23 %, ^{29}Si 4.68 %, ^{30}Si 3.08 %).

In conclusion, tracer analysis and to an even larger extent flux analysis are valuable tools for investigations on metabolism and alternative pathways. Nevertheless, this technique hides several pitfalls and therefore requires careful handling to avoid misinterpretations.

5 Methods and Material

5.1 Materials

D- and L-2-hydroxyglutarate, R- and S-5-oxotetrahydro-2-furancarboxylic acid, as well as pyridine, methyl chloroformate (MCF), and methoxylamine hydrochloride were from Sigma-Aldrich (Taufkirchen, Germany). Formic acid, methanol and ethyl acetate (LC-MS grade) from BDH Prolabo (VWR International, Vienna, Austria). N-Methyl-N-(trimethylsilyl)-trifluoroacetamide (MSTFA) was purchased from Macherey-Nagel (Dueren, Germany).

In all experiments purified water from a PURELAB Plus system (ELGA LabWater, Celle, Germany) was used.

5.2 Biological samples

5.2.1 Cell culture

For this thesis the following cell lines were cultured using the listed conditions:

HT1080 (a fibrosarcoma line; ATCC CCL-121, ATCC, Manassas, VA, USA) were cultured in DMEM (PAN, Aidenbach, Germany) supplemented with 10 % fetal calf serum (FCS, Biochrom AG, Berlin, Germany), 1 % penicillin-streptomycin (PAA, Pasching, Austria), and 2 mM L-glutamine (PAN). The HCT116 panel (colon carcinoma; Horizon Discovery, Waterbeach, UK; HD 104-013, HD 104-019, HD 104-020) consists of a parental line (WT-IDH1/2) and three cell lines carrying the mutations IDH1-R132H, IDH2-R172K, and IDH2-R140Q, respectively. This panel was cultured in RPMI (1640, PAN), supplemented with 10 % FCS, 1 % penicillin-streptomycin, and 2 mM L-glutamine. The same medium was used for cultivation of the LS174T-cell panel (colorectal adenocarcinoma, kindly provided by M. Kreutz, Regensburg) and CCRF-CEM-C7H2 (acute lymphoblastic T-cell line; kindly provided by R. Kofler, Innsbruck, Austria). The breast cancer cell line MCF7 (ATCC HTB-22) was cultured in DMEM supplemented with 10 % FCS, 1 % penicillin-streptomycin and 2 mM L-glutamine. The MCF7 cells formed clusters after trypsinization and, therefore, could not be counted, but sub-cultured and seeded based on ratios. All other cells were counted using the Casy TT System (OLS OMNI Life Science, Bremen, Germany).

Adherent cells were sub-cultured by trypsinization, while suspension cells were diluted in fresh medium and once a week centrifuged (800 rpm, 5 min) to completely remove the old medium. Cells were sub-cultured two or three times a week and incubated at 37°C, 5 % CO_2.

For experiments with treatment of cells, adherent cells were seeded into 6-well plates the day before treatment was started. Cell count was 0.25-0.5×10^6/ well but was adapted to the intended incubation time.

TRACER ANALYSIS

Cells were seeded into plates and kept under standard conditions overnight. The next day, the medium was replaced with RPMI (+10% FCS, 1% P/S, +2 g/L glucose, w/o L-glutamine) supplemented with 2 mM $^{13}C_5$-L-glutamine (CIL, Andover MA, USA), for glucose tracing with RPMI (+10% FCS, 1% P/S, w/o glucose, +2 mM L-glutamine) supplemented with 2 g/L $^{13}C_6$-D-glucose (CIL), respectively. Cells were incubated for 24 h or 48 h. Sample collection and extraction were performed using the routine protocol, but without addition of internal standard solution(s).

OCTYL-2-HG

Cells were seeded into plates and kept under standard conditions overnight. The next day, the medium was replaced with medium supplemented with (2R)-2-hydroxyglutaric acid octyl ester (Toronto Research Chemicals, Toronto, Canada). For control cells, the medium was replaced with fresh standard medium. Cells were incubated for 24 h. Sample collection and extraction were performed using the routine protocol.

5.2.2 Serum samples

Serum samples were collected at the Department of Internal Medicine III at the University Hospital Regensburg. Written informed consent was obtained from all participants. The study was approved by the local ethics committee and registered in the national registry for clinical studies (05-097). Serum was stored at -80°C until sample preparation, which was an extraction by methanol precipitation (see chapter 5.4.1).

5.2.3 Glioma tissue samples

With approval by the Ethics Committee of the University Medical Center Regensburg, Germany (10-248-0219), and written informed consent by the patients, frozen biopsies of human glioblastoma multiforme of known IDH mutational status were provided by the Department of Neurosurgery at the University Hospital Regensburg. The frozen tissues were immersed immediately into liquid nitrogen and stored at −80°C for a minimum of 24 h until sample preparation. For tissue homogenization, 30-120 mg of frozen tissue were transferred to Precellys 2 ml cups (pre-filled with 1.4 mm ceramic beads, Bertin Technologies, Montigny-le-Bretonneux, France), spiked with 40 µl internal standard (20 µl for smaller sample sizes) and covered with 1000 µl of 80% ice-cold methanol followed by two cycles of homogenization using a Precellys homogenizer (Peqlab Biotechnologie GmbH, Erlangen, Germany). Metabolite extraction was performed similarly to chapter 5.4.1: tissue homogenates were washed twice with 500 µl 80% methanol and additionally washed with 600 µl H_2O. After drying in the evaporator, samples were reconstituted in 200 µl H_2O (100 µl for smaller sample sizes) prior to LC-MS/MS measurements (see chapter 5.5.1). Metabolite concentrations in tissue extracts determined by LC-MS/MS analysis were normalized to tissue weight.

5.3 Enzyme assays

For enzyme assays, pellets of trypsinated cells were washed twice with PBS (phosphate buffered saline) to remove excreted protein and FCS. Cells were lysed in the respective assay buffer by sonication on ice, followed by centrifugation at 10.000 x*g* at 4°C for 5 min to remove cellular debris. The supernatant comprises the lysate used for the assay. An aliquot is taken to determine protein content for normalization.

For **assaying D2HDH activity** the buffer consisted of 20 mM HEPES, 25 mM KCl, 0.05 mM $ZnCl_2$, and protease inhibitor cocktail. To start the assay, the lysate is spiked with D-2-HG (various concentrations, as stated) and 2 mM PMS (phenazine methosulfate) as redox equivalent. For control, buffer without lysate was incubated with the same concentrations of D-2-HG and PMS. Incubation was performed under gentle shaking (400 rpm) at 37 °C. Aliquots of 20 µL were taken over a period up to 5 hours and mixed with stable isotope-labeled standard ([2,3,3]-D_3-2-HG, C/D/N Isotopes Inc.,

Pointe-Claire, Canada; 100 µM in water). Precipitation with ice-cold methanol stopped the enzymatic reaction. After extraction, samples were analyzed by LC-MS/MS.

For **assaying D-2-HG production by mutIDH1/2,** assay buffer consisted of 50 mM Tris-HCl (pH 7.4), 10 mM NaCl, 2 mM $MgCl_2$ and protease inhibitor cocktail (adapted from Pusch[8]). Here, the assay was started by addition of α-ketoglutarate and 10 mM NADPH. The following steps were identical to those for the D2HDH assay.

5.4 MS-sample preparation

5.4.1 Methanol precipitation and sample extraction

Samples analyzed for this thesis included serum or plasma, cell pellets and supernatant. For most analyses, it was necessary to remove the protein, which was done by methanol precipitation, which at the same time stopped any metabolic activity. For liquid samples like serum, plasma and cell culture supernatant, usually 50 µL-aliquots were precipitated in 200 µL 100 % cold methanol (MeOH). For quantitative analysis, the respective (stable isotope labeled) internal standard was added before methanol precipitation. Suspension cells were pelleted by centrifugation; supernatants were collected separately and treated as described above. The pellet was thoroughly washed three times with PBS to remove metabolites sticking to the outer surface of the cells, before addition of internal standard and protein precipitation with 80 % cold MeOH. For adherent cells the medium was collected and treated as described above. Cells in the well were washed three times with PBS, before the internal standard was added followed by scrapping the cells in 80 % cold methanol (600 µL are used for wells of a 6-well plate). The well is washed with additional 400 µL MeOH and combined with the first precipitate. All precipitates were further processed by pelleting the precipitated protein at 9560 x*g,* 4°C, 5 min and two further washing steps using 80 % (cell pellets) or 100 % MeOH (liquid samples), respectively. The methanolic phase, containing the analytes, was collected and combined in glass vials. Samples were dried using an infrared vortex vacuum evaporator (CombiDancer, Hettich AG, Baech, Switzerland). Further processing is dependent on the respective MS-method.

5.4.2 Derivatization for GC-analysis

For GC-analysis, dried sample extracts or dried medium (10 µL) residues were subjected to derivatization as previously described (Dietl *et al*. 2009[107]). The protocol includes methoximation (using methoxylamine hydrochloride in pyridine) and silylation (with *N*-methyl-*N*-trimethylsilyl-trifluoroacetamide MSTFA, Macherey-Nagel). The derivatization is carried out by an MPS-2 Prepstation sample robot (Gerstel, Mülheim/Ruhr, Germany) for automated sample handling.

For tracer analysis of 2-HG/-lactone and other metabolites, derivatization needed to be adapted to avoid interconversion of 2-HG/-lactone. Therefore, dried sample extracts were subjected to a two-step incubation regimen consisting of addition of MSTFA followed by incubation with methoxylamine hydrochloride in pyridine (as proton acceptor). Ten µL of a 1 mM undecanoic acid solution in isooctane were added to the dried residues as retention and injection standard. Silylation was carried out by the addition of 25 µL of MSTFA, and incubation for 30 min at 60°C. Then 25 µL of 20 mg/mL methoxylamine hydrochloride in pyridine were added to the sample and incubated at 60°C for 30 min. Finally, the sample was diluted further with 25 µL MeOx-reagent. Derivatization was carried out fully automated on the MPS-2 Prepstation sample robot.

Further attempts to establish derivatization of 2-HG and its lactone are summarized in chapter 7.

5.4.3 PCF-derivatization for amino acid analysis

For amino acid analysis, derivatization with PCF (propyl chloroformate) was performed to increase retention of these polar compounds on a C18 column. Dried cell pellet extracts were reconstituted in 100 µL of water of which 10 µL were subjected to PCF-derivatization for amino acid analysis (as described in van der Goot *et al*. 2014[108]). For medium 5-10 µL were directly used for derivatization. Internal standard mix contained a commercially available Amino Acid Standard Mix (Cambridge Isotopes, MSK-A2-1.2) spiked with D_7-ornithine (Cambridge Isotopes), L-tryptophan-D_5) (Eurisotop, Saint-Aubin, France), U$^{13}C_5$-glutamine (Cambridge Isotopes), $^{13}C_4$,$^{15}N_2$-L-asparagine (Cortecnet, Voisins-Le-Bretonneux, France), and D_5-hippuric Acid (Biozol, Eching, Germany), to yield a concentration of 1 mM for each labeled compound. Ten µL of a

1:10-dilution of this standard mix were added to cell pellets before methanol precipitation, and a 1:100-dilution was added to medium samples directly before PCF-derivatization. After derivatization, derivatives were extracted with ethyl acetate, dried under a nitrogen stream and reconstituted in 100 µL water/methanol (38%/ 62%, v/v).

5.5 MS methods

5.5.1 2-HG/-lactone quantification by HPLC-MS/MS

For analysis of 2-HG/-lactone, samples were reconstituted in 50 µL ddH_2O and transferred into a glass insert. HPLC-MS/MS analysis was performed as described in Voelxen *et al.* [92] and Berger *et al.* [109]. Briefly, HPLC-MS/MS analysis was achieved using a HPLC (Agilent 1200, Waldbronn, Germany) coupled to an API 4000 QTRAP (AB SCIEX, Darmstadt, Germany) operated in negative ionization mode. The HPLC column used was a Discovery HS F5-3 HPLC column (15 cm x 2.1 mm, 3 µm; Supelco, Bellefonte, USA) equipped with a Security Guard column (C18, Phenomenex, Aschaffenburg, Germany) and kept at 30°C. Gradient elution was achieved with mobile phase A consisting of 0.1 % formic acid in water (v/v) and 100 % acetonitrile as mobile phase B. The gradient for chromatographic separation started with 0 % B, 200 µL/min, increased to 100 % B from 6.50 min to 8 min at 350 µL/min, and stayed at 100 % B for 2 min, followed by a reconditioning of the column at the starting condition for 8 min. An injection volume of 5 µL was used. Detection was performed in MRM-mode using the following ion transitions: m/z 147.1 $[M-H]^-$ to m/z 84.8 for 2-HG, m/z 150.1 $[M-H]^-$ to m/z 87.8 for 2-HG-D_3 and m/z 128.8 $[M-H]^-$ to m/z 100.8 for 2-HG-lactone, m/z 131.8 $[M-H]^-$ to m/z 87.9 for 2-HG-lactone-D_3. Data analysis was done using the Analyst Software (version 1.6.2, AB Sciex). Quantification was achieved using a calibration curve with the area of target compounds normalized by the area of the corresponding stable isotope-labeled standard.

5.5.2 Amino acid quantification and tracer analysis by HPLC-MS/MS

Quantitative amino acids analysis was performed as described in van der Goot *et al*. (2014)[108]. Briefly, HPLC-MS/MS instrumentation was an Agilent 1200 coupled to an

API 4000 QTRAP (see above) operated in positive ionization mode. An EZ:faast AAA-MS (250 × 3 mm i.d., 4 µm, Phenomenex) reversed-phase column was used and kept at 30 °C. Mobile phases A was 10 mM ammonium formate and 0.1 % (vol/vol) heptafluorobutyric acid in water and mobile phase B was 10 mM ammonium formate and 0.1 % (vol/vol) heptafluorobutyric acid in methanol. The gradient for chromatographic separation started with 62 % B, increased to 79 % B within 12 min, further increased to 98 % B within 0.01 min, and kept at 98 % B for 3 min before reconditioning of the column at the starting condition for 8 min. The column flow rate was 350 µL/min. Injection volume was 5 µL for cell pellet samples and 10 µL for cell supernatant. The MS/MS was operated in MRM using one transition each for the analyte and the internal standard. Quantification was performed using calibration curves. Data analysis was done using the Analyst Software (version 1.6.2, AB Sciex).

For tracer analysis, MRM-transitions are programmed for all possible isotopologues and peak areas are used directly for data analysis. The R-package IsoCorrectoR was used to correct for natural abundance of ^{13}C and other naturally occurring stable isotopes and for impurities of the tracer[106].

5.5.3 Organic acid quantification by GC-EI-MS

For quantification of glucose and organic acids, a previously published method was used[107]. The internal standard mix contained 1 mM each of $^{13}C_3$-pyruvate, [2,3,3]-D_3-malate acid, $^{13}C_4$-succinate, $^{13}C_3$-lactate, [2,2,4,4]-D_4-citrate, $^{13}C_4$-fumarate, and D_6-α-ketoglutarate. Dried sample residues were subjected to derivatization using methoximation and silylation. First, 50 µL of 20 mg/mL methoxylamine hydrochloride in pyridine were added to the sample and incubated at 60°C for 60 min, then the injection standard undecanoic acid (10 µL of 1mM solution in isooctane) was added followed by 50 µL MSTFA and incubation at 60°C for 60 min. The derivatization is carried out on an MPS-2 Prepstation sample robot (Gerstel, Mülheim/Ruhr, Germany). Derivatized samples were analyzed by an Agilent model 6890 GC (Agilent, Palo Alto, CA) equipped with a Mass Selective Detector model 5975 Inert XL. Chromatographic separation was carried out on an RXI-5MS column, 30 m x 0.25 mm i.d. x 0.25 µm film thickness (Restek, Bad Homburg, Germany), which was connected to a 2 m deactivated pre-column (Agilent Technologies, Palo Alto, CA, USA). A sample volume of 1 µL and an injection temperature of 280°C was used. Cell pellet extracts were

injected splitless (splitless time 1 min), while medium samples were injected with a split ratio of 1:8. The initial oven temperature was set at 50°C, ramped at 5°C/min to 120°C, changed to 8°C/min up to 300°C, and held for 5 min. Helium was used as carrier gas at a flow-rate of 0.7 mL/min. Data analysis was done with Mass Hunter Quantitative Analysis Workstation Software (Agilent, version B.07.01).

5.5.4 Organic acid tracer analysis

Here, two different methods were used, which are explained in more detail in chapter 8.1.1.

The first method comprised HPLC-ESI-MS/MS analysis using an Agilent 1200 SL HPLC and a 4000 QTRAP mass spectrometer. A Discovery HS F5-3 HPLC column (15 cm × 2.1 mm, 3 µm; Supelco) equipped with a Security Guard column (C18, Phenomenex) was used with mobile phase A consisting of 0.1% formic acid in water (v/v) and acetonitrile as mobile phase B. Gradient elution started with an isocratic hold at 0% B for 5 min and a flow rate of 300 µL/min, followed by a linear increase to 100% B in 2 min, which was held for 4 min. For equilibration, the solvent was changed back to 0% B from 11 min to 11.1 min and held until 18 min. The flow rate was increased to 350 µL/min at 11.1 min. The column was kept at 30°C, and an injection volume of 10 µL was used. The mass spectrometer was operated in negative mode and detection was performed in MRM-mode using transitions for each metabolite.

Furthermore, a tracer analysis by GC-APCI-TOF-MS was implemented (see chapter 8.1.1). Sample derivatization consists of silylation followed by methoximation, as described in chapter 5.4.2. Instrumentation included a model 450-GC (Bruker Daltonics GmbH, Bremen, Germany) that was equipped with an autosampler (model PAL COMBI-xt from CTC Analytics, Zwingen, Switzerland) for sample injection with a 10 µL Hamilton syringe. The GC was coupled to a microTOF mass spectrometer (Bruker Daltonics) via an APCI II source. For separation of analytes, an RXI-5MS column, 30 m x 0.25 mm i.d. x 0.25 µm film thickness (Restek) was used with a 2 m deactivated pre- and a 0.5 m post-column of matching inner diameter (Agilent). The GC parameters were identical to those for organic acid quantification on an Agilent model 6890 GC/ MSD 5975 Inert XL. A sample volume of 1 µL was introduced at 280°C performing hot needle splitless injection (preinjection dwell of 1 s) with a splitless time

of 1 min. Helium served as the carrier gas at a constant flow rate of 0.7 mL/min. The transfer line to the MS instrument was maintained at 290°C. The APCI II source was operated as follows: ionization mode, positive; drying gas (nitrogen) temperature, 150°C; drying gas flow rate, 2.0 L/min; APCI vaporizer temperature, 300°C; nebulizer gas (nitrogen) pressure, 2.5 bar; current of the corona discharge needle, +4000 nA; capillary voltage, -3000 V; end-plate offset, -500 V. Data analysis was done with Compass QuantAnalysis software (Bruker, version 2.2).

For tracer analysis, peak areas of all isotopologues are used directly for data analysis. The R-package IsoCorrectoR was used to correct for natural abundance of ^{13}C and other naturally occurring stable isotopes and for impurities of the tracer[106].

5.5.5 Enantioselective analysis of D-/L-2-HG

Enantioselective analysis was performed by GC-MS after chiral derivatization adapting a protocol by Gibson *et a*l. (1993)[79]. Briefly, standard solutions or biological samples were dried under a nitrogen stream. The residues were re-dissolved in 50 µL of S-2-butanol (Sigma-Aldrich), acidified with 5 µL of 12 M HCl, and heated for 3 h at 90°C. Samples were extracted with 500 µL of hexane and dried under nitrogen. For acetylation, 30 µL of pyridine and 30 µL of acetic anhydride were added to the residue and incubated for 1 h at 80°C. Again, samples were dried under nitrogen and re-dissolved in 50-100 µL of hexane. Analyses were performed on an Agilent 6890N GC equipped with a Mass Selective Detector Model 5975 Inert using a DB-Wax UI (Agilent; 30 m × 0.25 mm ID × 0.25 mm film thickness) column. The following parameters were used: injection volume 1 µL in splitless mode (splitless time 1 min), helium flow 1.0 mL/min, full scan mode from 50–600 m/z. The initial oven temperature was set at 50°C, ramped at 5°C/min to 245°C, and held for 10 min. Data analysis was done with Mass Hunter Qualitative Analysis Workstation Software (Agilent, version B.07.00).

5.6 LysoTracker staining

The day before performing the staining experiment, cells were seeded at a density of $0.2x10^6$ cells/well on 24 mm cover glasses for microscopy in a 6-well plate aiming at scattered individual cells.

On the next day, cells were incubated with LysoTracker Deep Red (Invitrogen - Thermofischer, Karlsruhe, Germany; 1:10.000) and Hoechst 33342-Dye (Invitrogen - Thermofischer; 1:300 from a $5*10^{-4}$ M stock solution) in standard medium for 30 min at 37 °C. Prior to imaging, the medium was discarded and the cells were overlaid with colorless medium (without phenol-red). Glass coverslips were mounted and staged on an inverted microscope Axio Observer Z.1 (Carl Zeiss Microscopy GmbH, Jena Germany) equipped with a Fluar 40x/1.30 Oil M27 objective. Excitation wavelength was 622-655 nm for LysoTracker Red and 335-383 nm for Hoe33342 with emission light filtered at 665-715 nm and 420-470 nm, respectively. Images were acquired using Zen software (blue edition, 1.0.0.0, Carl Zeiss MicroImaging GmbH)

For analysis, single channel images were exported as .tif files. Further processing was done with ImageJ (2.0.0-rc-43/1.51j, National Institute of Health, USA), which provides sum of stained area per image. Spots from Hoe-staining represents nuclei and is used to normalize lysosomal staining.

5.7 Miscellaneous

Western Blot and qPCR were performed as described in the experimental section of Berger *et al.*[109].

(Intracellular) metabolite concentrations were normalized to total protein content determined using the FluoroProfile® Protein Quantification Kit (Sigma-Aldrich) according to manufacturer's instructions. Briefly, cell pellets and enzyme assay aliquots for protein determination were lysed in a sodium phosphate buffer (20 mM) with 1.2 % SDS. Samples were diluted in water when necessary. A calibration curve was generated using a BSA-standard solution (Sigma-Aldrich), which was diluted in water. The assay buffer was prepared from water, dye (FluoroProfile Fluorescent Reagent) and quantification buffer (25 % acetonitrile, 3 % SDS, 200 mM sodium

bicarbonate in water) (8:1:1). Later the dye was replaced by the fluorescent dye SERVA Purple (Serva, Heidelberg, Germany). Assay buffer and BSA-standard or (diluted) sample were mixed in equal amounts in a black 96-well plate (Greiner, Frickenhausen, Germany) and incubated for about 1.5 h. The assay is measured with a fluorimeter at an excitation wavelength of 485 nm and an emission wavelength of 600 nm.

5.8 Statistics

Basic statistics were performed with MS Excel 2013. ANOVA, as well as post hoc-tests (Tukey´s HSD, Dunnett) were performed with R (version 1.1.383). Plots were prepared with Excel; data represent means and error bars standard deviations, if not stated otherwise. Bland-Altman-plots were created (using Excel) by plotting differences between measurements against the mean of measurements. For differences, normal distribution was assumed when found to be within mean differences ± 1.96*SD.

For calculation of the K_m-value for D2HDH, OriginPro 8 was used (hill function; n=1 for a single substrate model). Plots showing enzyme kinetics are generated based on these calculations by OriginPro 8.

6 Quantitative analysis of 2-HG/-lactone

6.1 Development and validation of a quantitative LC-MS/MS method

A quantitative LC-MS/MS-method for 2-HG&-lactone analysis was established to confirm the finding of 2-HG-lactone in serum extracts of AML-patients carrying an *IDH1/2* mutation. In contrast to GC-MS analysis, entailing the risk of artefact detection from derivatization, LC-MS/MS benefits form a straightforward sample preparation, namely methanol precipitation. Quantification of 2-HG and 2-HG-lactone was achieved by running an LC-ESI-QqQ-MS method. Detection was performed in MRM mode using the following ion transitions: m/z 147.1 $[M - H]^-$ to m/z 84.8 for 2-HG, and m/z 150.1 to m/z 87.8 for 2-HG-D_3, as well as m/z 128 $[M - H]^-$ to m/z 84.8 for 2-HG-lactone and m/z 131 to m/z 87.8 for 2-HG-lactone-D_3. This analysis yielded two well resolved peaks, one each for 2-HG and its respective lactone (Figure 7). Chromatographic separation of the two compounds was found to be necessary, as 2-HG, due to the loss of H_2O during ionization, yielded a signal for the transition of 2-HG-lactone. But the two compounds could be distinguished readily based on their different retention times. However, this non-chiral method is not able to separate D- and L- enantiomers.

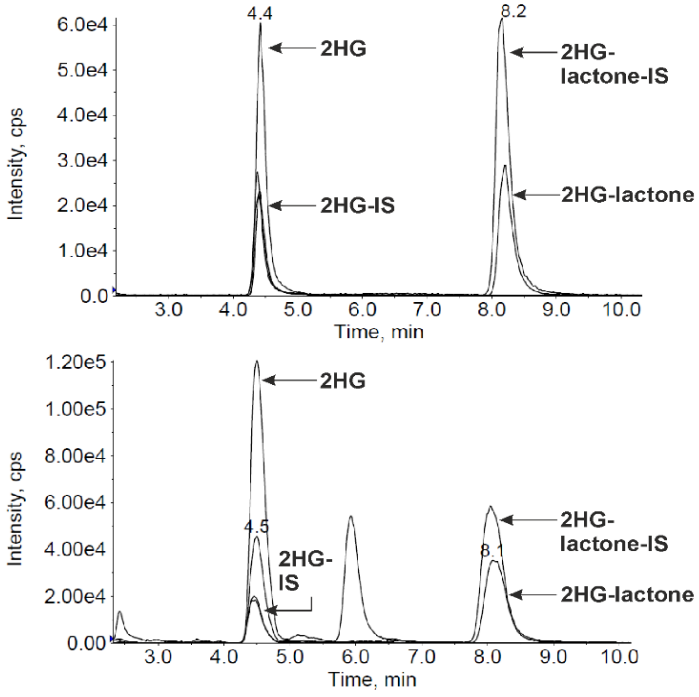

Figure 7. Representative chromatograms (EICs of 2-HG&-lactone) of a standard (upper panel) and serum sample of an AML patient with IDH(1-R132L) mutation (lower panel). 2-HG elutes at RT 4.4 min, 2-HG-lactone at RT 8.2 min. The peak at RT 6.0 min is due to an unidentified matrix compound.

Calibration curves were calculated from the area ratios of analyte and stable isotope labeled standard in pure standards, applying a 1/x-weighing. Internal standard solution consisted of [2,3,3]-D_3-2-HG (C/D/N Isotopes Inc.), which was incubated with HCl at 100°C for 30 min to form the 2-HG-lactone-D_3. This solution was evaporated to complete dryness and re-suspended in ddH_2O to yield a final concentration of 100 µM 2-HG-D_3 and 2-HG-lactone-D_3. Ten µL of this internal standard were added to the sample before precipitation, unless stated otherwise. Table 1 summarizes characteristic parameters established for this targeted LC-MS/MS analysis from pure standards in water and cell culture samples.

Table 1. Figures of merit for the LC-MS/MS method employed for quantification of 2-HG&-lactone. Mean accuracy was calculated from blank medium spiked with 2-HG in known concentration. Precision was calculated from repeated injections. Recovery represents relative amount of 2-HG contained in extracted samples (medium with and without FCS) in comparison to known concentration used for spike-in (three levels), that represent 100% recovery. (r=correlation coefficient for calibration curve). (This table is partially reproduced from Berger et al.[109])

	2-HG	**2-HG-lactone**
LOD (S/N>3)	< 0.05 µM	< 0.05 µM
LLOQ	0.2 µM	0.3 µM
ULOQ	900 µM	1000 µM
r	> 0.9988	> 0.9995
internal standard	D_3-2-HG	D_3-2-HG-lactone
Accuracy/precision from spike at 3 levels (n=5)		
0.5 µM	97.8 % ± 5.7	95.9 % ± 7.1
25 µM	100.8 % ± 1.5	103.2 % ± 3.2
500 µM	97.7 % ± 2.0	95.8 % ± 1.4
Recovery (n=6) from cell culture media +FCS, -FCS		
0.5 µM	101.8 %, 107.7 %	100.1 %, 110.8 %
25 µM	118.6 %, 125.5 %	110.8 %, 114.1 %
500 µM	111.9 %, 120.1 %	101.3 %, 114.4 %

Samples analyzed by means of this LC-MS/MS-method included extracts of serum, tissue and both cell pellets and supernatant. Figure 7 shows exemplary chromatograms of 2-HG/-lactone analysis in standard and AML-serum. For samples with an *IDH1/2* mutation background, the values were assumed to reflect the D-enantiomers. Some enantioselective test measurements with extracts from HCT116 and HT1080 cells confirmed this assumption (Supplemental Figure S1).

6.2 Enzymatic assay to measure degradation of D-2-HG

As mentioned earlier, D-2-HG produced in certain cancer cells carrying an *IDH1/2* mutation is accumulating to high levels and is therefore regarded as an oncometabolite. In contrast to 2-HG-aciduria, where the degrading enzyme *D2HGDH*, is mutated, it is supposed to be fully active in cells with *IDH1/2* mutation. However, it was never investigated on an experimental basis, whether this is really the case and how D2HDH activity might be regulated in response to elevated levels of its substrate. As part of this thesis, experimental evidence was collected on this issue and published in 2019 (Berger *et al*.[109]). This chapter summarizes the results of this study:

A cell-based assay was developed with concomitant 2-HG quantification by LC-MS/MS. The work-flow of the assay is explained in a schematic representation (Figure 8).

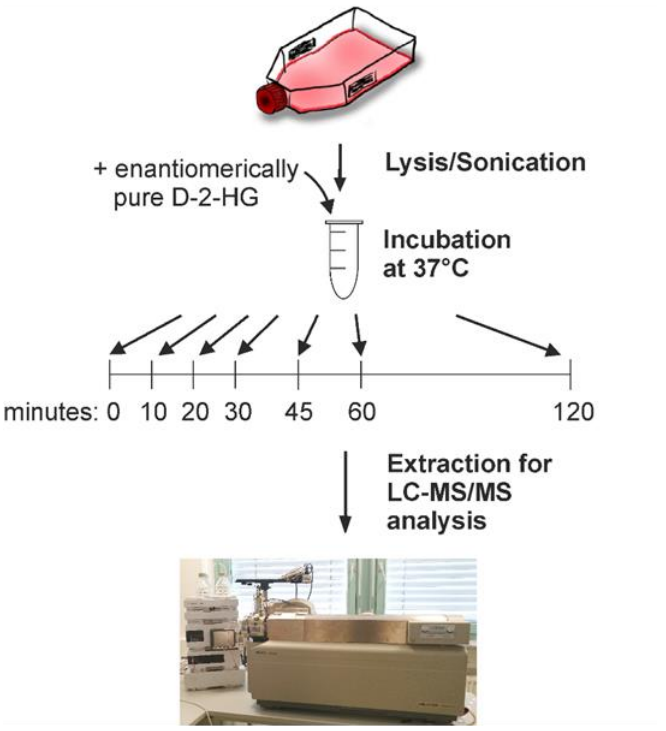

Figure 8. A cell-based enzyme assay was established to measure the rate of oxidation of D-2-HG to α-ketoglutarate by D2HDH. First, cells were sonicated in an assay buffer containing a redox reagent. Enantiomerically pure D-2-HG was added, as the LC-MS/MS method employed was not enantioselective. Then, lysate was incubated at 37°C with gentle shaking for up to several hours. Aliquots were taken repeatedly over this time period and enzymatic reaction was stopped by methanol precipitation. Aliquots were extracted and subjected to LC-MS/MS to determine 2-HG concentration.

For calculation of degradation rates, only values within the linear range were used. This assay was optimized regarding the assay buffer composition: FAD (flavin adenine dinucleotide), as the endogenous redox partner, was compared against other artificial redox agents, namely INT (iodonitrotetrazolium) and PMS (phenazine methosulfate). The latter showed the significant highest degradation rates and was therefore chosen to ensure maximal sensitivity. pH of the buffer was also investigated and found to be optimal at pH 7.6, which reflects mitochondrial pH, the compartment D2HDH is located to.

As explained earlier, in enzymatic assays it is also possible to follow the product of the enzymatic reaction under investigation. In the case of D-2-HG degradation, the product, α-ketoglutarate, was not a favorable analyte. With an established GC-EI-qMS method (see chapter 5.5.3) including also α-KG, it was not possible for assay aliquot to get values above the LLOQ. α-KG is a rather low abundant metabolite which is substrate to many enzymes. Activity of those enzymes, while performing the D-2-HG degradation assay, cannot be excluded, although co-factors etc. might be limiting as not supplied in surplus. With this in mind, it was assumed that D-2-HG, which in

humans - to the best of my knowledge - is only substrate to D2HDH, is the more reliable analyte. Furthermore, it was assumed, that after addition of D-2-HG in surplus to the cell lysate, degradation of total 2-HG equals to D-2-HG. A test measurement of assay aliquots from MCF7 cell homogenates using a chiral method (according to Gibson[79]) showed that this assumption is valid (Figure 9).

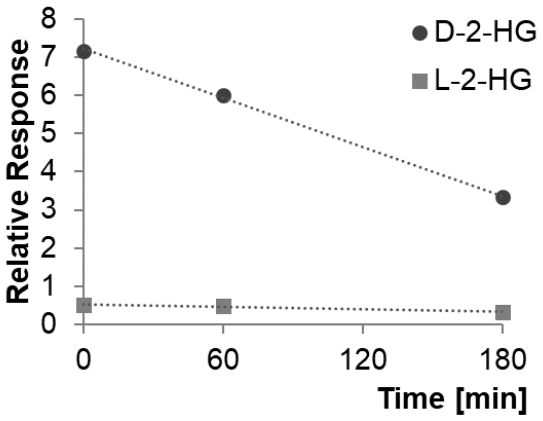

Figure 9. Enantioselective analysis of 2-HG degradation in aliquots of MCF7 homogenates. The assay was started by the addition of D-2-HG (>95% purity). Data points represent three pooled replicate aliquots. Degradation rate of D-2-HG agrees well with 2-HG data from LC-MS/MS analysis. Figure reproduced from Berger et al[109].

The assay was applied to lysates of MCF7 cells to determine the K_m-value. D2HDH in these cells has a K_m of 26.4 µM (standard error 1.65, R^2_{adj}=0.99718; n=3 per data point, two independent experiments; Figure 10), which is similar to published results from other mammalian cells[110,111], but different from *Arabidopsis thaliana* (~580 µM)[26]. Furthermore, this rather low K_m is in line with the suggestion that D2HDH is a metabolic repair enzyme, acting already at low substrate concentrations. We additionally found that other cell lines, like HT1080 cells, show different enzyme kinetics as v_{max} of those cells was lower compared to MCF7. This is especially interesting as HT1080 cells carry an IDH1-R132C mutation and therefore have elevated D-2-HG levels in comparison to WT-IDH1/2 cell like MCF7.

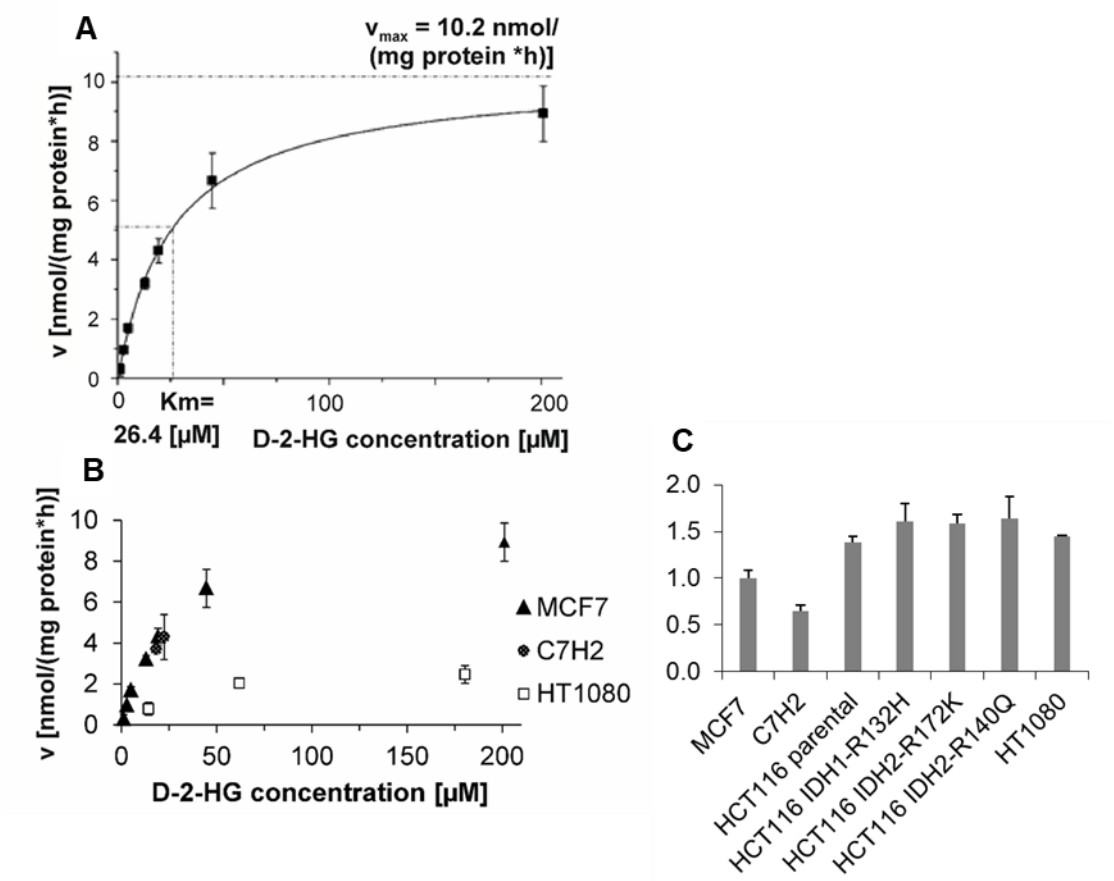

Figure 10. Analysis of D-2-HG degradation in several cell lines. ***A****) The described D2HDH-assay was applied to homogenates of MCF7 cells, and established a K_m-value of 26.4 µM D-2-HG.* ***B****) Degradation capacitiy was found to differ between cell lines tested, but this was not reflected in protein abundance of D2HDH as measured by Western Blot (****C****). Figure reproduced from Berger et al*[109]*.*

MCF7 cells were treated with 1 mM or 5 mM D-2-HG for both 24 h and 48 h, respectively, to check for D2HDH regulation in response to this treatment. However, significant differences between treated and untreated MCF7 cells neither in the enzyme assay, nor on protein or mRNA level of D2HDH expression could be observed (Figure 11). To investigate long-term effects of D-2-HG, we took cells from the HCT116 panel, comprising the parental HCT116 cell line with WT-IDH1/2 and cell lines with the following mutations: *IDH1-R132H/+*, *IDH2-R172K/+*, and *IDH2-R140Q /+.* These mutated cells produce endogenous D-2-HG and show similar levels to HT1080 cells. However, regulation of D2HDH activity and expression does not give a clear picture. For the enzyme assay, results show a high variance making a fit of the Michaelis-Menten-kinetic impossible. Protein expression in the HCT116 panel is found to be higher compared to MCF7 cells, but within the panel only HCT116 IDH2-R140Q is

significantly higher (ANOVA p=0.028, Tukey´s HSD parental vs IDH2-R140Q: p_{adj}=0.032). Together with data from several publications this hints at a more complex regulation of D2HDH on the protein level[31,46,112].

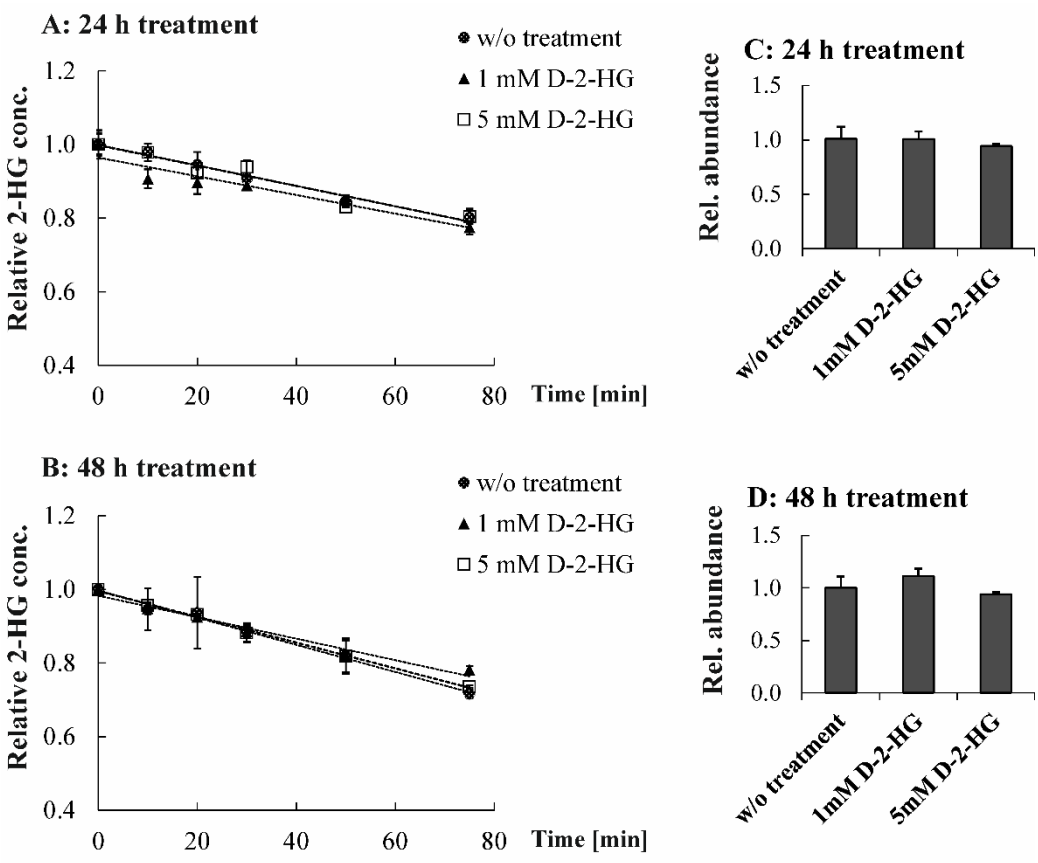

*Figure 11. MCF7 cells were treated with 1 mM and 5 mM D-2-HG for 24 h and 48 h (including a control without treatment). Comparison of D2HDH activities (**A&B**) did not show significant differences (24 h: ANOVA p=0.779; 48 h: ANOVA p=0.069). Protein abundance of D2HDH was measured by Western Blot (**C&D**) and did not uncover significant changes (24 h: ANOVA p=0.505; 48 h: ANOVA p=0.069). Figure reproduced from Berger et al[109].*

Finally, we compared D-2-HG degradation by D2HDH to production of D-2-HG by mutIDH1/2, both measured in cell homogenates from HCT116 cell panel. Buffer composition for mutIDH1/2 assay was adapted according to a protocol from the Pusch lab[8]. Both assays were run close to saturating substrate concentrations and after addition of the endogenous redox partner, which is FAD for D2HDH and NADPH for IDH1/2. Under these experimental conditions, which are supposed to reflect physiological conditions in mutIDH1/2 cancer cells, D-2-HG production clearly exceeded its degradation (Figure 12).

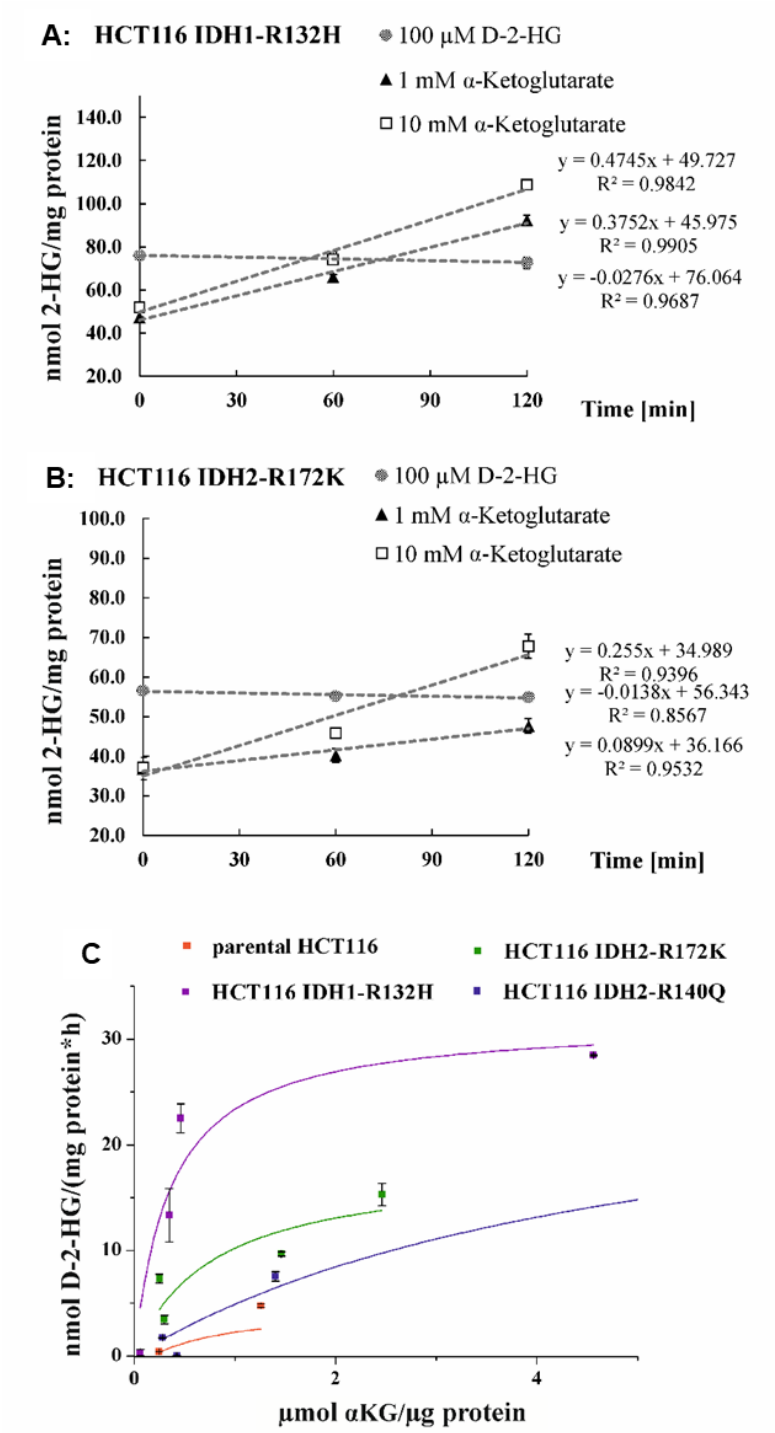

*Figure 12. Comparison of D-2-HG production by mutIDH1/2 (using 1 mM or 10 mM α-KG as substrate) with its degradation (100 µM) by D2HDH in HCT116 IDH1-R132H (**A**) and HCT116 IDH2-R172K cells (**B**). Both reactions run approximately at maximal velocity, but production clearly exceeds degradation. **C**) shows enzymatic 2-HG production capacity in cell homogenates reflecting 2-HG production by the HCT116 panel as observed under standard culture conditions. Figure reproduced from Berger et al[109].*

In conclusion, these data provide experimental evidence on the accumulation of D-2-HG in mutIDH1/2 cancer cells and tissue due to production exceeding degradation. Explanation of *in vivo* D-2-HG levels is more complicated because of additional events like distribution across other body fluids (especially in AML patients) and many factors apparently impacting on the regulation of D2HDH.

7 Strategies for chiral analysis of 2-HG/-lactone

For chiral analysis by hyphenated MS, two approaches could be considered given the equipment available at the Institute of Functional Genomics: one is using a chiral column, which can separate enantiomers because of different retention behavior. The other way is performing derivatization with specific reagents yielding diastereomers, which are no longer mirror images of each other and can be separated on standard columns due to different physicochemical properties.

Cyclodextrin-based columns resolve chiral compounds based on the formation of inclusion complexes and are commonly used for enantioselective chromatographic separation. Kaunzinger *et al*. (1996) used a beta-cyclodextrin column for the enantioselective analysis of 2-hydroxyglutaric acids in urine[113]. Similarly, the method, which led to the discovery of the novel metabolite 2-HG-lactone in our lab, was a GC-EI-qMS method using a cyclodextrin column (Rt-γDEXsa). Sample preparation here included a methyl chloroformate (MCF)-derivatization. In general, alkyl chloroformates are frequently used reagents for the derivatization of metabolites as the reaction is fast, takes place at room temperature and can be performed in aqueous solution. MCF converts amino groups into volatile carbamates and carboxylic groups (-COOH) of organic acids into esters. For 2-HG two derivatization products were observed (Figure 13, see also Figure 2, chapter 3.1).

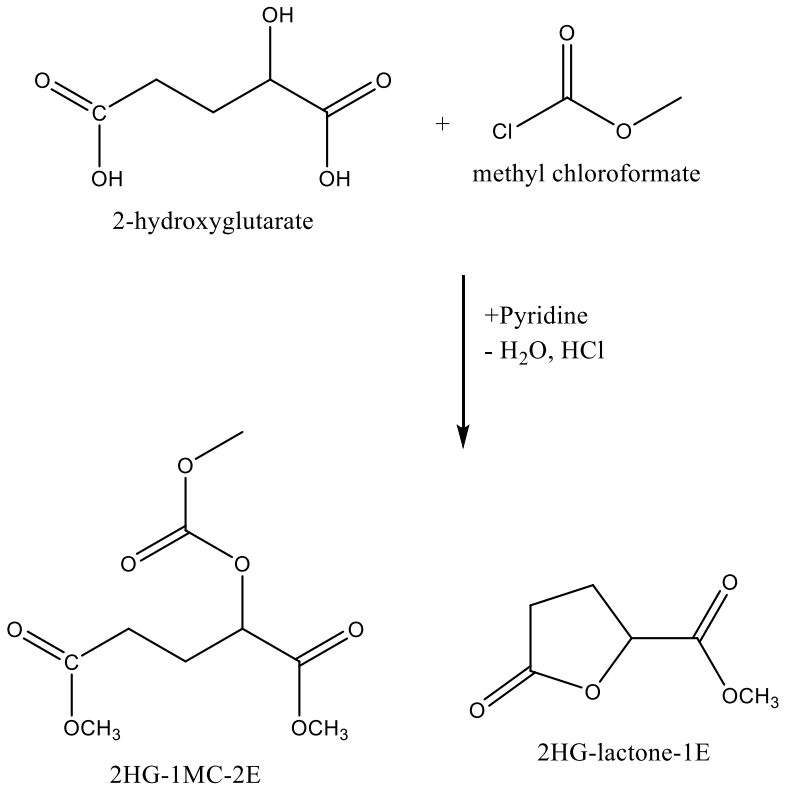

Figure 13. Reaction scheme for MCF derivatization of 2-hydroxyglutarate. Derivatization of 2-HG standards yielded two products: the ester of the 2-HG-lactone (2-HG-lactone-1E) as major product, but also the 3-fold derivative of 2-HG (2-HG-1MC-2E).
(MC, methoxycarbonyl group; E, methyl ester group.)

The observation, that ratios of the two derivatives are stable for standard samples, but not for serum samples (of AML patients with *IDH1/2* mutation) lead to the discovery of R-5-Oxo-2-tetrahydro-furancarboxylic acid (2-HG-lactone) as a novel metabolite (see also chapter 3.1, Figure 2). The formation of the one metabolite (2-HG-lactone) from the other metabolite (2-HG) during derivatization made this method redundant for simultaneous quantitative and enantioselective analysis of both metabolites. Nevertheless, a MS-method providing quantitative information on D- and L-2-HG and their corresponding lactones would be of great value to the analysis of biological samples.

A very frequent derivatization in GC-analysis is silylation using reagents like MSTFA (N-methyl-N-(trimethylsilyl)-trifluoroacetamide). Through silylation, acidic hydrogen atoms in functional groups, such as -COOH, -OH, -NH and -SH, are replaced with a trimethylsilyl (TMS) group. As silyl derivatives are prone to hydrolysis in the presence of traces of water, anhydrous conditions are obligatory. Silylation is often combined with methoximation for a two-step derivatization strategy (methoximation followed by silylation) to extend coverage of derivatized metabolites. Oximation reagents, such as hydroxylamines or alkoxyamines, react with aldehyde and keto groups under basic conditions. This derivatization reaction is preventing ring formation of reducing sugars or keto-enol-tautomerism. Nevertheless, for analysis of 2-HG/-lactone on a cyclodextrin column, this strategy cannot be applied. As mentioned above silylation takes place at -OH groups, which are present on the cyclodextrin stationary phase, as well. Derivatization reagents are added in surplus and do not react completely but to a certain percentage remain in the sample. Thus, injecting samples after silylation would change column affinity and shorten its lifetime. Additionally, it was noticed that the derivatization regimen of methoximation followed by silylation causes ring opening of 2-HG-lactone and can therefore not be used for the intended purpose. In chapter 8.1.1 it is described, how derivatization including silylation still can be used for analysis of 2-HG/-lactone.

To circumvent the need for an enantioselective cyclodextrin column, it is possible to alternatively produce diastereomers by derivatization with respective reagents. Interestingly, Weibel *et al.* (2000)[114] synthesized chiral silylation reagents for determination of absolute configuration by NMR spectroscopy. By using these reagents, separation of chiral analytes would be achievable on standard GC-columns.

However, synthesis of those chiral silylation reagents is quite laborious and they are not stable. Therefore, this approach is not feasible for rather small studies as needed here in the context of 2-HG-lactone in AML serum. Ding *et al.* (2018) described a GC-method for separation of lactic acid and 2-hydroxyglutaric acid enantiomers by chiral derivatization using L-menthol and acetyl chloride, combined with determination by MS[115]. Derivatization reagents here attack OH-groups, which is esterified in the lactone-form. Hence, this protocol is again not adaptable to 2-HG-lactone analysis.

In addition, I tried enantioselective derivatization according to Gibson (see also 4.3.3). S-2-butanol was used for esterification of carboxyl-groups followed by acetylation with acetic anhydride. Applying this protocol to 2-HG and –lactone standard samples, the diastereomers of 2-HG were separated after analysis on a DB-Wax UI column (coupled to an EI-qMS; Figure 14; method details see chapter 5.5.5). For 2-HG-lactone the chromatogram basically looked the same, with the major peak corresponding to the 2-HG-derivates. An additional, low abundant peak both, in 2-HG and –lactone standards, could be assigned to the 2-HG-lactone-derivative, but no separation of diastereomers was observed here (as described already by Duran *et al*. 1980[2]). These observations are the result of a transesterification reaction of the intramolecular ester of 2-HG (=2-HG-lactone) and 2-HG-butyl-esters (which are the major and desired reaction products). This in the end means, that the Gibson-protocol cannot be applied to chiral analysis of 2-HG/-lactone.

I also tried N-methyl-bis(trifluoroacetamide) (MBTFA) for derivatization. This reagent is used for acylation under mild, neutral conditions, instead of acetic anhydride, and would be combined with S-2-butanol for esterification. The milder conditions were expected to inhibit the formation of 2-HG-lactone from 2-HG (and vice versa). However, in practice, the method yielded poor derivatization efficiency and interconversion of the two metabolites.

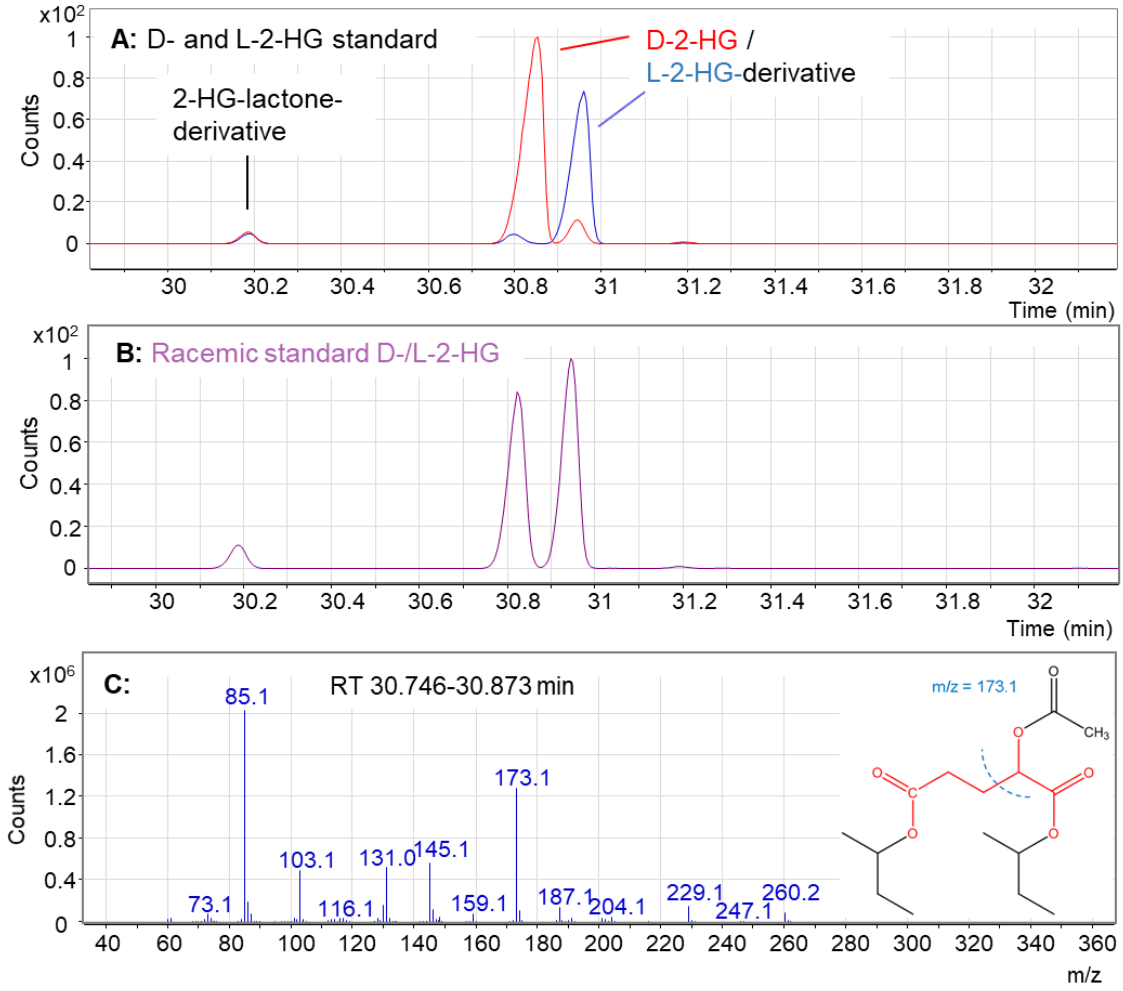

Figure 14. Separation of D-2-HG (red) and L-2-HG (blue) after derivatization with S-2-butanol and acetic anhydride. (TIC of ***A****= two separate standards,* ***B****= racemic standard). Derivatization gives rise to a derivative of 2-HG-lactone at RT~30.18 min, which is also of minor abundance for 2-HG-lactone standard samples (not shown).* ***C****) shows the mass spectrum of the 2-HG-derivative. Structure of 2-HG (core in red) after derivatization with S-2-butanol and acetic anhydride. The blue line indicates the most intense specific fragment, m/z 173.1.*

Similar to these approaches by GC-MS, it is possible to derivatize chiral analytes to form diastereomers for separation on non-chiral LC-columns. There are different reagents available and some of those already were used in analysis of 2-HG. As mentioned in chapter 4.3.3, Struys *et al.* used DATAN to produce diastereomers of 2-HG, which were analyzed on a C18 HPLC column[80]. Similarly, Cheng *et al.* (2015) formed diastereomers by TSPC (N-(p-toluenesulfonyl)-L-phenylalanyl chloride) labeling prior to LC-ESI-MS/MS analysis. This derivatization approach not only enables separation of D-/L-HG on a C18 HPLC column (VP-ODS, Shimadzu), but also offers enhanced sensitivity in comparison to DATAN derivatives[116]. Again, these

derivatization reagents attack the -OH of 2-HG, making them unsuitable for 2-HG-lactone analysis. Moreover, there are also reagent for derivatization of carboxyl groups, such as (S)(+)-1-(2-pyrrolidinylmethyl)-pyrrolidine (S-PMP). Tsutsui *et al.* (2012) used this reagent for chiral analysis of lactic acid and 3-hydroxybutyric acid by LC-ESI-MS/MS[117]. However, for derivatization (which is an esterification of the carboxyl group) of 2-HG-lactone transesterification is expected to occur as described before. Thus, it would not be possible to quantitatively discriminate 2-HG and –lactone derivatives.

Besides chiral GC-columns, there are also commercially available chiral LC-columns. But they are quite expensive. For instance, a Chirobiotic R column (glycopeptide antibiotic silica bonded column) was used for separation of 2-HG enantiomers in urine[118]. Here, LC was coupled to a Triple Quad MS run in MRM-mode. The method is reported to be sensitive and rapid, outperforming established chiral GC-methods with typically longer run times. Additionally, a chiral LC-column based on tert-butylcarbamoyl-quinine and –quinidine (QN-AX, QD-AX) has been reported for the separation of D- and L-2-HG. Here, LC is coupled to a Charged Aerosol Detection (CAD), although LC-conditions are stated to be MS-compatible. Resolution for the two enantiomers is about 2.0 for a 20 min run[119]. None of these methods included 2-HG-lactone. It might be worth trying whether a method separating D-/L-2-HG-lactone (and D-/L-2-HG in the same run) could be set up with such columns. Nevertheless, for this thesis such a column was not available and, therefore, it was not possible to perform these tests.

Finally, an enantioselective (and quantitative) analysis of D-/L-2-HG and D-/L-2-HG-lactone could not be established, although various methods were tested. Mainly interconversion of 2-HG and -lactone hampered this comprehensive investigation. Generally, chiral analysis can also be accomplished by further techniques, which were beyond the scope of this thesis. By interfacing an ion mobility cell to a mass spectrometer, a further dimension of separation is gained. Dwevedi *et al*. (2006)[120] introduced the concept of chiral IMS (ion mobility spectrometry), where ions are separated based on their stereospecific interaction with a chiral gas (e.g. S-2-butanol) which is mixed with the drift gas. Furthermore, for CE there are applications that are able to separate enantiomers[121,122]. In chiral-CZE (capillary zone electrophoresis) and MEKC (micellar electrokinetic chromatography), chiral selectors

(CS) such as cyclodextrines are mixed with the buffer used as mobile phase. The CS and chiral analytes interact in an enantioselective fashion resulting in specific mobility. The coupling of this separations to MS, however, is somewhat problematical as chiral selectors are often non-volatile. In CEC (capillary electrochromatography), the chiral selectors are immobilized on the column, overcoming the problems at the interface to MS. Disadvantages with this mode are low robustness and low peak capacity. Finally, it can be said that further possibilities for chiral analysis of 2-HG&-lactone exist but would require extensive and systematic tests.

8 Investigating metabolism in mutIDH1/2 cells by tracer analysis

To unravel the origin of the novel metabolite 2-HG-lactone, a tracer analysis was conducted. Metabolites, which are in high or even complete exchange and share the same carbon backbone, become apparent with matching MIDs. Beneath, labeling of metabolites with high exchange but different backbone can provide further information about metabolic changes in the respective system. Therefore, data on several metabolites generated by tracer analysis in the HCT116 panel (colon carcinoma) were collected and interpreted.

8.1.1 GC-APCI-TOF-MS for tracer analysis

Tracer analysis in this thesis was performed mainly using a GC-APCI-TOF-MS. The advantage in comparison to a GC-EI-qMS instrument is that APCI shows less or hardly any fragmentation. Because of extensive fragmentation EI-spectra are complex and

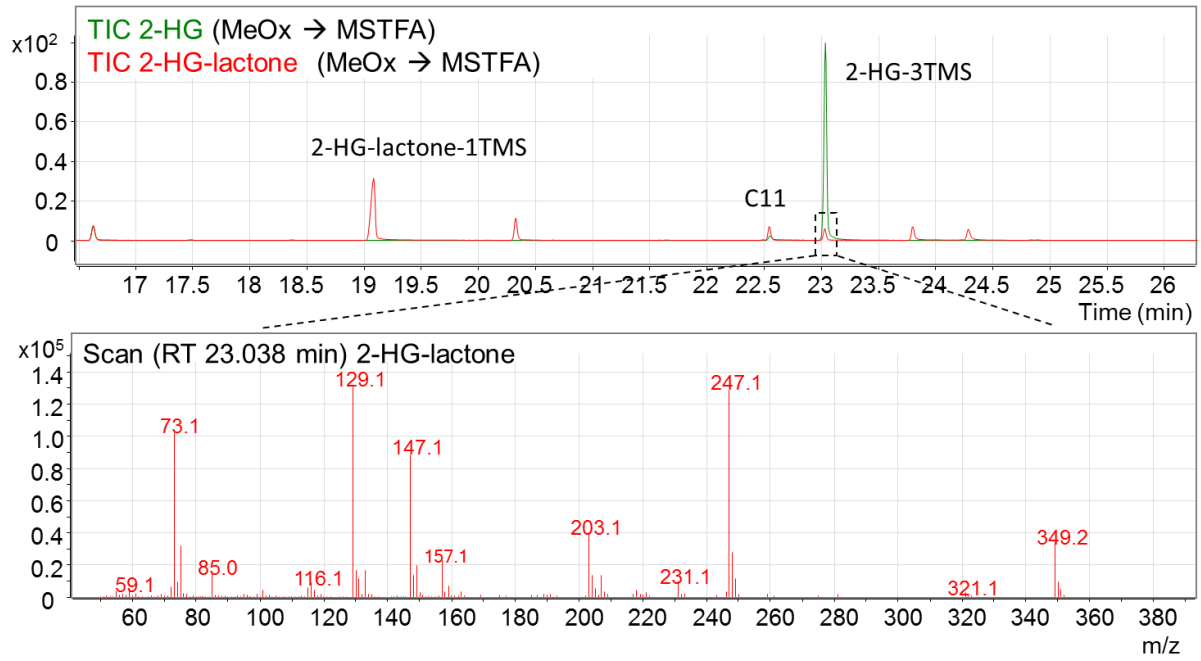

Figure 15: Derivatization, methoximation followed by silylation, of 2-HG and 2-HG-lactone standards. For 2-HG lactone (red) several peaks are detected: RT~19.05 min is the 1TMS-derivative, RT~23.05 min the 2-HG-3TMS formed by hydrolysis of the intramolecular ester of 2-HG-lactone. The lower panel shows the spectrum of the latter peak, which is equal to that of the 2-HG standard (see also Figure 17).

unique fragment ions for all compounds of interest have to be identified. Contrarily, for APCI, detection of the intact $[M+H]^+$-ion is possible, which facilitates interpretation and identification of labeling pattern. Additionally, the coupling to a TOF-analyzer provides high-resolution, resolving compounds and their isotopologues in full scan mode. In contrast, a Triple Quad instrument requires programming of transitions for all possible isotopologues, which can limit the number of compounds analyzed simultaneously.

From the previous chapter it can be seen, that (GC-)MS-analysis of 2-HG and -lactone is challenging because of frequent interconversion of the two metabolites. Nevertheless, analysis of samples from this tracing experiments by GC-APCI-TOF-MS requires derivatization. For the enantioselective GC-application, as described before, silylation was not compatible. Contrarily, GC-separation of labeled metabolites is achieved on a standard non-polar 5 % diphenyl-dimethyl-polysiloxane column (Restek, Rxi-5ms). Standard procedure for methoximation followed by silylation in our lab (see also chapter 5.4.2) was found to result in identical spectra for 2-HG&-lactone because of transesterification of the intramolecular ester in 2-HG-lactone during derivatization (Figure 15).

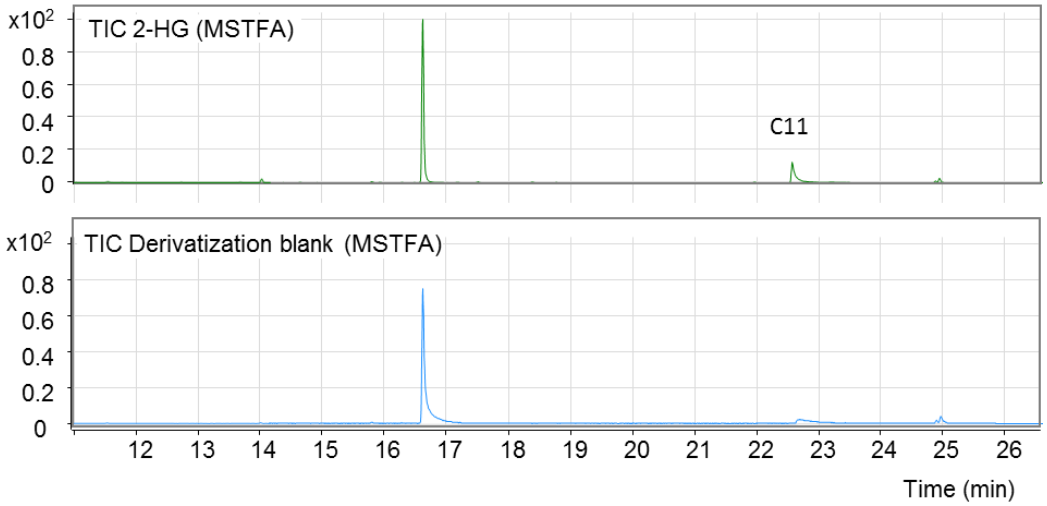

Figure 16. Silylation of 2-HG with MSTFA did not result in specific signals. The peak at ~16.5 min is also detected in a derivatization blank. The signal at ~22.5 min belongs to the derivative of the internal standard undecanoic acid (C11).

Silylation alone (incubation with MSTFA without addition of MeOx/pyridine) did not give intense signals, reaction efficiency was low (see Figure 16). But doing the reverse derivatization regime, starting with silylation followed by incubation with MeOx/pyridine worked out. Thus, obviously by addition of methoxylamine hydrochloride in pyridine

the reaction is facilitated. Pyridine is an acid scavenger and will drive the reaction forward by trapping the protons produced from the silylation reaction. Methoxylamine does not take over any function and could be left out. This derivatization produces a 3-fold TMS derivative for 2-HG and for 2-HG-lactone the 1-fold TMS derivative (Figure 17).

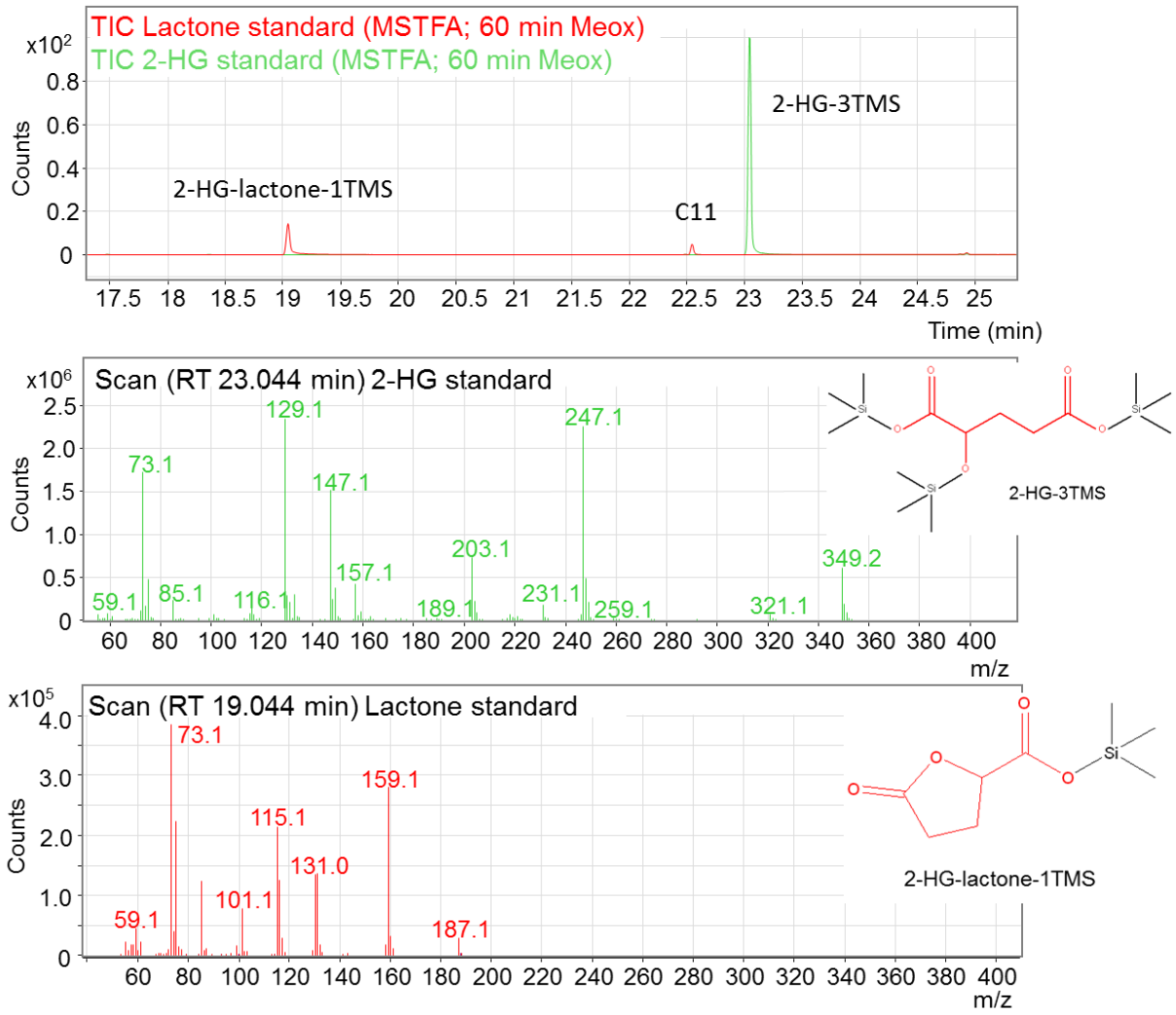

Figure 17. The upper panel shows a chromatogram of 2-HG (green) and -lactone (red) standards after silylation with MSTFA and further incubation with pyridine. The peak at ~23.05 min originates from the 2-HG-derivative. The corresponding spectrum is shown in the mid panel. The lower panel represents the spectrum of the 2-HG-lactone-derivative, which elutes at ~19.05 min. No side products for both 2-HG&-lactone(-derivatives) are detected.

In addition to 2-HG and -lactone, other metabolites, e.g. TCA intermediates could be detected. Table 2 lists *m/z*-values and retention times used for data extraction with Compass QuantAnalysis software (Bruker, version 2.2).

Table 2. Overview of compounds included in the tracer analysis by GC-APCI-TOF-MS analysis including m/z-values of the $[M+H]^+$-ion and retention times. The number of carbon atoms indicates mass shift of the fully labeled isotopologue.

Compound	**m/z for $[M+H]^+$**	**retention time [min]**	**Number of carbon atoms**
2-HG	365.1 (3TMS)	23.3	5
2-HG-lactone	203.1 (1TMS)	19.4	5
α-KG	363.1 (3TMS)	24.2	5
Succinate	263.1 (2TMS)	18.5	4
Fumarate	261.1 (2TMS)	19.2	4
Malate	351.2 (3TMS)	21.9	4
Citrate	481.2 (4TMS)	26.8	6

At the Institute of Functional Genomics there is an established method for LC-ESI-QqQ-MS analysis of organic acids. For analysis of labeling pattern, this analysis requires transitions for all possible isotopologues. For some analytes this even entails two transitions per isotopologue, when differentially labeled fragments are produced. On the other hand, this can provide structural information on which C-atom is labeled. Nevertheless, the new GC-APCI-TOF-MS method was expected to be more convenient including several analytes like organic acids, 2-HG &-lactone and further analytes amendable to silylation. A systematic evaluation of available analytes and sensitivity (especially in comparison to LC-ESI-QqQ-MS) was not feasible for time reasons. Yet, tracing data for TCA intermediates and 2-HG/-lactone from GC-APCI-TOF-MS and LC-ESI-QqQ-MS after correction for natural abundance were readily comparable (Figure 18). Bland-Altman plot for mean enrichment of TCA-intermediates do not show a systematic error across all metabolites and variances are within the acceptable range (average mean difference ± 1.96 SD, represented by the doted lines). Succinate shows the highest differences between the two measurements (~4.8%) which is probably due to its low abundance and peaks close to the LOD, where variation is expected to be higher. α-KG analysis by LC is also known to be difficult because of bad peak shapes. Therefore, GC-data are expected to be more reliable.

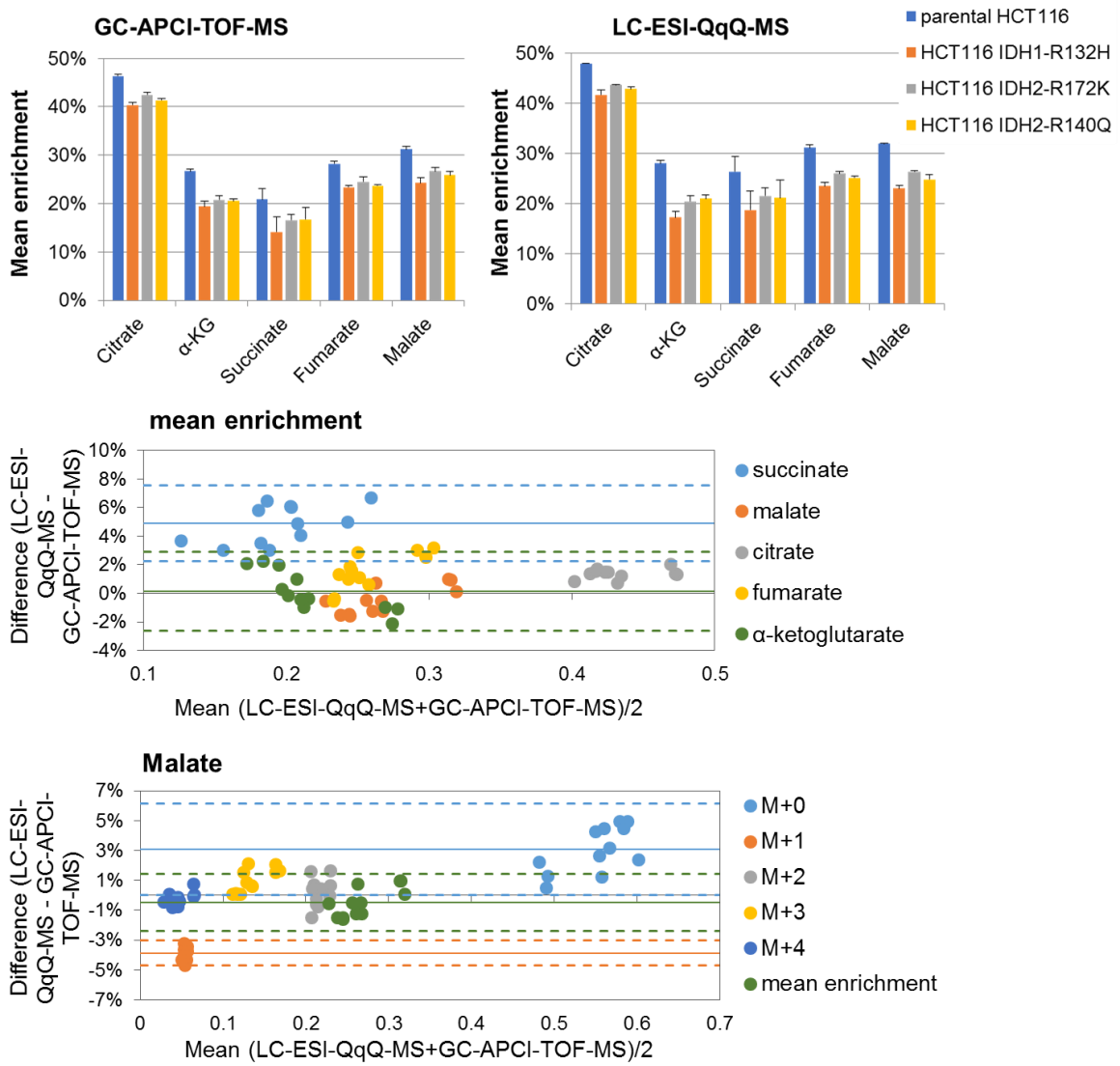

Figure 18. Method comparison for tracer analysis by GC-APCI-TOF-MS and LC-ESI-QqQ-MS. The upper panel shows mean enrichment for glucose tracing in the HCT116 panel calculated from data aquired by both, GC-APCI-TOF-MS and LC-ESI-QqQ-MS. Bland-Altman plots for mean enrichment of all metabolites shown in the upper panel and in the lower panel for malate isotopologues and mean enrichment (continous lines represent mean difference, dotted line mean difference ± 1.96 SD; shown for metabolites/ isotopologues with most pronounced differences).

Exemplary Bland-Altman plots for malate isotopologues (relative fractions) and mean enrichment reveal for M+0 and M+1 the most pronounced differences between the two approaches. M+0-fraction from LC-ESI-QqQ-MS is ~3% higher than from GC-APCI-TOF-MS, which results in an opposite difference for M+1 due to correction for natural abundance. The M+1 signal in the raw data can be attributed to either naturally labeled analytes or compounds labeled with one ^{13}C originating from the

tracer. The correction algorithm calculates and subtracts the natural fraction based on the M+0 signal, thus reducing the M+1 fraction in this case for the LC-ESI-QqQ-MS data. Nevertheless, mean enrichment does not show much difference and is used for comparisons in the following chapters. Comparisons across isotopologues of one metabolite are not calculated.

8.1.2 2-HG is the endogenous precursor of its lactone

2-HG and its lactone are closely related metabolites with 2-HG-lactone being the intramolecular ester of 2-HG. Therefore, it can be assumed that 2-HG was the endogenous precursor of 2-HG-lactone. A tracing experiment was conducted to test this hypothesis. $^{13}C_5$-glutamine is a frequently used tracer and is promising in this context. Glutamine is rapidly transformed via glutamate and α-KG into 2-HG (Figure 20) theoretically resulting in acceptable enrichment to corroborate the expected connection between 2-HG and its lactone.

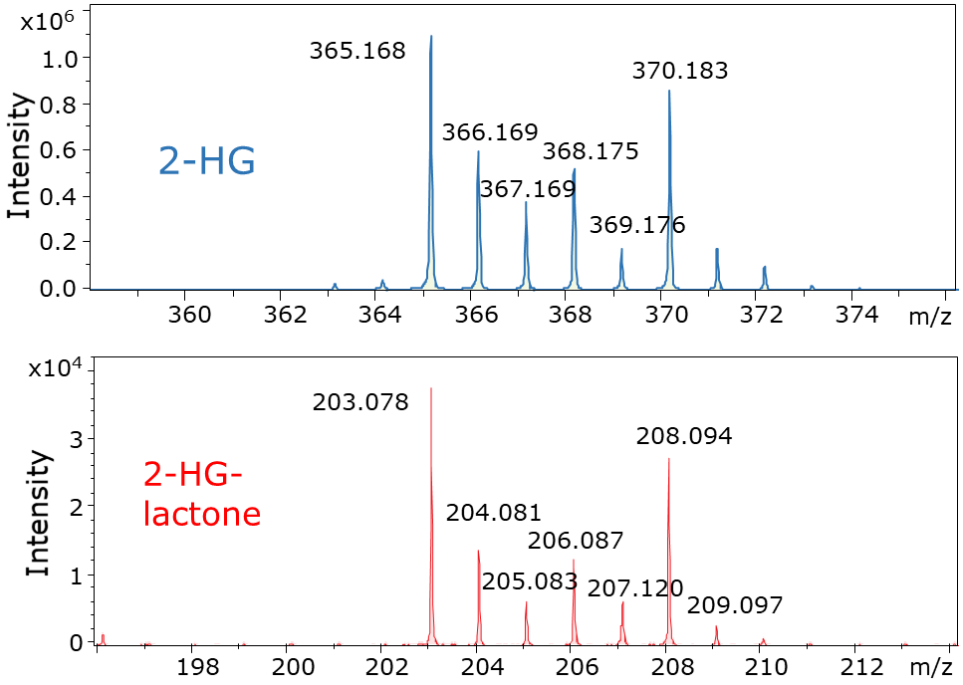

Figure 19. Labeling pattern of 2-HG (3-TMS-derivative, upper panel) and 2-HG-lactone (1-TMS-derivative, lower panel) from 13C5-glutamine tracing in HCT116 IDH1 R132H cells.

Figure 19 shows an exemplary spectrum of 2-HG and -lactone from this tracing experiment. The m/z-values 203.1 and 365.2 correspond to the respective $[M+H]^+$ and show the highest intensity. The m/z-values 208.1 and 370.2 represent the

corresponding M+5 isotopologues and derive from the production of 2-HG and -lactone from $^{13}C_5$-glutamine. Other isotopologues are products of converging pathways, some of which can be found in Figure 20. In summary, the labeling patterns of the two metabolites reveal a similar isotopologue distribution, indicating that indeed 2-HG-lactone is formed endogenously via intramolecular esterification of 2-HG. There are no hints that 2-HG-lactone is further metabolized other than by hydrolysis back to 2-HG.

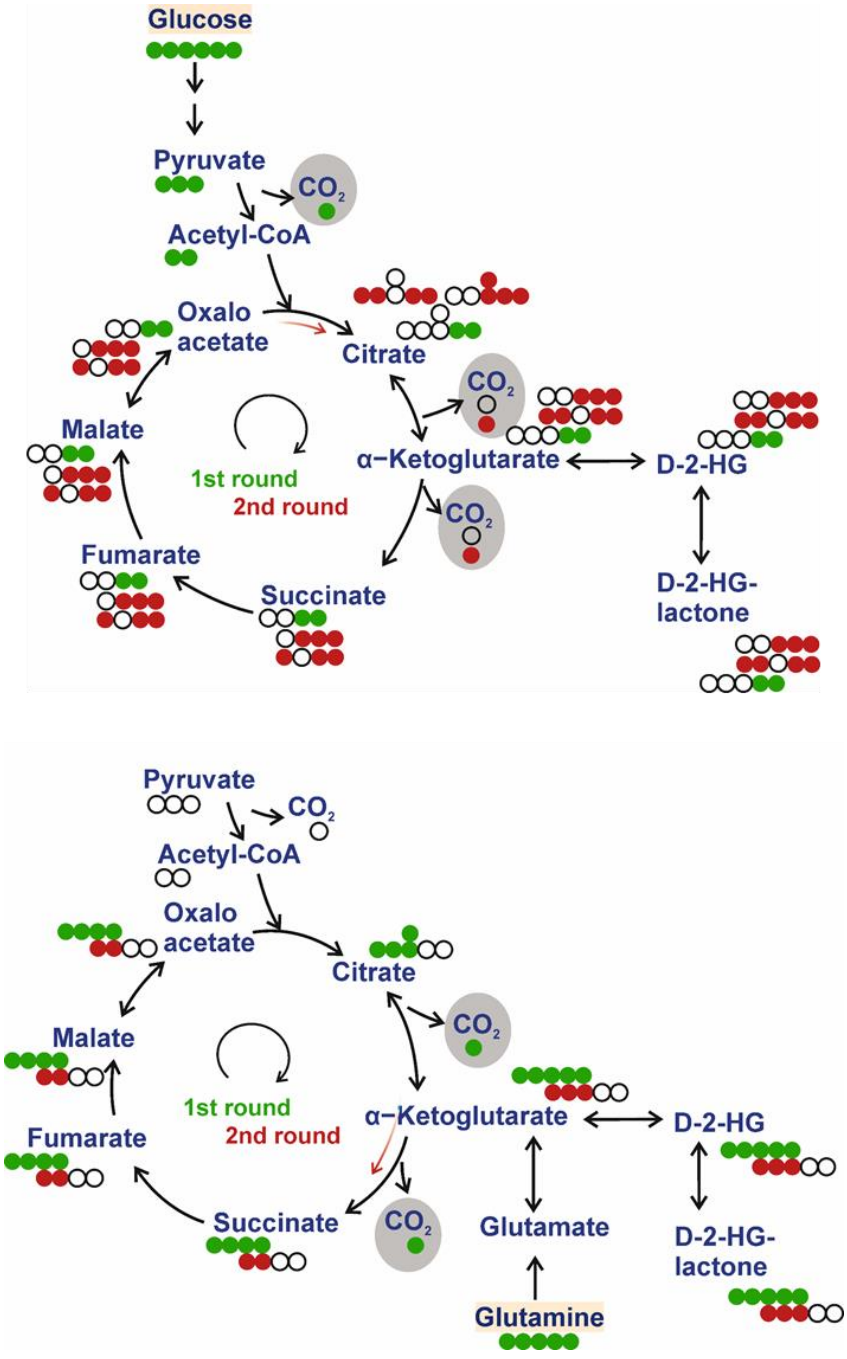

Figure 20. Schemes depicting the expected isotopologues for TCA intermediates from $^{13}C_6$-glucose (upper panel) and $^{13}C_5$-glutamine tracing (lower panel), respectively. Each circle represents a carbon atom. Green circles originate directly from the tracer and are produced within the first round of the TCA cycle. Red circles represent tracer carbons incorporated during a second round of the TCA cycle. For glucose, the TCA is replenished from pyruvate/ acetyl-CoA, for glutamine from α-KG, which is indicated by the red arrows.

8.1.3 Tracer analysis in HCT116 cell panel

By means of this tracer analysis, differences in cellular metabolism between cell lines of the HCT116 panel can be made visible. As mutIDH1/2 consumes an increased amount of α-KG, pathways for regeneration of α-KG might be upregulated. Furthermore, α-KG reduction by mutIDH1/2 is coupled to consumption of NADPH, which has to be regenerated to balance the cellular redox status. There are several enzymes which can produce NADPH, including WT-IDH1/2. Therefore, cells with mutation in *IDH1/2* are affected twice with reduced production of NADPH while consumption is increased. Metabolic adaptation might differ between *mutIDH1* and *mutIDH2* cells due of the different localization of IDH1 and IDH2 to the cytosol and mitochondrion, respectively. For mitochondria, α-KG concentration is higher than in the cytosol[123] and re-generation of the α-KG pool is expected to be higher due to the TCA cylce e.g. flux through IDH3. The fact that IDH2 is located in the mitochondrion is responsible for its independency on WT-IDH2 activity, in contrast to mutIDH1, which is dependent on WT-IDH1 for α-KG supply[13].

For this thesis, two different tracers were used, $^{13}C_5$-glutamine (48 h of incubation) and $^{13}C_6$-glucose (24 h of incubation), which reveal a comparable mean isotopic enrichment in most of the TCA intermediates under these conditions. However, it has to be noted that maximal enrichment as a function of isotopic steady state was not tested systematically. Therefore, fractional contributions of glucose and glutamine cannot be compared directly and do not sum up to 100%. Mean enrichment might be increased by longer cultivation times. In addition, in glutamine tracing experiments, there was still FCS in the medium, contributing low amounts of unlabeled L-glutamine slightly diluting $^{13}C_5$-glutamine. Thus, in these experiments enrichment form glutamine is always underestimated.

Interestingly, the two cell lines with the highest 2-HG levels, HCT116 IDH1-R132H and -IDH2-R172K, show a higher mean isotopic enrichment in all TCA intermediates upon incubation with $^{13}C_5$-glutamine compared to parental HCT116 and -IDH2-R140Q (Figure 21). Consequently, it can be concluded that the TCA cycle is replenished by glutaminolysis to compensate for the high α-KG demand. This is further supported by MIDs from glutamate, α-KG and 2-HG representing labeling from $^{13}C_5$-glutamine (Figure 23), as well as higher mean enrichment in amino acids which can be formed from glutamine via the TCA cycle, e.g. Asp (Figure 22). Especially, M+5 of glutamate,

α-KG and 2-HG agree quite perfectly for mutIDH1/2 cells (statistics see Supplemental Table S 5).

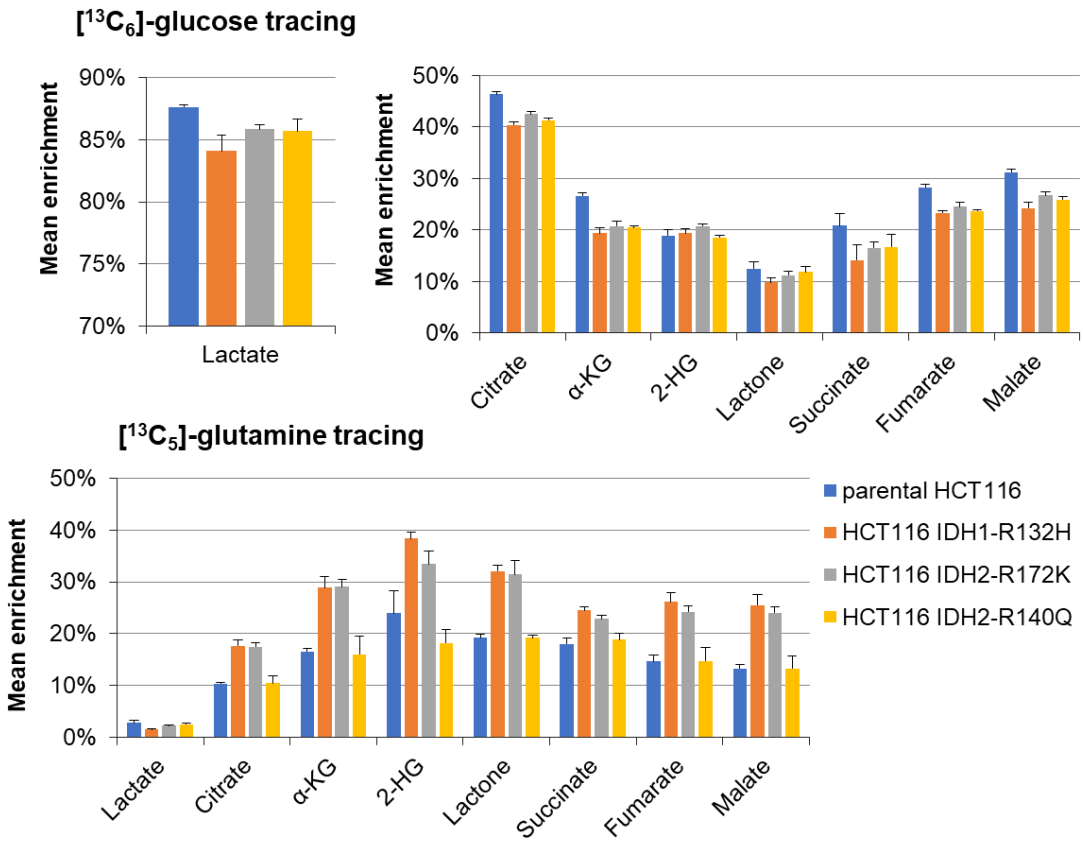

Figure 21. Mean isotopic enrichment in lactate, TCA intermediates and 2-HG/-lactone from $^{13}C_6$-glucose (upper panels) and $^{13}C_5$-glutamine (lower panel). Labeling in lactate from glucose is not significantly different (ANOVA p= 0.891), for TCA intermediates differences are significant. For further statistics see Supplemental Table S 1 and Supplemental Table S 2.

Notably, the parental HCT116 cell line, which does not have to compensate for increased α-KG consumption, shows the highest mean enrichment from $^{13}C_6$-glucose in all TCA intermediates and other products which (can) contain carbon from glucose (e.g. Ala, Ser, Asp, Glu; Figure 21 and Figure 22). For HCT116 IDH1-R132H and -IDH2-R172K, higher glutaminolysis was already detected, which ends up with lower mean enrichment in $^{13}C_6$-glucose tracing. HCT116 IDH2-R140Q exhibit a lower 2-HG production than the other two mutant cell lines, but still are supposed to have a higher α-KG demand than the parental line. Nevertheless, this cell line shows lower enrichment for both, glucose and glutamine. This could be explained by further substrates used for replenishment of TCA cycle. For instance, it is known that other (unlabeled) substrates, like amino acids (α-KG anaplerosis via His, Pro, Arg[124,125],

Asp/Asn-conversion into oxaloacetate[126]) and acetyl-CoA derived from fatty acid oxidation can refuel the TCA cycle for simultaneous energy production and supply of carbon backbones for biomass production. Contradictory is the labeling in amino acids like Asn, Ala and Ser from both tracers, which is not lower for HCT116 IDH2-R140Q, but for HCT116 IDH1-R132H.

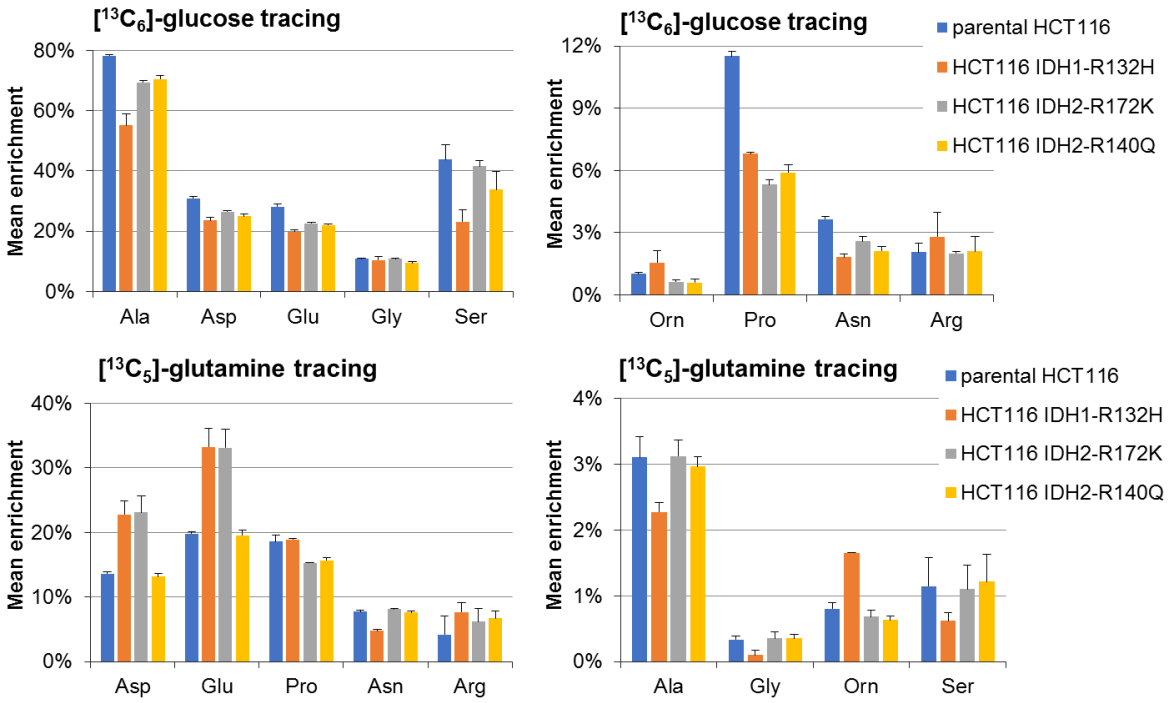

Figure 22. Mean isotopic enrichment in amino acids from $^{13}C_6$-glucose (upper panels) and $^{13}C_5$-glutamine (lower panels). For further statistics, see Supplemental Table S 3 and Supplemental Table S 4.

Lower mean enrichment from $^{13}C_6$-glucose in TCA intermediates does not reveal a lower glycolytic flux in *mutIDH1/2* cells. TCA anaplerosis from amino acids allows to forward glycolytic products to other pathways than TCA cycle, e.g. glucose-6-phosphate into pentose phosphate pathway (PPP) and acetyl-CoA into fatty acid synthesis. Especially PPP might be important in *mutIDH1* cell, as it is the major source for cytosolic NADPH production[127]. Further measurements of the labeling pattern in the respective metabolites (e.g. ribose-5-phosphate, fatty acids) could clarify this issue.

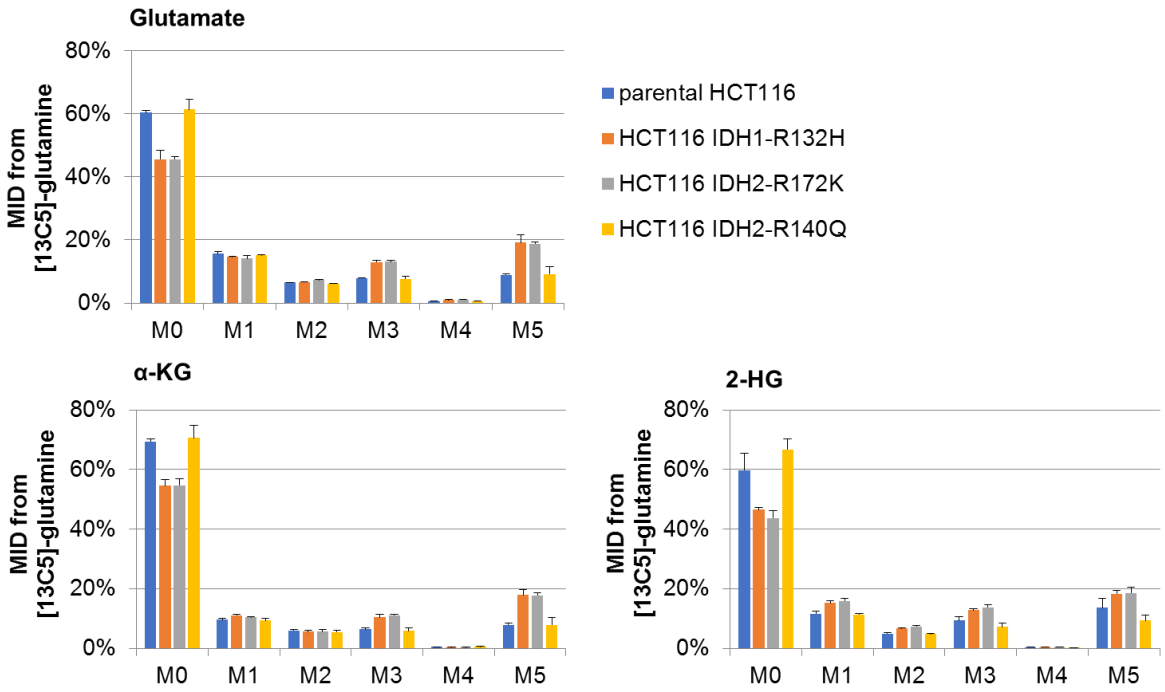

Figure 23. MIDs from $^{13}C_5$-glutamine tracing of glutamate, α-KG and 2-HG. The highly similar labeling patterns indicate a high exchange between glutamate, α-KG and 2-HG. M+5 isotopologues (as direct products of $^{13}C_5$-glutamine) are only significantly different in HCT116 IDH2-R140Q, ANOVA p= 0.0161(further statistics see Supplemental Table S 5).

The TCA cycle can also be replenished via pyruvate carboxylase (PC) activity. Thereby, pyruvate from glycolysis is metabolized to oxaloacetate, which can run the TCA in the reverse direction into malate and fumarate yielding M+3 isotopologues[128,129]. In the data from $^{13}C_6$-glucose tracing in the HCT116 panel, M+3 for fumarate and malate is higher than succinate M+3 indicating that pyruvate carboxylase is active (Figure 21, statistics see Supplemental Table S 9). This was already described for both, parental and HCT116-IDH1-R132H cells, and therefore might not be activated merely to compensate for 2-HG production. Contrarily, for astrocytes it was described that PC-flux is increased with *mutIDH1/2* to maintain TCA activity[130].

For HCT116 IDH1-R132H cells, it has to be noted that labeling after incubation with $^{13}C_6$-glucose in alanine and serine differ from all other cell lines (also for $^{13}C_5$-glutamine tracing, however, at a much lower level). These two metabolites are products of glycolysis and alanine is supposed to reflect mitochondrial pyruvate[97,131]. Contrarily, lactate reflects cytosolic pyruvate, but differences here in mean enrichment within the HCT116 cell panel are not significant. The reaction from pyruvate to alanine in

mitochondria is catalyzed by ALT2, which removes an amino-group form glutamate giving rise to α-KG. Especially in *mutIDH2* cells, this represents another possibility to fuel α-KG into 2-HG production. However, in *mutIDH1* cells with increased cytosolic α-KG consumption this obviously is regulated differently. Serine can be produced from glucose via D-3-phosphoglycerate dehydrogenase and degraded into pyruvate and similarly to alanine shows a lower M+3 and mean enrichment for HCT116 IDH1-R132H cells (statistics see Supplemental Table S 3 and Supplemental Table S 7). In contrast to other metabolites with contribution from glucose, this *mutIDH1* cell line is not only lower than the parental line, but also lower than the two *mutIDH2* cell lines. This is a trend, which can be observed in further metabolites, but is the most evident (~20% lower than parental) for serine and alanine.

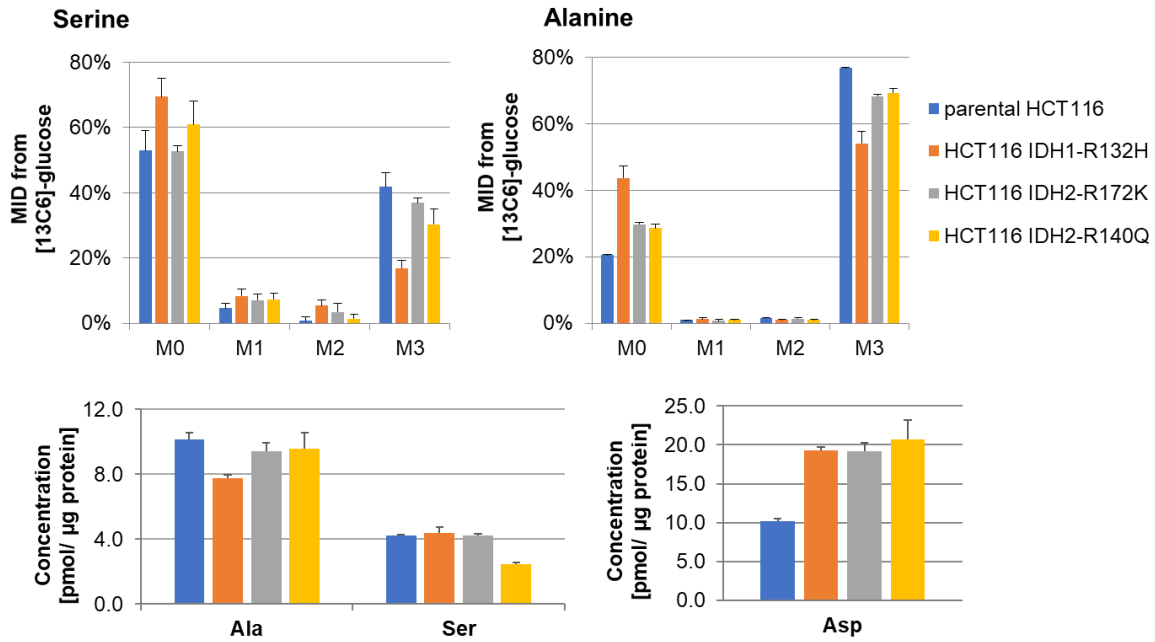

*Figure 24. MIDs for alanine (mean enrichment ANOVA p=3.59*10-6) and serine (ANOVA p=3.86*10-5) from $^{13}C_6$-glucose. Absolute concentrations of selected amino acids in cell extracts: alanine (ANOVA p= 4.10*10-3), serine (ANOVA, p= 3.86*10-5) and aspartate (ANOVA p=5.15*10-5); For further statistics see Supplemental Table S 6 and intracellular amino acids see Supplemental Figure S2*.

8.1.4 Mutant IDH1/2-related effects on cellular metabolism

The described data on labeling pattern from culturing cells with $^{13}C_5$-glutamine and $^{13}C_6$-glucose can be combined with quantitative data to interpret changes in context of mutations in *IDH1/2*. For details about acquisition of quantitative data see chapter 6.5.2 and 6.5.3.

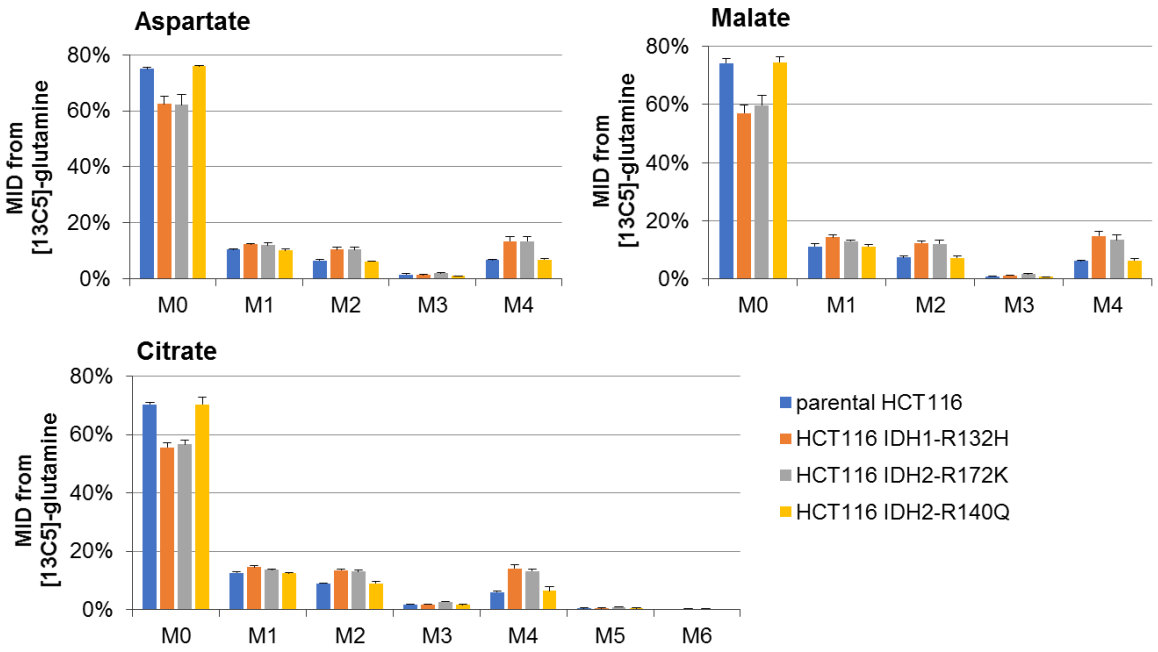

Figure 25. MIDs of aspartate, malate and citrate from $^{13}C_5$-glutamine. Aspartate aminotransferase produces aspartate from malate, which causes matching labeling pattern. Reductive carboxylation generates citrate M+5 from $^{13}C_5$-glutamine and hereinafter malate M+3, which is hardly observable, here. Thus, this pathway is not active.

Glutaminolysis in *mutIDH1/2* cells to enable 2-HG production was already described in several reports[132-134]. Accordingly, glutamate dehydrogenase (*GLUD*; for direct conversion of glutamate into α-KG) is upregulated in certain cancers including *mutIDH1* glioma[135]. Besides, α-KG can be produced by aspartate aminotransferase (AAT; *GOT1* cytosolic, *GOT2* mitochondrial) using oxaloacetate and glutamate. By-product of this reaction is aspartate, which was found elevated in cell extracts of all *mutIDH1/2* cell lines in comparison to the parental HCT116 (Figure 24). As oxaloacetate used by AAT is formed from malate in the TCA cycle and rapidly converted into aspartate, the latter has a similar labeling pattern to malate (Figure 25).

As mentioned before, the TCA can be replenished from other amino acids taken up from the environment, in this case cell culture medium. Remarkably, parental HCT116

cells tends to take up lower amounts of certain amino acids or even release more than the *mutIDH1/2* cell lines (Figure 26, intracellular levels see Supplemental Figure S 2). The HCT116 IDH1-R132H clone shows the highest uptake and the lowest release, respectively. (High variances from calculating uptake/release make most differences not significant.) Increased uptake of amino acids for anaplerosis could be seen in mean enrichment of all downstream metabolites, as it dilutes the labeling from the main carbon sources, glucose and glutamine, in the respective tracing experiment. The most striking difference in mean enrichment and labeling pattern within the HCT116 panel was detected for alanine and serine. Thus, these two metabolites are apparently produced from sources other than glucose and glutamine in HCT116 IDH1-R132H cells. This might be a compartment specific effect, as this cell line is the only one with increased cytosolic α-KG demand and significantly decreased intracellular alanine levels (Figure 24). Serine is found at a lower concentration in HCT116 IDH2-R140Q cells. Generally, this amino acid is associated with purine synthesis and cytosolic redox balance. Still, the available data do not give a clear picture. For instance, it could not be unraveled, which alternative precursors were used for alanine and serine synthesis by using further tracers.

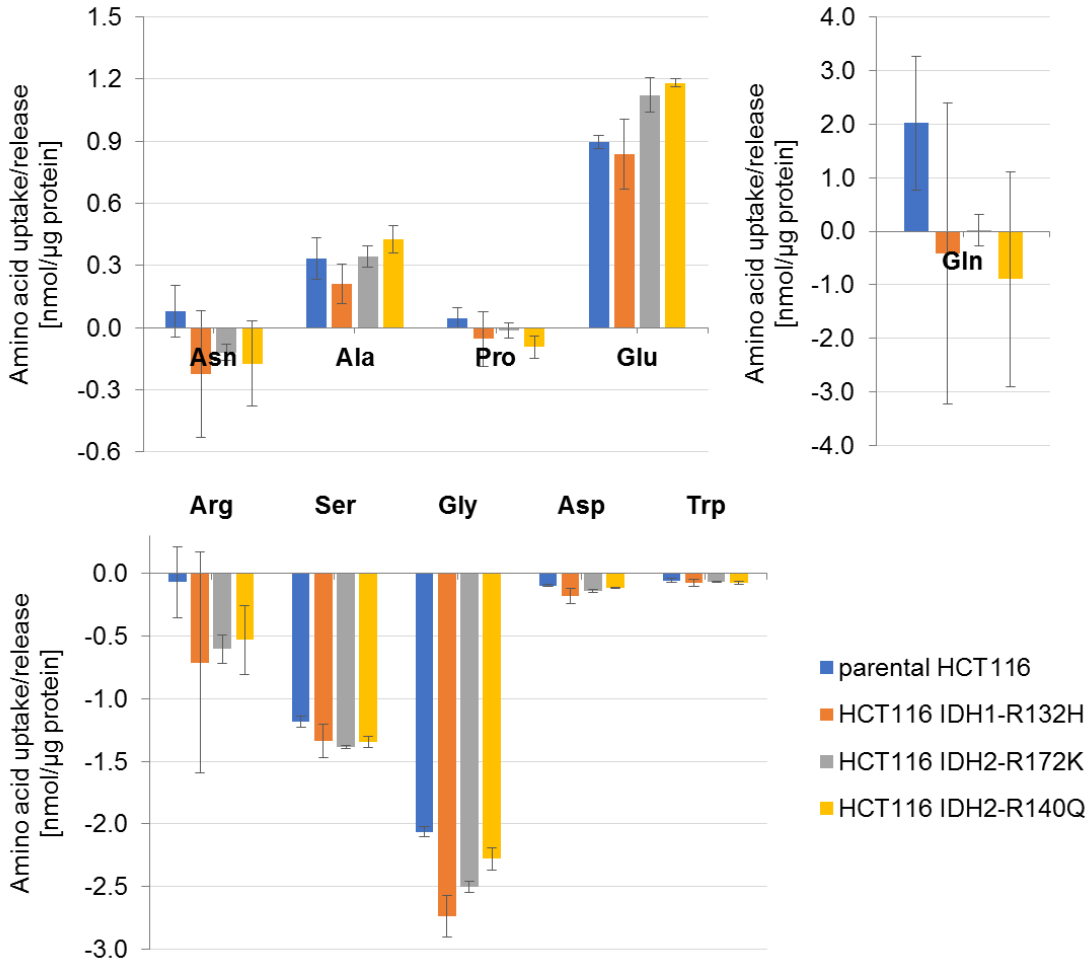

Figure 26. Uptake and release of selected amino acids (medium incubated with cells subtracted with blank medium, and normalized to cellular protein content). Significant differences were detected for glycine (ANOVA p=0.0087, Tukey´s HSD parental vs. IDH1-R132H $p_{adj}=1.55*10^{-4}$, parental vs. IDH2-R172K $p_{adj}=2.97*10^{-3}$, IDH1-R132H vs IDH2-R140Q $p_{adj}=2.17*10^{-3}$) and serine (ANOVA p=0.0407, Tukey´s HSD parental vs. IDH2-R172K $p_{adj}=3.8*10^{-2}$).

Regarding the adaptation to increased NADPH consumption by mutIDH1/2, the here presented data only provide minor information. Labeling from $^{13}C_6$-glucose was found to be altered in all mutated HCT116 cell lines relative to the WT-cells. Using a different approach, Gelman *et al.* (2018) found increased glucose uptake and PPP-flux in HCT116 IDH1R132H cells compared to their wild-type counterpart[136]. This was deemed necessary to maintain lipogenesis, which requires NAPDH[137]. At the same time, uptake of palmitate from medium in *mutIDH1* cells was observed and growth in delipidated medium was limited. Further, Molenaar *et al.* (2015) found decreased $NADP^+$-dependent IDH activity in HCT116 IDH1-R132H cells in comparison to *WT-IDH1/2* cells[138]. Similarly, NADPH production capacity was found to be reduced in

IDH1-R132H glioblastoma[139]. In contrast, in other tissues/cells, like in myeloid cells, PPP is responsible for most of the NADPH production capacity[140]. Besides, GLUD activity (see above glutaminolysis) for conversion of glutamate into α-KG uses $NADP^+$ as cofactor, therefore producing NADPH while refueling the TCA. Additionally, *mutIDH1* glioma cells can upregulate mitochondrial proline production from glutamine to maintain redox homeostasis[141]. However, labeling in proline in the here presented data does not support this finding for HCT116 cells.

Maintaining fatty acid synthesis is critical to *mutIDH1/2* cells. As mentioned above, lipogenic NADPH is increasingly produced by PPP and uptake of palmitate is essential for growth. Furthermore, it was shown that *mutIDH1* cells exploit additional exogenous carbon sources such as acetate (if supplied with the medium) to produce acetyl-CoA for fatty acid synthesis[136]. Contrarily, cells with WT-IDH1/2 use (cytosolic) acetyl-CoA originating from mitochondrial citrate/TCA. Contribution of glutamine to fatty acid synthesis requires intact IDH1 activity and reductive carboxylation to derive citrate from glutamine. Reductive carboxylation is revealed by the formation of citrate M+5 upon feeding cells with $^{13}C_5$-glutamine. In the cytosol, citrate (M+5) can be further converted to malate (M+3), which is also indicative of reductive glutamine metabolism[142,143]. Neither citrate M+5 nor malate M+3 were observed in the HCT116 panel (Figure 25). Nevertheless, reductive glutaminolysis is rather active (in HCT116 cells) under hypoxic conditions[133], when oxidative TCA flux needs to be down-regulated. Likewise, Badur *et al.* (2018) showed that *mutIDH1* cells (HT1080), compared to *WT-IDH1* cells, convert less glutamine to citrate/acetyl-CoA, while uptake of glutamine was increased[137]. Accordingly, glucose contribution to lipogenic acetyl-CoA in HT1080 cells is increased. If this is indeed the case for the HCT116 panel, this might be confirmed by measuring isotopic enrichment from $^{13}C_6$-glucose and $^{13}C_5$-glutamine, respectively, in fatty acids/palmitate. However, this was beyond the scope of the present study.

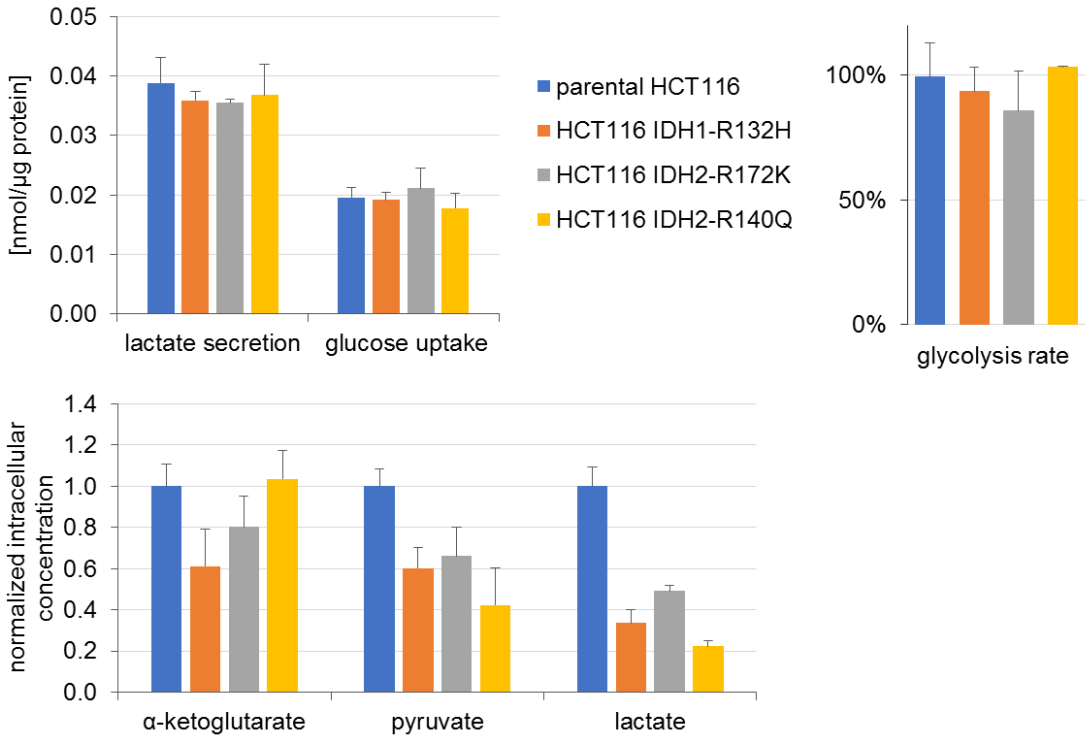

Figure 27. Glycolysis and TCA in HCT116: Lactate secretion is lactate concentration in the supernatant minus the backgound signal detected in blank medium, normalized to cell protein content; glucose uptake is calculated likewise (lactate secretion ANOVA p=0.662, glucose uptake ANOVA p=0.557; n=2-3). Intracellular α-KG, pyruvate and lactate (normalized to parental HCT116; ANOVA: α-KG $p=3.0*10^{-4}$, pyruvte $p=4.83*10^{-6}$, lactate $p=7.62*10^{-6}$; n=5-6). Glycolysis rate is the percentage of one molecule glucose being converted into two molecules of lactate (ANOVA p=0.479). For further statistics see Supplemental Table S 8.

Moreover, reduced glycolysis and lactate production in *mutIDH1* glioma was reported[144]. In accordance, LDHA (L-lactate dehydrogenase A catalyzing pyruvate conversion to lactate) and MCT1&4, responsible for lactate export, were found to be downregulated[145,146]. Similar results were presented by Mustafa *et al*. (2014), with overexpression of LDHA in glioma without *IDH1* mutation and overexpression of LDHB (L-lactate dehydrogenase B) in *mutIDH1* glioma to increasingly feed pyruvate into the TCA (see also Kurshed *et al*. 2017)[135,144]. For this thesis, neither lactate secretion nor glycolysis rate differed significantly between parental and *mutIDH1/2* HCT116 cells (Figure 27). Glycolysis rate was calculated as percentage of one molecule glucose being converted into two molecules of lactate. Thus, increased PPP-flux towards ribose-5-phosphate for nucleotide synthesis (as an alternative way to use glucose not ending in lactate) would result in an altered glycolysis rate. Furthermore, enrichment

in lactate is not significantly different within the HCT116 panel (ANOVA p=0.891; Figure 21). Consequently, the data presented here, do not indicate changes in the way glucose is consumed and the amount lactate is produced within the HCT116 cell panel. Further insights could be provided by measurements of PPP-metabolites and from additional experiments using 1,2-$^{13}C_2$-glucose as tracer. Additionally, discrepancies between our finding of unaltered glucose uptake (see also Grassian *et a*l. 2014[133]) in parental HCT116 cells vs ~IDH1-R132H and increased glucose uptake in HCT116 IDH1-R132H reported by Gelman *et al*. (2018)[136] might be due to different cell culture conditions (glucose concentration in medium, incubation time). Rewiring of cell metabolism, especially (entry into) TCA cycle can also be seen from intracellular levels of α-KG, pyruvate and lactate (Figure 27). Levels of other TCA intermediates do not change significantly (data not shown).

The main compensation mechanism for increased α-KG consumption is glutaminolysis and it is primarily dependent on the amount of 2-HG production. Regarding the localisation of mutIDH1/2, differences found were of minor impact. The most striking difference between HCT116 IDH1-R132H cells and HCT116 mutIDH2 cells is found in the labeling pattern of some amino acids, especially alanine and serine. It is assumed that depletion of *IDH1* or *IDH2*, respectively, can be compensated by flux through the other isoform(s) and metabolite shuttles across the mitochondrial membrane. Likewise, Khurshed *et al*. (2017) concluded, based on gene expression data, that mitochondrial isocitrate production in *mutIDH1* glioma is enhanced and shuttled to the cytosol for α-KG and 2-HG production[144]. Moreover, it was found that impaired mitochondrial IDH-flux (e.g. by *IDH2* depletion) could be compensated by cytosolic WT-IDH1. For cells with a monoallelic *IDH1* mutation, this increased WT-IDH1 flux even caused an increase of 2-HG production due to higher substrate availability for mutIDH1[13]. The same was observed in HCT116 IDH1-R132H cells under hypoxic conditions, which increased oxidative IDH1-flux (citrate → α-KG + CO_2)[133]. Interestingly, under these conditions, cells without *IDH1* mutation increase reductive IDH1 flux to produce citrate for fatty acid synthesis. An *IDH1* mutation results in the loss of this metabolic flexibility and, thus, in compromised growth under hypoxic conditions. As a result, there is also

a difference in nutrient supply (glucose vs. glutamine) for FA synthesis in *mutIDH1* cells under hypoxic conditions.

In conclusion, the here presented data on metabolic adaptation in *mutIDH1/2* cells using ^{13}C-labeled compounds provide insight in the potential of this technique. The data are useful for understanding effects of increased 2-HG production by *mutIDH1/2* on cellular metabolism. However, to draw a complete picture, measurements need to be extended to further metabolites, like PPP and fatty acids. Additionally, based on these results, incubation times with tracers can be optimized. A paper summarizing all these efforts is planned for publication.

9 Origin and fate of 2-hydroxyglutarate-lactone

This chapter summarizes the efforts made to study the novel metabolite 2-HG-lactone. The detection and confirmation of 2-HG-lactone was accomplished by applying different bioanalytical methods to serum samples obtained from AML-patients with mutated *IDH1/2*. Cell culture experiments using cells with *mutIDH* and *WT-IDH* provided evidence on the formation of 2-HG-lactone from 2-HG.

9.1 2-HG and -lactone in various biological specimens

Initially, the LC-MS/MS method described in chapter 5.5.1 was applied to a set of AML-serum samples to investigate the respective serum levels of both, 2-HG and its metabolite 2-HG-lactone. This investigation led to the following insights (see also Figure 28A&B):

- 2-HG is only present at elevated concentrations in patients with *IDH1/2* mutation and decreases upon treatment, which is in agreement with the literature[147-149].
- 2-HG-lactone is only detected in samples with increased 2-HG concentrations, the ratio, however, varies.
- The amount of 2-HG-lactone is not dependent on the type of IDH1/2 mutation, nor on the 2-HG level.

In tissue extracts of glioma patients with *IDH1/2* mutation, 2-HG-lactone concentration was just above the LLOQ, while 2-HG was detected in the mmolar range (Figure 28C). Thus, the ratio of 2-HG/-lactone was not comparable to AML-sera. This led to the assumption, that lactonization is a specific (enzymatic) reaction, which is hardly observable in the brain. Direct lactonization of 2-HG in the blood by serum enzymes was excluded by incubation of (fresh) serum and blood specimens with 2-HG at 37°C. These experiments did not reveal formation of 2-HG-lactone. Similarly, incubation of 2-HG and α-KG with microsomal fractions (human microsomes & S9-fractions; life technologies; Carlsbad, USA) and recombinant IDH1/2 enzyme (Biomol, Hamburg & Amsbio, Abingdon, UK) did not result in 2-HG-lactone production (data not shown).

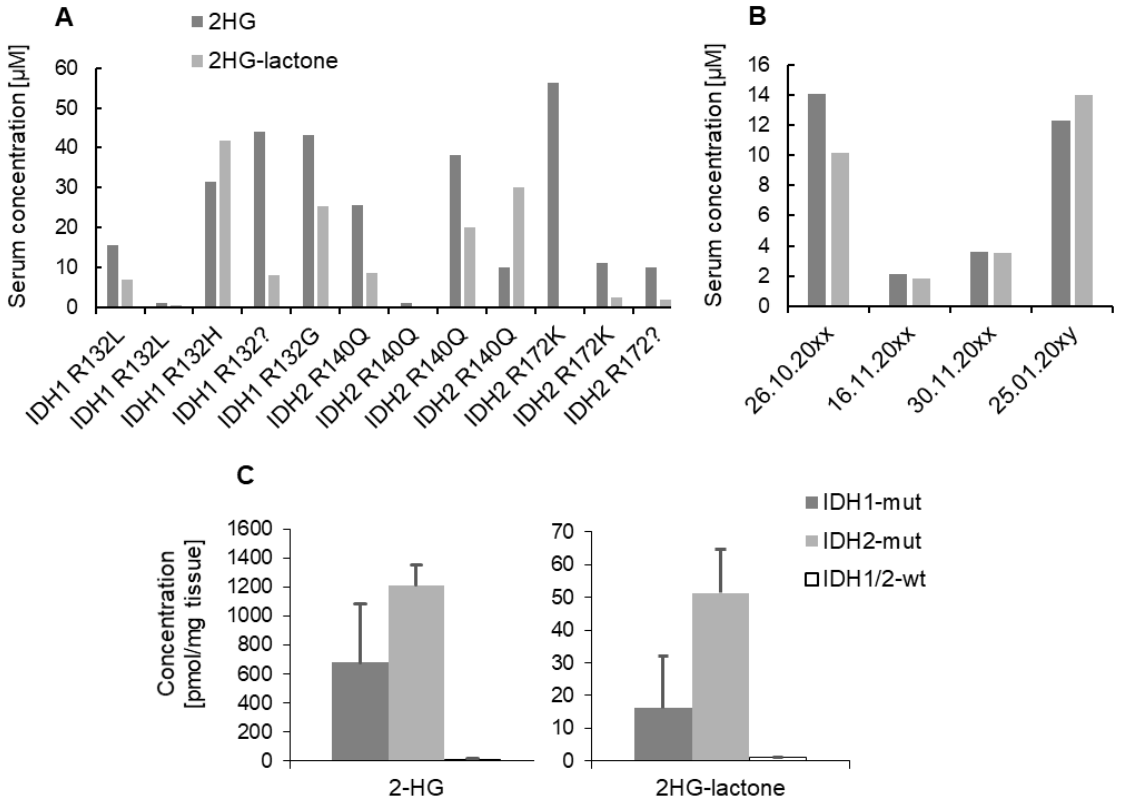

Figure 28. Analysis of 2-HG/-lactone in different biological specimens. ***A****) Serum samples (bars represent meaurements of one patient each) of patients with IDH1/2 mutations.* ***B****) Follow-up of 2-HG/-lactone levels in serum (n=1) of a patient with an IDH2-R140Q mutation from diagnosis (first date) to ongoing treatment (causing a decrease in both metabolites) to relapse (last date).* ***C****) Glioma tissue with mutated and wild type IDH1/2 (IDH1-mut: n=6, IDH2-mut: n=3, WT-IDH: n=5). 1000 pmol/mg tissue weight roughly translates to 1 mM assuming a tissue density of 1 g/mL. 2-HG-lactone constitutes about 3-4% of 2-HG, which is much lower than for AML-sera, where some samples show even higher levels of 2-HG-lactone than 2-HG.*

Furthermore, we asked, whether lactonization of 2-HG is specific to AML-patients with mutation in *IDH1/2* and therefore elevated 2-HG concentrations or whether it can be found for instance in serum of 2-HG-aciduria patients, as well. Those patients also typically have augmented 2-HG serum concentrations, but we unfortunately did not get hold of such a sample for ethical reasons.

In extracts of both, cell pellets and supernatants (e.g. from MCF7 and C7H2 cells), as expected, 2-HG was only found at baseline levels and 2-HG-lactone was below LLOQ or even LOD. Treatment of cells with D-2-HG led to increased intracellular D-2-HG concentrations, but it did not result in detectable production of 2-HG-lactone from 2-HG (Figure 29A&B). Interestingly, uptake of 2-HG&-lactone and intracellular hydrolysis of

2-HG-lactone varied across the cell lines tested. 2-HG is probably substrate to several transmembrane transporters: OAT1/4 (SLC22A6, SLC22A11)[150] and the dicarboxylate transporter 3 (SLC13A3)[151]. 2-HG-lactone, as a monocarboxylate, is assumed to be transported by the widely expressed monocarboxylate transporters MCT1&4. Therefore, differences in the expression level of these transporters and intracellular esterases might explain alterations in intracellular 2-HG and -lactone levels across different cell lines.

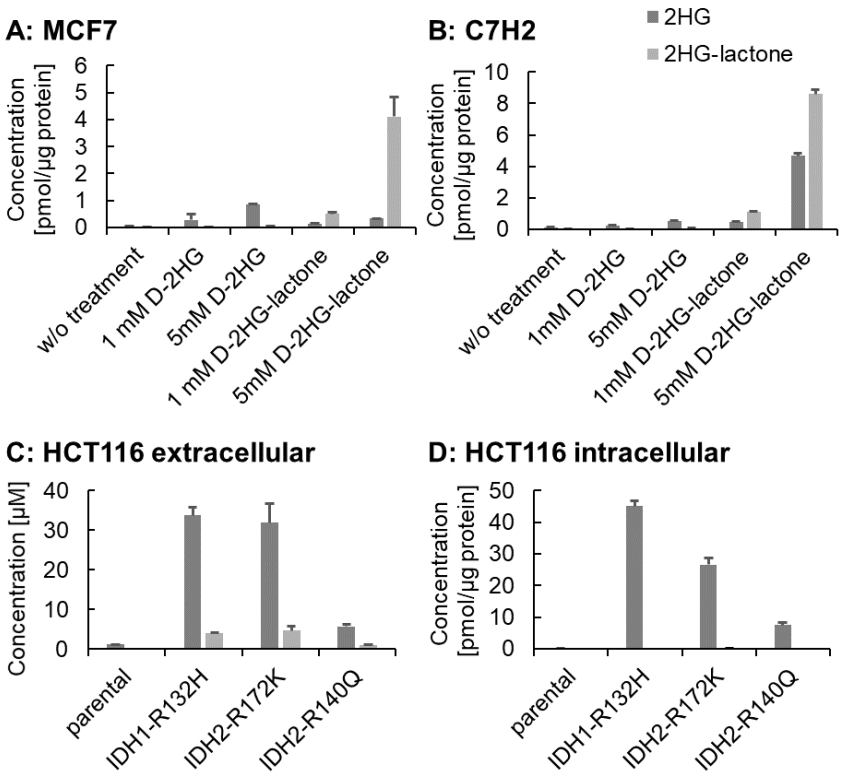

*Figure 29. 2-HG/-lactone concentrations in cell extracts and supernatants. **A**) and **B**) show intracellular concentrations in two cell lines with WT-IDH1/2 (MCF7 and C7H2) after treatment with D-2-HG/-lactone for 72 h, as indicated (n=3). 2-HG-lactone is only detected intracellularly, when used for treatment but not as product of cellular 2-HG lactonization. Without treatment hardly any of the two metabolites are detected. **C**) depicts endogenous metabolite levels in media, and **D**) in cell extracts of the HCT116 panel (n=2-6). Here 2-HG-lactone is also detected, especially in supernatants of mutIDH1/2 cell lines.*

Administration of different concentrations (1-10 mM in medium) of D- and L-2-HG to various cell types (including primary macrophages, Supplemental Figure S 3) did not lead to the detection of significant amounts of 2-HG-lactone. These experiments suffered from low uptake rates of 2-HG. Therefore, I started to work on cells with an

IDH1 or *IDH2* mutation, which produce 2-HG endogenously, namely HT1080 (IDH1-R132C) and the HCT116 panel (IDH1-R132H, IDH2-R172K, and IDH2-R140Q mutant lines and parental line with baseline 2-HG). Indeed, all cell lines with an *IDH1/2* mutation had elevated intra- and extracellular 2-HG concentrations. Remarkably, no 2-HG lactone was found in HT1080 extracts (*Figure 33*), whereas mutIDH1/2 HCT116 contained 2-HG-lactone, especially in the supernatant (Figure 29C&D). The absolute concentrations of 2-HG-lactone, as well as the 2-HG/-lactone ratio, were altered within those three cell lines. Subsequently, the HCT116 panel was used as a model system to investigate the production, metabolism and effects of 2-HG-lactone.

It has to be mentioned, that 2-HG-lactone is not stable in aqueous solutions, due to spontaneous hydrolysis into 2-HG. Preliminary data showed that the concentration of 2-HG-lactone would be decreased by ~8% by this effect (see Supplemental Figure S 4).

9.2 2-HG-lactone formation is independent of IDH1/2 mutation

During my work on this thesis, 2-HG-lactone was exclusively detected in the presence of *IDH1/2* mutation. However, it was assumed that mutIDH1/2 was not directly involved in 2-HG-lactonization but necessary to provide sufficient 2-HG concentrations to detect 2-HG-lactone formation. This question was addressed by administering 100 µM (2R)-2-hydroxyglutaric acid octyl ester (octyl-D-2-HG, structure see Figure 30) to parental HCT116 cells (*WT-IDH1/2*). The octyl-D-2-HG can diffuse across the cell membrane with intracellular hydrolysis of the ester giving rise to free 2-HG. Therefore, this treatment results in elevated intracellular D-2-HG concentrations even in *WT-IDH1/2* cells. LC-MS/MS analysis confirmed elevated 2-HG levels both, in cell extracts and supernatant, as shown in Figure 30 A+B. Additionally, 2-HG-lactone was detected in samples from octyl-D-2-HG treated cells. In particular, extracellular concentrations of 2-HG-lactone were abundant, which agreed with endogenous 2-HG/-lactone levels measured in *mutIDH1/2* HCT116 cell lines (Figure 29).

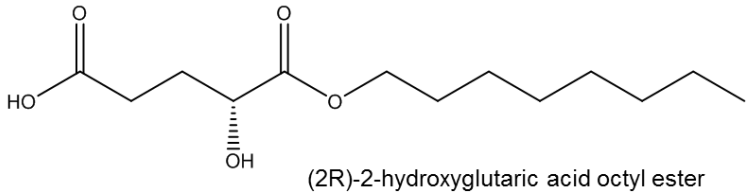

(2R)-2-hydroxyglutaric acid octyl ester

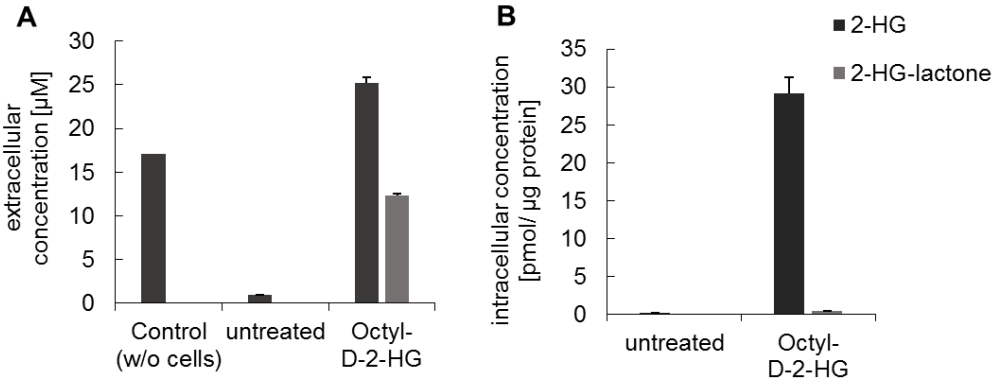

*Figure 30. 2-HG/-lactone concentrations in **A**) supernatant and **B**) cell extracts of octyl-D-2-HG (100 µM) treated parental HCT116 cells in comparison to untreated cells (n=2-3). Control medium, incubated without cells, reveals hydrolysis of octyl-D-2-HG even in absence of cells.*

However, elevated (intracellular) 2-HG levels alone do not entail detection of 2-HG-lactone. In extracts of HT1080 cells for instance, there is endogenous 2-HG production from an IDH1-R132C mutation but 2-HG-lactone is not detectable. Therefore, it is assumed, that another factor, like an enzyme, is involved into 2-HG lactonization.

Treatment of cells with octyl-D-2-HG was repeated with several other cell lines to test those cells for their capability to lactonize 2-HG (Figure 31). All tested cell lines were able to produce 2-HG-lactone upon octyl-D-2-HG treatment. Correlation of intra- or extracellular 2-HG and –lactone levels was not observed, but the concentrations of both metabolites and their ratio covered a wide range. Further work is needed to unravel what regulates the total amounts and the ratio of 2-HG and -lactone.

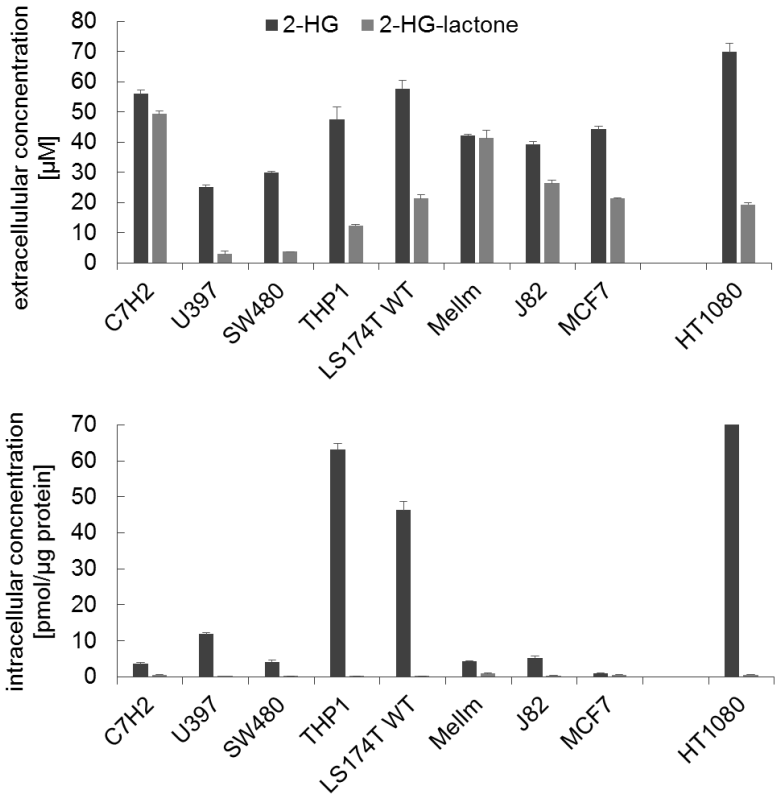

Figure 31. Extracellular (upper panel) and intracellular (lower panel) 2-HG/-lactone concentrations of selected cell lines of different origin treated with 100 µM Octyl-2-HG for 24 h (n=3). All cell lines have WT-IDH1/2, except HT1080 (IDH1-R132C; intracellular 2-HG is 144.5 pmol/ µg protein). (Cell lines are of following origin: C7H2 - acute lymphoblastic T cell line, U397 and THP1 - monocytic leukemia , SW480 and LS174T - colorectal adenocarcinoma, MelIm - melanoma, J82 - bladder cancer, MCF7 - breast cancer, HT1080 - fibrosarcoma)

9.3 Impact of pH on 2-HG-lactone formation

Lactones are intramolecular esters and, therefore, the formation is favored under acidic conditions. We take advantage of this fact in the synthesis of our stable isotope labeled standard ([2,3,3]-D_3-2-HG-lactone from [2,3,3]-D_3-2-HG) required for quantitative LC-MS/MS analysis. Interestingly, there is a report about urine from a 2-HG-aciduria patient, where not only 2-HG but also the 2-HG-lactone was detected[91]. However, the authors also explain this finding with the low pH of the sample, which is as low as pH 2.5 (due to the addition of HCl before the measurement).

To find out, what pH is low enough for lactonization of 2-HG, 1 mM D-2-HG was incubated in buffers of different pH values for 29 h at 37 °C. As shown in Figure 32,

the percentage of lactone formation increases with decreasing pH. At pH 5 2-HG-lactone amounts to ~3% of 2-HG concentration.

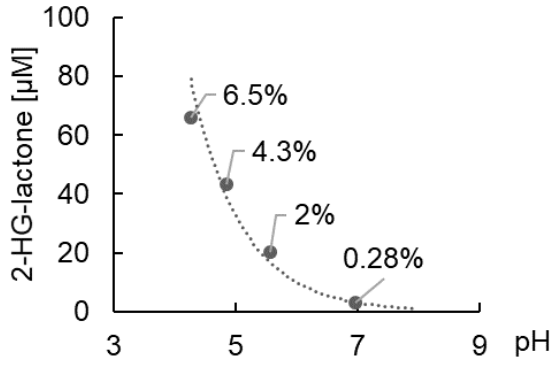

Figure 32: Spontaneous, non-enzymatic 2-HG lactonization under acidified conditions. 1 mM D-2-HG was incubated in HEPES-buffer (20 mM) acidified with HCl to different pH values (at 37°C, 29 h, n=2 per data point) and formed 2-HG-lactone was quantified.

Physiological pH, in cell compartments like cytosol and mitochondria or in blood is supposed to be too high as it is tightly regulated in a neutral range. Extracellular acidification is a hallmark of cancer and was also verified for bone marrow in AML rats[152]. In the latter study, the pH dropped from 6.9 in the bone marrow of healthy rats to 6.5 in leukemic rats. Incubation time of 29 h (like in the experiment shown in Figure 32) is rather short in comparison to an *in vivo*-situation like in an AML-patient. Besides, there is spontaneous hydrolysis of 2-HG-lactone released to the (strongly buffered) blood in AML-patients. Moreover, we know that 2-HG production by mutIDH1/2 is high; therefore, it seems unlikely that lactonization takes place already in the bone marrow of AML patients even in the case of pH being lowered by highly proliferating cancer cells. While peripheral myeloid cancer cells still can form 2-HG in the blood circulation, 2-HG-lactone formation should be limited to the bone marrow because of the lower pH there. Such a situation will probably not lead to serum samples which present with higher 2-HG-lactone than 2-HG levels.

To collect some evidence on lactonization as a function of environmental pH, cell culture experiments were preformed imitating alteration in extracellular pH. Namely, HT1080 cells (IDH1-R132C) were cultivated in acidified medium. (Cells were only cultivated for 6 h under these conditions to avoid a high number of dead cell in these samples due to the low pH). Although those cells produce 2-HG endogenously, lactonization cannot be observed under this experimental pH condition (Figure 33). Contrarily, for *mutIDH1/2* HCT116 cells, which already produce 2-HG-lactone under standard culture conditions, cultivation in acidified medium causes a higher percentage

of 2-HG-lactone. Maybe this external pH drop stabilized the 2-HG-lactone produced in *mutIDH1/2* HCT116 cells, but was not sufficient to induce lactonization in HT1080.

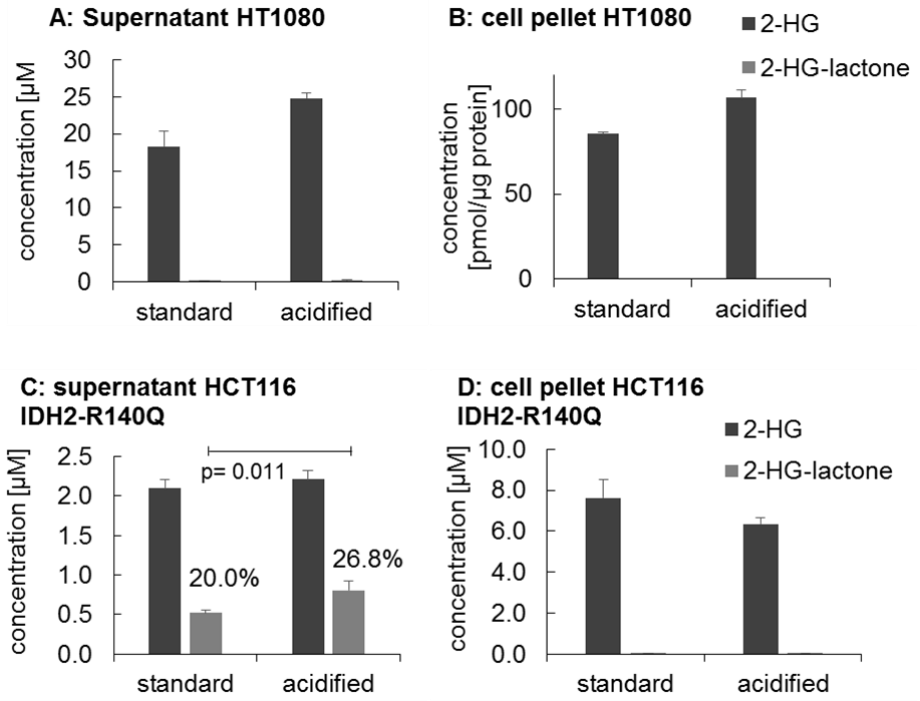

Figure 33. 2-HG/-lactone levels in cell culture supernatants (A&C) and cell pellets (B&D), respectively, for HT1080 and HCT116 IDH2-R140Q cells. Each cell line was cultured for 6 h under standard and acidified conditions (pH of medium at time of addition was ~6.5). (n=2-3, percentages represent amounts of 2-HG-lactone relative to the sum of 2-HG/+lactone). 2-HG-lactone is significantly different in HCT116 IDH2-R140Q (t-test: p=0.011).

9.4 Investigations on lysosomes in context of 2-HG-lactone formation

In cells the only compartment with low pH are lysosomes - intracellular vesicles responsible for degradation of waste products. Hydrolytic enzymes accomplish the breakdown of macromolecules targeted and internalized into lysosomes (via the endocytic pathway). To keep these enzymes active, the lysosomal lumen needs to maintain acidic pH, which is assured by the vacuolar-type H^+-ATPase[153]. The average luminal pH in lysosomes is pH 4.5-5. This pH seems to be appropriate to produce detectable amounts of 2-HG-lactone. Formation of 2-HG-lactone in lysosomes would require fast and efficient export by a high affinity transporter, as intracellular

2-HG-lactone levels were found at a low level with 2-HG-lactone accumulation in cell culture supernatant and AML-serum.

Moreover, it seems feasible that 2-HG is imported into lysosomes, which is a prerequisite for 2-HG-lactonization in lysosomes. For α-KG and other mono-/dicarboxylates transport across the lysosomal membrane by the human sialic acid transporter SLC17A5 was reported[154,155]. This anion transporter is rather unspecific and 2-HG and α-KG are very similar in their structure. Thus, it is assumed that 2-HG is a substrate of SLC17A5, as well.

The number of lysosomes within a cell can vary dependent on environmental conditions like nutrient availability and alternating biomass turnover with concomitant changing degradation requirements[156,157]. To elaborate whether lysosomes are the crucial factor for lactonization of 2-HG, a staining of these compartments was performed. The area of stained spots per image was used as measure for lysosomal number. LysoTracker Deep Red is a commercially available dye for fluorescence microscopy, which selectively accumulates in acidic compartments, namely lysosomes and to some extent late endosomes. The fluorophore of LysoTracker is a weak base

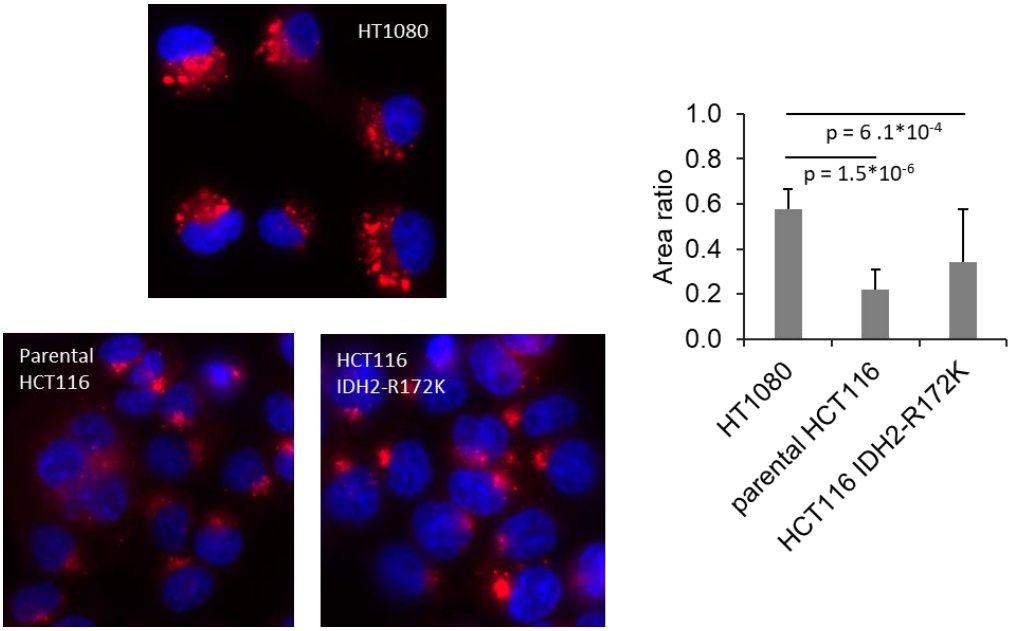

*Figure 34. Representative images of HT1080, parental HCT116 und -IDH2-R172K cells stained with Hoechst 33342 (blue; nuclei) and LysoTracker Deep Red (red; lysosomes). Quantitative data in the right panel: Lysosomal staining calculated as the ratio of LysoTracker staining normalized to staining of nuclei with Hoechst 33342 in three different cell lines. (n=10 images, ANOVA p=2.13*10$^{-6,}$ post hoc-test=Tukey´s HSD).*

and hardly protonated at neutral pH and can therefore easily cross cell membranes. At acidic pH, like in lysosomes, the fluorophore becomes protonated and is then trapped in that organelle. Consequently, this live cell imaging approach is highly selective and sensitive. For normalization, cell nuclei were simultaneously stained with Hoechst 33342 solution. Consequently, the relative staining (lysosomes/nuclei) should be higher for cells with more lysosomes. When assuming, that 2-HG-lactonization takes place in lysosomes, HT1080 cells should present significantly less lysosomal staining. However, staining of HT1080 cells and HCT116 cells does not reveal the expected differences (Figure 34). Comparison of LysoTracker staining (normalized to nuclei staining) rather showed the opposite difference. Consequently, lysosomes seem not to be solely responsible for 2-HG-lactonization.

9.5 Does 2-HG-lactone formation involve an enzyme?

Another aspect of lactone formation is the varying ratio of 2-HG and its lactone found in cell culture supernatant (but also in AML serum; Figure 28). The ratio seems not to be constant for a given type of IDH1/2 mutation.

To check for a potential correlation between the concentration of 2-HG and its lactone, parental HCT116 cells and HCT116 IDH2-R172K cells were treated with increasing octyl-D-2-HG concentrations. In agreement with previous data, 2-HG-lactone was not detected in significant amounts in cell extracts, but only in cell supernatants (Figure 35B). The extracellular 2-HG concentrations increased in a linear fashion (Figure 35A). This is true for control media incubated without cells, as well, but 2-HG concentrations are at a lower level. Thus, octyl-D-2-HG is to some extent hydrolyzed in culture medium releasing free 2-HG. The difference between control medium and cell supernatant, however, is due to export of intracellularly hydrolyzed/formed 2-HG. The 2-HG-lactone in supernatant of octyl-D-2-HG treated cells reveals a higher concentration for increasing (octyl-D-)2-HG levels. For the highest concentrations applied, 2-HG-lactone seems to reach saturation. Likewise, intracellular 2-HG concentrations seem to run into saturation, which however is not reached yet from the octyl-D-2-HG concentrations applied in this experiment (Figure 35C).

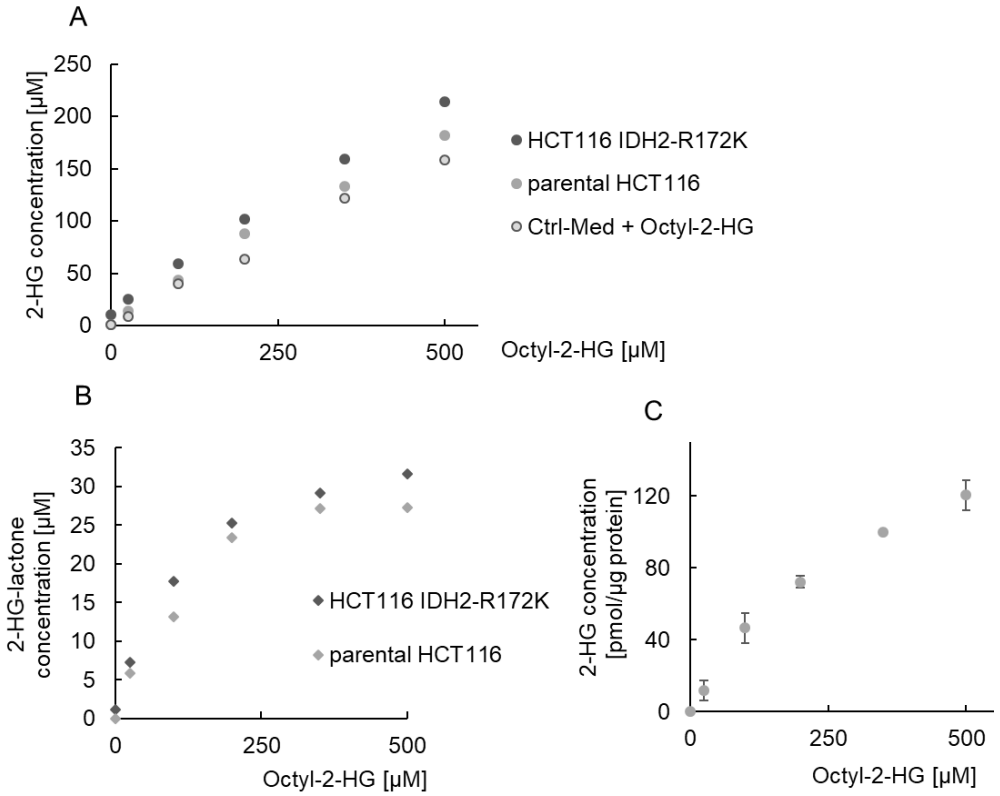

Figure 35. ***A****) Extracellular 2-HG concentrations for parental HCT116 and ~IDH2-R172K cells depend on the octyl-D-2-HG concentration used for treatment (24 h). The difference in 2-HG concentration in mutant cells is attributed to endogenous 2-HG production from mutIDH2. Control (Ctrl)-medium is incubated without cells and, therefore, shows spontanous hydrolysis of octyl-D-2-HG.* ***B****) Corresponding extracellular 2-HG-lactone concentrations in parental HCT116 and IDH2-R172K HCT116. (No 2-HG-lactone in control-medium).* ***C****) Intracellular 2-HG concentration depends on the octyl-D-2-HG concentration used for treatment of parental HCT116 from two independent experiments. Intracellular 2-HG-lactone is below the LLOQ.*

Finally, HT1080 cells were also treated with (different concentrations of) octyl-2-HG and now found to produce 2-HG-lactone (Figure 36). This is the more interesting, as intracellular 2-HG levels in treated HT1080 cells do not increase in comparison to untreated cells or with higher octyl-D-2-HG treatment as seen before for HCT116 cells. HT1080 cells show the highest (endogenous) intracellular 2-HG levels of all mutated cell lines measured (see also Figure 31). However, treatment with octyl-2-HG induces 2-HG lactonization. Maybe there is an intracellular level for 2-HG, which when exceeded initiates lactonization to facilitate 2-HG removal. This critical level would then be higher in HT1080 than e.g. HCT116 and for HT1080 cells it would reflect almost the endogenous 2-HG level. Here, more experiments are needed.

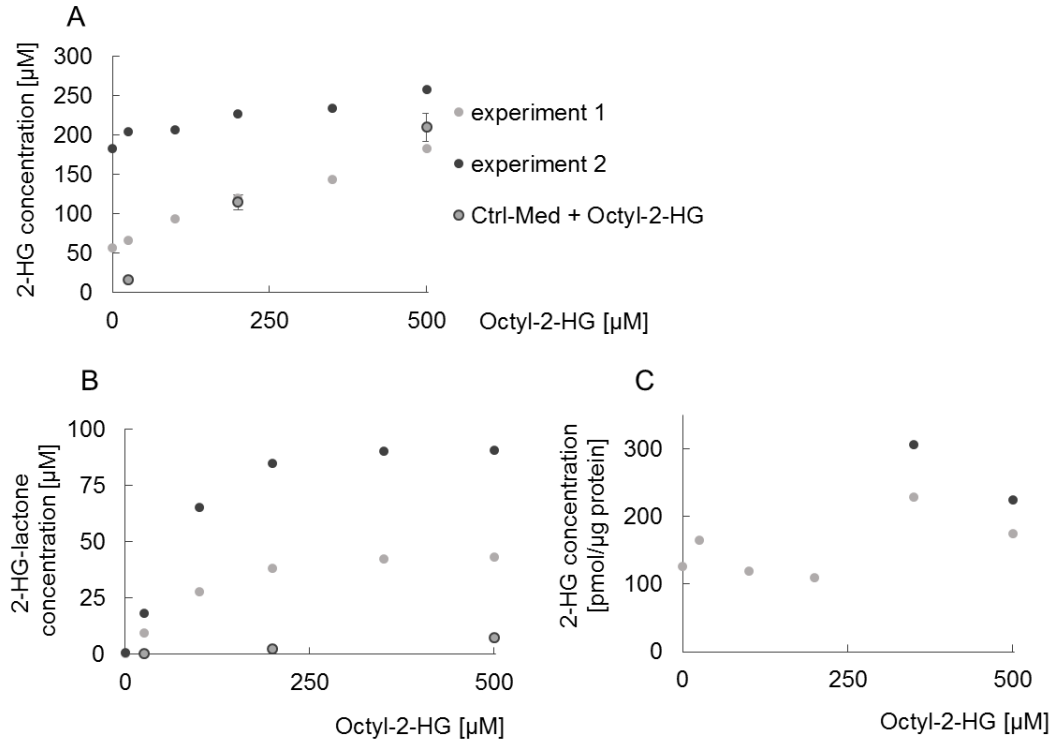

Figure 36. ***A****) Extracellular 2-HG concentrations for HT1080 cells depend on the octyl-D-2-HG concentration used for treatment (24 h). Control (Ctrl)-medium is incubated without cells and, therefore, shows spontanous hydrolysis of octyl-D-2-HG.* ***B****) Corresponding extracellular 2-HG-lactone concentrations in HT1080 cells from two independent experiments* ***C****) Intracellular 2-HG concentrations in octyl-D-2-HG treated HT1080 hardly correlate with octyl-D-2-HG amounts used for treatment. The fluctuation as well as differences between the two experiments are due to differences in protein amount in the cell pellets.*

The increase in 2-HG-lactone concentration seen upon increasing concentrations of octyl-2-HG applied resembles a Michaelis-Menten-kinetic. This suggests, that an enzyme is involved in 2-HG-lactone formation (and/or export). Two mechanisms can be imagined explaining these findings. Either lactonization takes place intracellularly, with a high affinity transporter clearing the cells from 2-HG-lactone. Alternatively, 2-HG-lactone is formed during export (by a transporter) to enhance 2-HG export. Both assumptions meet our findings of a more effective transport of the monocarboxylate 2-HG-lactone than the dicarboxylate 2-HG (see below).

In macrophages incubated separately with D- and L-2-HG-lactone, respectively, it was observed that lactone hydrolysis was enantiospecific. As shown in Figure 37A&B uptake of 2-HG-lactone was comparable for the D- and L-form with a concentration dependent, linear increase in intracellular levels. Intracellular 2-HG concentrations reflect hydrolysis of 2-HG-lactone into the open ring form. Here, hydrolysis of D-2-HG-lactone occurs more readily than that of L-2-HG-lactone (about 50-fold, Figure 37C&D)). While for L-2-HG-lactone treatment, intracellular 2-HG levels again increase in a linear fashion, for D-2-HG-lactone intracellular 2-HG seems to run into saturation (comparable to the findings in octyl-D-2-HG treated cells, Figure 35).

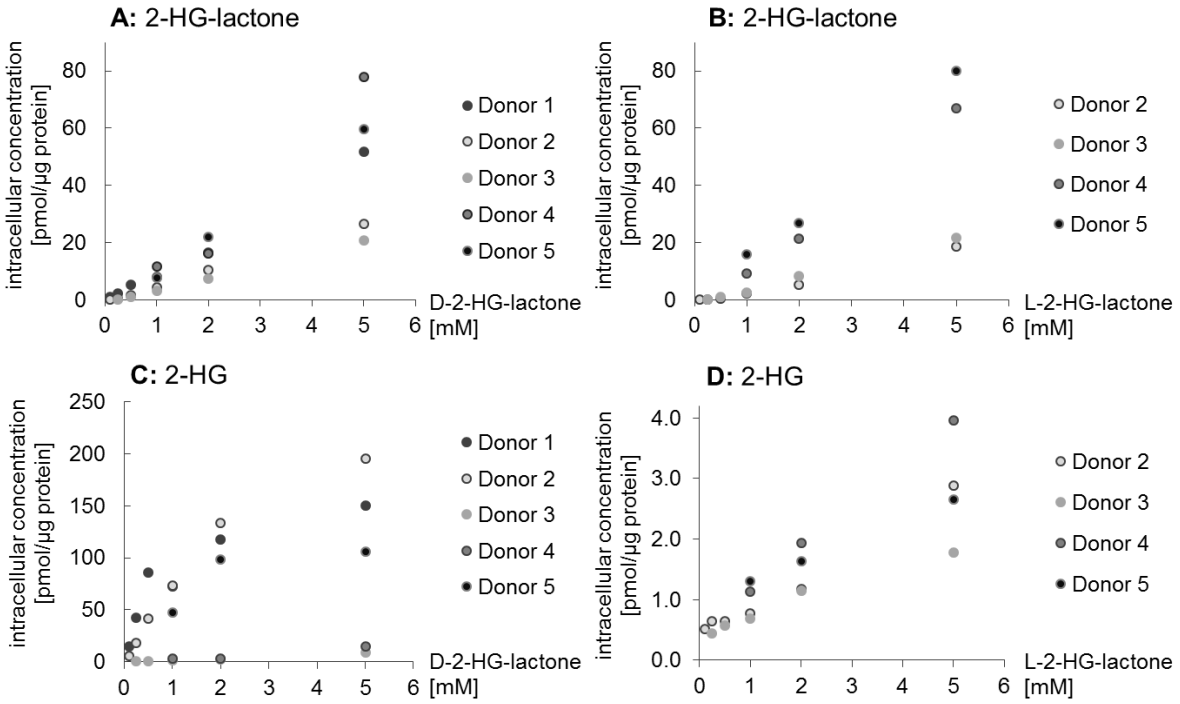

*Figure 37. Treatment of macrophages with D- and L-2-HG-lactone reveal enantiospecific effects. The upper panels give the intracellular 2-HG-lactone concentrations after treatment of cells with increasing amounts of **A**) D-2-HG-lactone and **B**) L-2-HG-lactone for 24 h. **C**) and **D**) give the respective intracellular 2-HG concentrations. For treatment enantiomerically pure solutions were prepared, LC-MS/MS measurements were not enantioselective but represent total 2-HG. Cells from Donor 1 were not treated with L-2-HG-lactone.*

It has to be noted that generally donor dependent variances are given. For hydrolysis of D-2-HG-lactone there are two donors which show a considerably lower hydrolysis rate than the other donors, but which is still higher than for L-2-HG-lactone. This phenomenon needs to be followed up. Meanwhile, it can be concluded that 2-HG-lactone hydrolysis is facilitated by an enzyme, because spontaneous hydrolysis

cannot occur in an enantioselective manner. However, it cannot be said whether this enzyme is also catalyzing the lactonization of (D-)2-HG.

9.6 2-HG-lactone formation in cell homogenates

To learn more about enzyme kinetics of 2-HG lactonization from the HCT116 panel, cells were lysed to perform enzyme assays. Cell homogenates were spiked with 2-HG as substrate and incubated at 37°C (similarly to D2HDH assay). Analysis of assay aliquots by LC-MS/MS do not reveal *in vitro* 2-HG-lactonization. Accordingly, no (active) enzyme catalyzing 2-HG-lactone formation is contained in cell homogenates. Inactivity could be explained by assay conditions, which do not recreate *in vivo* conditions. Altering assay conditions, like adding different salts/ ions (up to 25 mM potassium, 1 mM calcium, 2 mM zinc) and reducing agents (e.g. DTT), did not result in 2-HG-lactone formation. Interestingly, there are no human enzymes known that catalyze lactone formation. For other species there are, for instance the gluconolactonase (SMP30, regucalcin) involved into the vitamin C synthesis in mice[158]. Some lactonases can catalyze the reaction in both directions (lactone formation and hydrolysis) dependent on environmental conditions like pH. A lactonase (of unknown amino acids sequence) found in the bacterium *Burkholderia* sp. R-711, was described to hydrolyze D-2-HG-lactone, but lactone formation was not detected[159]. Nevertheless, is was considered that an esterase might be responsible for both, 2-HG lactonization and 2-HG-lactone hydrolysis. Variances in the 2-HG/-lactone ratio would then be a consequence of a shifted equilibrium, e.g. by changes in the pH.

When adding 2-HG-lactone to cell homogenates (for incubation at 37°C for 5 h) to measure its hydrolysis, assay data do not reveal significant degradation. In conclusion, HCT116 cell homogenates do not contain an active esterase or any other enzyme, acting on D-2-HG and its lactone. Hence this approach does not contribute to explain our findings of 2-HG lactonization in AML-patients with *IDH1/2* mutation.

Nevertheless, these results further support the hypothesis that 2-HG-lactone formation may be catalyzed by a transport protein embedded in the cell membrane. Such a protein (containing hydrophobic regions) is likely to be depleted during cell lysis and homogenate preparation in aqueous buffers. To increase solubility a detergent (DDM = n-dodecyl beta-D-maltoside) was added, which is assumed to retain enzyme activity, but again was not marked by success. Additionally, membrane gradients cannot be imitated in cell homogenates. Finally, there are several reasons which could hamper detection of 2-HG lactonization in cell homogenates.

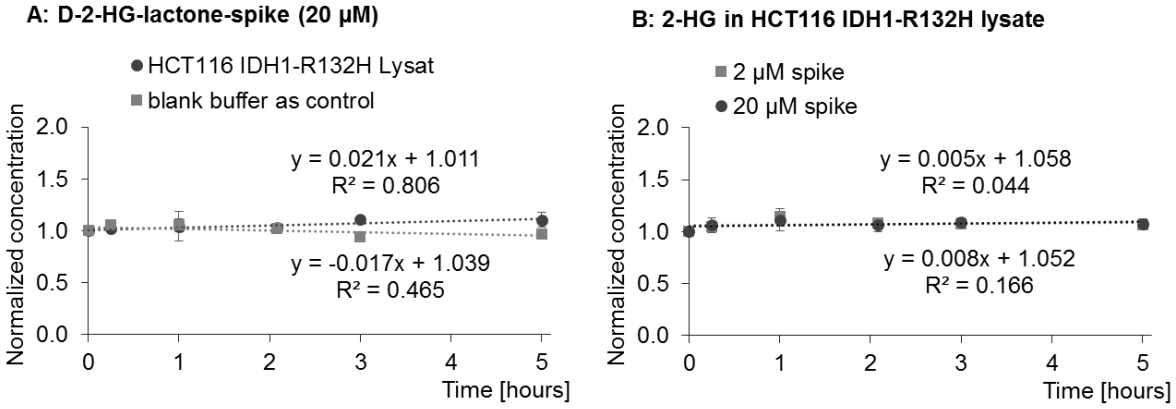

*Figure 38. Assays for 2-HG-lactone degradation or 2-HG production, respectively. **A**) Lysate of HCT116 IDH1-R132H was spiked with 20 µM 2-HG-lactone and its concentrations was followed over 5 hours (n=2). Changes in concentration (normalized to concentrations at 0 hours) was not significantly different from changes in 2-HG-lactone concentration incubated in blank buffer without protein (t-test p=0.139). Correspondingly, 2-HG concentrations (from incubation of 2 µM or 20 µM 2-HG-lactone) do not increase (**B**).*

9.7 2-HG and its lactone are two distinct metabolites

One could ask, why it is of importance to find the origin of 2-HG-lactone, if it is solely produced from and readily degraded to its precursor 2-HG. Investigation into potential biological effects of 2-HG/-lactone showed, for instance, a significant effect of D-2-HG and its lactone (in comparison to untreated controls) on the secretion of IL-6 from macrophages (Figure 39). In contrast, L-2-HG is not significantly different from controls. However, comparison to D-2-HG also does not give a significant difference (Tukey´s HSD p_{adj}=0.891).

More interesting would be the differences in effects from the open vs the esterified 2-HG. However, in the macrophage experiment, effects of D/-L-2-HG-lactone in comparison to D-/L-2-HG do not show a clear picture. IL6-secretion in L-2-HG-lactone-treated cells was basically unaffected by treatment, which agrees with the before mentioned finding that L-2-HG-lactone was hardly hydrolyzed intracellularly (Figure 37). Therefore, it appears that 2-HG is the compound evoking a (immune-) response, while the lactone does not. However, as the differences in lactone hydrolysis seem to be enantioselective and cell type specific, this issue needs further investigations.

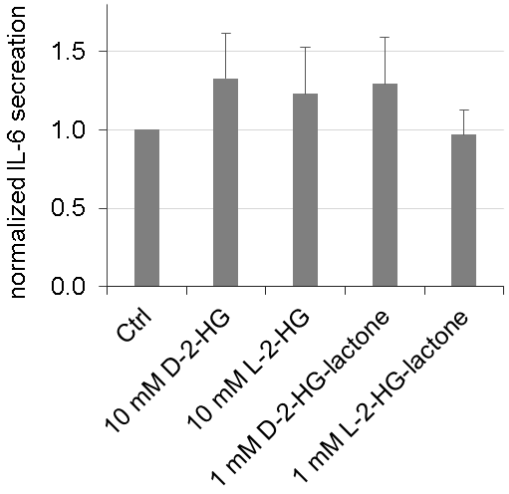

Figure 39. IL-6 secretion in primary macrophages from three different donors (normalized to untreated cells = Ctrl; all cells were stimulated with LPS). For 10 mM D-2-HG and 1 mM D-2-HG-lactone treatment increase in IL-6 secretion is significant (ANOVA p=0.021; Dunnett test for pairwais comparison to Ctrl – vs D-2-HG p=0.0132, - vs D-2-HG-lactone p=0.0225, -vs L-2-HG p=0.0612). Data were generated in cooperation with the group of M. Kreutz (Department of Hematology and Oncology, University Hospital Regensburg).

As mentioned before, 2-HG-lactone is assumed to be transported via MCT1&4. To investigate 2-HG-lactone transport by monocarboxylate transporters, a panel of LS174T cells was available comprising wild type and the knockout clones *MCT1*$^{-/-}$, *MCT4*$^{-/-}$, and *MCT1*$^{-/-}$ *4*$^{-/-}$, respectively[160]. Those four cell lines were again treated with 100 µM octyl-D-2-HG, which resulted in increased intracellular 2-HG levels and 2-HG lactonization. As reported before for cells with WT-IDH1/2, 2-HG-lactone was hardly observable in pellet and medium extracts from LS174T cells grown under standard conditions (Figure 40A&C). For medium extracts of octyl-D-2-HG treated cells, 2-HG-lactone was clearly detected for the full panel. Interestingly, when *MCT1* was knocked out, extracellular 2-HG-lactone concentrations were lower indicating that MCT1 is the more efficient transporter (Figure 40B). At the same time there was an intracellular accumulation of 2-HG-lactone in those cells compared to WT-cells (Figure 40E). In comparison to intracellular 2-HG, -lactone is still low abundant supporting the

hypothesis of an efficient clearing. On the contrary, *MCT4*$^{-/-}$ cells like WT-cells export 2-HG readily, and -lactone does not accumulate intracellularly. For the *MCT1*$^{-/-}$ *4*$^{-/-}$ cell line, -lactone is still found in the medium indicating that also other transporters are capable of exporting 2-HG-lactone. However, intracellular accumulation is significantly higher than in *MCT1*$^{-/-}$ cells (ANOVA $p=1.27*10^{-9}$, Tukey´s HSD $p_{adj}= 5.71*10^{-5}$), which might be due to intracellular acidification. MCTs are responsible for export of lactic acid, which was found elevated in pellet extracts of *MCT4*$^{-/-}$ and *MCT1*$^{-/-}$ *4*$^{-/-}$ cells (Figure 40F). If lactic acid is not removed from the cell, intracellular pH will drop which then pushes the equilibrium of 2-HG and –lactone towards lactone. These differences in intracellular pH might also explain the lower intracellular 2-HG amount in *MCT4*$^{-/-}$ cells. Low pH would not only stabilize the 2-HG-lactone, but also the octyl-D-2-HG. Therefore, it is supposed that measurement of intracellular octyl-D-2-HG would reveal higher levels of this compound for *MCT4*$^{-/-}$ and *MCT1*$^{-/-}$ *4*$^{-/-}$ cells. But as 2-HG-lactone can leave *MCT4*$^{-/-}$ cells via MCT1, the concentrations of both metabolites are on a lower level.

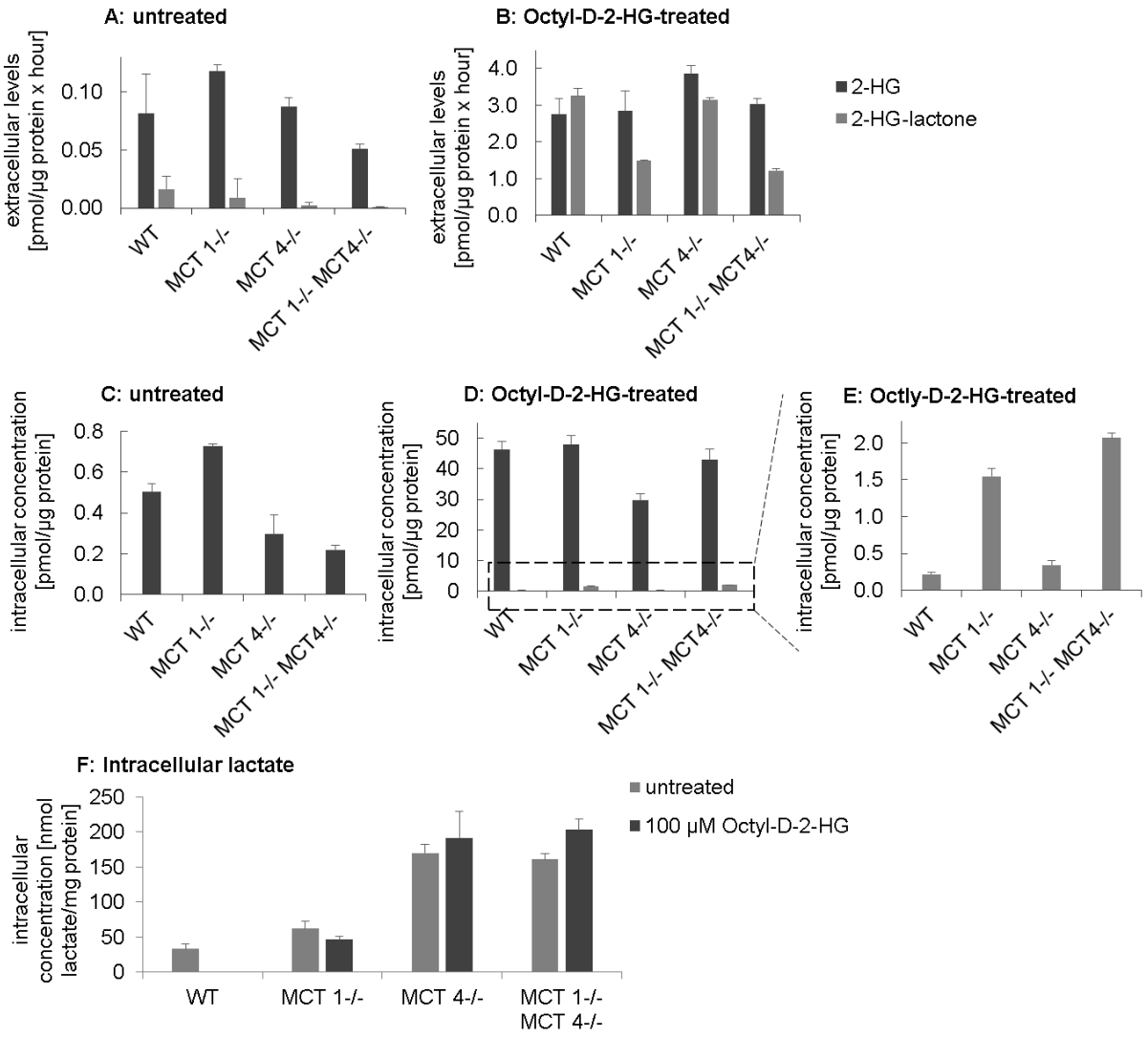

*Figure 40. LS174T panel treated with octyl-D-2-HG (100 µM, 24 h) reveals differences in 2-HG-lactone transport. Extracellular levels (**A&B**) were corrected by differences in growth (according to a method suggested by Jain 2012[161]) as cells of this panel show different growth rates. Furthermore spontanous release of 2-HG from Octyl-2-HG was quantified in mediums incubated without cells and substracted from media samples. (n=1-6, especially for 2-HG-lactone values were often below LLOQ). **C,D&E**) show intracelllar 2-HG/-lactone. Intracellular lactate (**F**) levels within the LS174T panel are significantly different (ANOVA untreated cells $p=2.69*10^{-7}$, Octyl-D-2-HG treated cells $p=3.09*10^{-4}$). Further statistics see Supplemental Table S 10 and Supplemental Table S 11 and Supplemental Table S 12.*

10 Conclusions and Perspectives

In this thesis, experiments were preformed to gain more insight into the oncometabolite D-2-hydroxyglutarate and its lactone. An enzymatic assay was developed to investigate the degradation of D-2-HG in the presence of *IDH1/2* mutation. It was found that D-2-HG degradation by D2HDH is at v_{max} and is not increased in response to extracellular elevated D-2-HG levels. Contrarily, production of D-2-HG by mutated IDH1/2 is of higher capacity, which was hypothesized before in the literature. With this work this assumption was further supported by experimental evidence. For analysis of both metabolites, 2-HG and its lactone, an LC-MS/MS method was established and thoroughly validated. The origin of 2-HG-lactone, an intramolecular ester of 2-HG, is still unclear. It could be detected in cell lines when 2-HG concentrations are elevated either due to mutations in *IDH1/2* or by treatment with cell permeable octyl-2-HG. However, high 2-HG-levels are not the only factor necessary for 2-HG-lactonization. With the evidence collected in this thesis, we hypothesize that a so far unidentified enzyme contributes to this intramolecular ester formation. Remarkably, lactone forming enzymes are not described for humans, rather lactonases catalyzing the reverse reaction of lactone hydrolysis.

2-HG-lactone was found to exceed 2-HG concentrations in several AML-sera, while in glioma tissue it was detected only at 3-4% of 2-HG. Consequently, either the unknown enzyme is present at different levels and/or altered activity (dependent on environmental factors) or the level to which 2-HG needs to accumulate to start lactonization is cell type specific. Furthermore, 2-HG-lactone is mainly found in extracellular fluids like serum and cell culture supernatant. One might speculate that the lactone is formed to be exported acting in a kind of paracrine fashion. We investigated the effects of D-2-HG-lactone on immune cells, namely macrophages (regarding cytokine secretion). Further investigations need to focus on whether or to what degree those biological effects are distinct from D-2-HG. Besides, effects on other functional levels e.g. inhibitions of β-glucosidase would be of interest. Another question is, what effect 2-HG-lactone has for instance on progression and prognosis of AML. In general, identification of the mechanism behind 2-HG-lactonization and its manipulation would help to distinguish 2-HG and 2-HG-lactone mediated effects in cells of identical biological background. Also, a knock-out of the 2-HG-lactone

hydrolyzing esterase would aid in separating out effects of both, 2-HG and -lactone. Besides, it is of interest whether the 2-HG-lactone can be detected in patients with 2-HG-aciduria, who also have increased serum 2-HG concentrations.

Performing all these analyses was challenged by the fact that 2-HG and -lactone can be interconverted spontaneously. This fact made several established methods redundant and needed the development of new analytical methods and there are still areas for further improvement.

11 References

1 Wachsmuth, C. J. Implementation and applications of gas chromatography/ atmospheric pressure chemical ionization time-of-flight mass spectrometry in metabolomics. Dissertation, *University of Regensburg* (2015).

2 Duran, M., Kamerling, J. P., Bakker, H. D., van Gennip, A. H. & Wadman, S. K. L-2-Hydroxyglutaric aciduria: an inborn error of metabolism? *J Inherit Metab Dis* **3**, 109 (1980).

3 Parsons, D. W., Jones, S., Zhang, X. S., Lin, J. C. H., Leary, R. J., Angenendt, P. *et al.* An integrated genomic analysis of human glioblastoma Multiforme. *Science* **321**, 1807 (2008).

4 Dalziel, K. Isocitrate dehydrogenase and related oxidative decarboxylases. *FEBS Lett* **117 Suppl**, K45 (1980).

5 Yan, H., Parsons, D. W., Jin, G. L., McLendon, R., Rasheed, B. A., Yuan, W. S. *et al.* IDH1 and IDH2 mutations in gliomas. *New Engl J Med* **360**, 765 (2009).

6 Sjöblom T, Jones S, Wood LD, Parsons DW, Lin J, Barber TD *et al.* The consensus coding sequences of human breast and colorectal cancers. *Science* **314**, 268 (2006).

7 Mardis, E. R., Ding, L., Dooling, D. J., Larson, D. E., McLellan, M. D., Chen, K. *et al.* Recurring mutations found by sequencing an acute myeloid leukemia genome. *New Engl J Med* **361**, 1058 (2009).

8 Pusch, S., Schweizer, L., Beck, A. C., Lehmler, J. M., Weissert, S., Balss, J. *et al.* D-2-hydroxyglutarate producing neo-enzymatic activity inversely correlates with frequency of the type of isocitrate dehydrogenase 1 mutations found in glioma. *Acta Neuropathol* **2**, 19 (2014).

9 Waitkus, M. S., Diplas, B. H. & Yan, H. Isocitrate dehydrogenase mutations in gliomas. *Neuro Oncol* **18**, 16 (2015).

10 Ward, P. S., Patel, J., Wise, D. R., Abdel-Wahab, O., Bennett, B. D., Coller, H. A. *et al.* The common feature of leukemia-associated IDH1 and IDH2 mutations is a neomorphic enzyme activity converting alpha-ketoglutarate to 2-hydroxyglutarate. *Cancer Cell* **17**, 225 (2010).

11 Dang, L., White, D. W., Gross, S., Bennett, B. D., Bittinger, M. A., Driggers, E. M. *et al.* Cancer-associated IDH1 mutations produce 2-hydroxyglutarate. *Nature* **462**, 739 (2009).

12 Gross, S., Cairns, R. A., Minden, M. D., Driggers, E. M., Bittinger, M. A., Jang, H. G. *et al.* Cancer-associated metabolite 2-hydroxyglutarate accumulates in acute myelogenous leukemia with isocitrate dehydrogenase 1 and 2 mutations. *J Exp Med* **207**, 339 (2010).

13 Ward, P. S., Lu, C., Cross, J. R., Abdel-Wahab, O., Levine, R. L., Schwartz, G. K. *et al.* The potential for isocitrate dehydrogenase mutations to produce 2-hydroxyglutarate depends on allele specificity and subcellular compartmentalization. *J Biol Chem* **288**, 3804 (2013).

14 Wen, H., Cho, H. R., Yun, T., Kim, H., Park, C. K., Lee, S. H. *et al.* Metabolomic comparison between cells over-expressing isocitrate dehydrogenase 1 and 2 mutants and the effects of an inhibitor on the metabolism. *J Neurochem* **132**, 183 (2015).

15 Pichler, M. M., Bodner, C., Fischer, C., Deutsch, A. J., Hiden, K., Beham-Schmid, C. *et al.* Evaluation of mutations in the isocitrate dehydrogenase genes in therapy-related and secondary acute myeloid leukaemia identifies a patient with clonal evolution to IDH2 R172K homozygosity due to uniparental disomy. *Br J Haematol* **152**, 669 (2011).

16 Dang, L., White, D. W., Gross, S., Bennett, B. D., Bittinger, M. A., Driggers, E. M. *et al.* Cancer-associated IDH1 mutations produce 2-hydroxyglutarate. *Nature* **465**, 966 (2010).

17 Losman, J. A. & Kaelin, W. G. What a difference a hydroxyl makes: mutant IDH, (R)-2-hydroxyglutarate, and cancer. *Gene Dev* **27**, 836 (2013).

18 Kaufman, E. E., Nelson, T., Fales, H. M. & Levin, D. M. Isolation and characterization of a hydroxyacid-oxoacid transhydrogenase from rat kidney mitochondria. *J Biol Chem* **263**, 16872 (1988).

19 Fan, J., Teng, X., Liu, L., Mattaini, K. R., Looper, R. E., Vander Heiden, M. G. *et al.* Human phosphoglycerate dehydrogenase produces the oncometabolite D-2-hydroxyglutarate. *ACS Chem Biol* **10**, 510 (2015).

20 Chalmers, R. A., Lawson, A. M., Watts, R. W., Tavill, A. S., Kamerling, J. P., Hey, E. *et al.* D-2-hydroxyglutaric aciduria: case report and biochemical studies. *J Inherit Metab Dis* **3**, 11 (1980).

21 Matsunaga, H., Futakuchi-Tsuchida, A., Takahashi, M., Ishikawa, T., Tsuji, M. & Ando, O. IDH1 and IDH2 have critical roles in 2-hydroxyglutarate production in D-2-hydroxyglutarate dehydrogenase depleted cells. *Biochem Bioph Res Co* **423**, 553 (2012).

22 Aghili, M., Zahedi, F. & Rafiee, E. Hydroxyglutaric aciduria and malignant brain tumor: a case report and literature review. *J Neuro-Oncol* **91**, 233 (2009).

23 Struys, E. A. D-2-Hydroxyglutaric aciduria: Unravelling the biochemical pathway and the genetic defect. *J Inherit Metab Dis* **29**, 21 (2006).

24 Kranendijk, M., Struys, E. A., van Schaftingen, E., Gibson, K. M., Kanhai, W. A., van der Knaap, M. S. *et al.* IDH2 mutations in patients with D-2-hydroxyglutaric aciduria. *Science* **330**, 336 (2010).

25 Nota, B., Hamilton, E. M., Sie, D., Ozturk, S., van Dooren, S. J. M., Ojeda, M. R. F. *et al.* Novel cases of D-2-hydroxyglutaric aciduria with IDH1 or IDH2 mosaic mutations identified by amplicon deep sequencing. *J Med Genet* **50**, 754 (2013).

26 Engqvist, M., Drincovich, M. F., Flugge, U. I. & Maurino, V. G. Two D-2-hydroxy-acid dehydrogenases in Arabidopsis thaliana with catalytic capacities to participate in the last reactions of the methylglyoxal and beta-oxidation pathways. *J Biol Chem* **284**, 25026 (2009).

27 Chaturvedi, A., Cruz, M. M. A., Jyotsana, N., Sharma, A., Goparaju, R., Schwarzer, A. *et al.* Enantiomer-specific and paracrine leukemogenicity of mutant IDH metabolite 2-hydroxyglutarate. *Leukemia* **30**, 1708 (2016).

28 Chowdhury, R., Yeoh, K. K., Tian, Y. M., Hillringhaus, L., Bagg, E. A., Rose, N. R. *et al.* The oncometabolite 2-hydroxyglutarate inhibits histone lysine demethylases. *Embo Reports* **12**, 463 (2011).

29 Figueroa, M. E., Abdel-Wahab, O., Lu, C., Ward, P. S., Patel, J., Shih, A. *et al.* Leukemic IDH1 and IDH2 mutations result in a hypermethylation phenotype, disrupt TET2 function, and impair hematopoietic differentiation. *Cancer Cell* **18**, 553 (2010).

30 Intlekofer, A. M., Wang, B., Liu, H., Shah, H., Carmona-Fontaine, C., Rustenburg, A. S. *et al.* L-2-hydroxyglutarate production arises from noncanonical enzyme function at acidic pH. *Nat Chem Biol* **13**, 494 (2017).

31 Koivunen, P., Lee, S., Duncan, C. G., Lopez, G., Lu, G., Ramkissoon, S. *et al.* Transformation by the (R)-enantiomer of 2-hydroxyglutarate linked to EGLN activation. *Nature* **483**, 484 (2012).

32 Xu, W., Yang, H., Liu, Y., Yang, Y., Wang, P., Kim, S. H. *et al.* Oncometabolite 2-hydroxyglutarate is a competitive inhibitor of alpha-ketoglutarate-dependent dioxygenases. *Cancer Cell* **19**, 17 (2011).

33 Kaelin, W. G. SDH5 mutations and familial paraganglioma: Somewhere warburg is smiling. *Cancer Cell* **16**, 180 (2009).

34 Shim, E. H., Livi, C. B., Rakheja, D., Tan, J., Benson, D., Parekh, V. *et al.* L-2-hydroxyglutarate: an epigenetic modifier and putative oncometabolite in renal cancer. *Cancer Discov* **4**, 1290 (2014).

35 Latini, A., Scussiato, K., Rosa, R. B., Llesuy, S., Bello-Klein, A., Dutra-Filho, C. S. *et al.* D-2-hydroxyglutaric acid induces oxidative stress in cerebral cortex of young rats. *Eur J Neurosci* **17**, 2017 (2003).

36 Mohrenz, I. V., Antonietti, P., Pusch, S., Capper, D., Balss, J., Voigt, S. *et al.* Isocitrate dehydrogenase 1 mutant R132H sensitizes glioma cells to BCNU-induced oxidative stress and cell death. *Apoptosis* **18**, 1416 (2013).

37 Forni, L. G. & Willson, R. L. Thiyl and phenoxyl free radicals and NADH. Direct observation of one-electron oxidation. *Biochem J* **240**, 897 (1986).

38 Sulkowski, P. L., Corso, C. D., Robinson, N. D., Scanlon, S. E., Purshouse, K. R., Bai, H. *et al.* 2-hydroxyglutarate produced by neomorphic IDH mutations suppresses homologous recombination and induces PARP inhibitor sensitivity. *Sci Transl Med* **9**, 1 (2017).

39 Losman, J. A., Looper, R. E., Koivunen, P., Lee, S., Schneider, R. K., McMahon, C. *et al.* (R)-2-hydroxyglutarate is sufficient to promote leukemogenesis and its effects are reversible. *Science* **339**, 1621 (2013).

40 Ma, S., Jiang, B., Deng, W., Gu, Z.-K., Wu, F.-Z., Li, T. *et al.* D-2-hydroxyglutarate is essential for maintaining oncogenic property of mutant IDH-containing cancer cells but dispensable for cell growth. *Oncotarget* **6**, 8606 (2015).

41 van den Bent, M. J., Dubbink, H. J., Marie, Y., Brandes, A. A., Taphoorn, M. J., Wesseling, P. *et al.* IDH1 and IDH2 mutations are prognostic but not predictive for outcome in anaplastic oligodendroglial tumors: a report of the european organization for research and treatment of cancer brain tumor group. *Clin Cancer Res* **16**, 1597 (2010).

42 Boissel, N., Nibourel, O., Renneville, A., Huchette, P., Dombret, H. & Preudhomme, C. Differential prognosis impact of IDH2 mutations in cytogenetically normal acute myeloid leukemia. *Blood* **117**, 3696 (2011).

43 DiNardo, C. D., Ravandi, F., Agresta, S., Konopleva, M., Takahashi, K., Kadia, T. *et al.* Characteristics, clinical outcome and prognostic significance of IDH mutations in AML. *Am J Hematol* **90**, 732 (2015).

44 Green, C. L., Evans, C. M., Zhao, L., Hills, R. K., Burnett, A. K., Linch, D. C. *et al.* The prognostic significance of IDH2 mutations in AML depends on the location of the mutation. *Blood* **118**, 409 (2011).

45 Patel, J. P., Gonen, M., Figueroa, M. E., Fernandez, H., Sun, Z., Racevskis, J. *et al.* Prognostic relevance of integrated genetic profiling in acute myeloid leukemia. *New Engl J Med* **366**, 1079 (2012).

46 Böttcher, M., Renner, K., Berger, R., Mentz, K., Thomas, S., Cardenas-Conejo, Z. E. *et al.* D-2-hydroxyglutarate interferes with HIF-1α stability skewing T-cell metabolism towards oxidative phosphorylation and impairing Th17 polarization. *Oncoimmunology* **7**, e1445454 (2018).

47 Kohanbash, G., Carrera, D. A., Shrivastav, S., Ahn, B. J., Jahan, N., Mazor, T. *et al.* Isocitrate dehydrogenase mutations suppress STAT1 and CD8+ T cell accumulation in gliomas. *J Clin Invest* **127**, 1425 (2017).

48 Zhang, X., Rao, A., Sette, P., Deibert, C., Pomerantz, A., Kim, W. J. *et al.* IDH mutant gliomas escape natural killer cell immune surveillance by downregulation of NKG2D ligand expression. *Neuro Oncol* **18**, 1402 (2016).

49 Linster, C. L., Van Schaftingen, E. & Hanson, A. D. Metabolite damage and its repair or pre-emption. *Nat Chem Biol* **9**, 72 (2013).

50 Briggs, G. E. & Haldane, J. B. A note on the kinetics of enzyme action. *Biochem J* **19**, 338 (1925).

51 Michaelis, L., Menten, M. L. . Die Kinetik der Invertinwirkung. *Biochemische Zeitung* **49**, 333 (1913).

52 Bisswanger, H. Enzyme assays. *Perspectives in Science* **1**, 41 (2014).

53 Chan, P., Lovrić, J. & Warwicker, J. Subcellular pH and predicted pH-dependent features of proteins. *Proteomics* **6**, 3494 (2006).

54 Talley, K. & Alexov, E. On the pH-optimum of activity and stability of proteins. *Proteins* **78**, 2699 (2010).

55 Balss, J., Pusch, S., Beck, A.-C., Herold-Mende, C., Krämer, A., Thiede, C. *et al.* Enzymatic assay for quantitative analysis of D-2-hydroxyglutarate. *Acta Neuropathol* **124**, 883 (2012).

56 Mann, M. & Jensen, O. N. Proteomic analysis of post-translational modifications. *Nat Biotechnol* **21**, 255 (2003).

57 Zhao, Y. & Jensen, O. N. Modification-specific proteomics: Strategies for characterization of post-translational modifications using enrichment techniques. *Proteomics* **9**, 4632 (2009).

58 Oliver, S. G., Winson, M. K., Kell, D. B. & Baganz, F. Systematic functional analysis of the yeast genome. *Trends Biotechnol* **16**, 373 (1998).

59 Fiehn, O. Metabolomics – the link between genotypes and phenotypes. *Plant Mol Biol* **48**, 155 (2002).

60 Bino, R. J., Hall, R. D., Fiehn, O., Kopka, J., Saito, K., Draper, J. *et al.* Potential of metabolomics as a functional genomics tool. *Trends Plant Sci* **9**, 418 (2004).

61 Nicholson, J. K., Connelly, J., Lindon, J. C. & Holmes, E. Metabonomics: a platform for studying drug toxicity and gene function. *Nat Rev Drug Discov* **1**, 153 (2002).

62 Nicholson, J. K. & Wilson, I. D. Understanding ´global` systems biology: Metabonomics and the continuum of metabolism. *Nat Rev Drug Discov* **2**, 668 (2003).

63 Ward, J. L., Harris, C., Lewis, J. & Beale, M. H. Assessment of 1H NMR spectroscopy and multivariate analysis as a technique for metabolite fingerprinting of Arabidopsis thaliana. *Phytochemistry* **62**, 949 (2003).

64 Kebarle, P. & Tang, L. From ions in solution to ions in the gas phase - the mechanism of electrospray mass spectrometry. *Anal Chem* **65**, 972A (1993).

65 Matuszewski, B. K., Constanzer, M. L. & Chavez-Eng, C. M. Matrix effect in quantitative LC/MS/MS analyses of biological fluids: a method for determination of finasteride in human plasma at picogram per milliliter concentrations. *Anal Chem* **70**, 882 (1998).

66 Schmitz, O. in *The HPLC Expert: Possibilities and Limitations of Modern High Performance Liquid Chromatography* (ed S. Kromidas) Ch. 1, 1 Wiley (2016).

67 Dettmer, K. & Hammock, B. D. Metabolomics-a new exciting field within the "omics" sciences. *Environ Health Persp* **112**, A396 (2004).

68 Lu, W., Bennett, B. D. & Rabinowitz, J. D. Analytical strategies for LC-MS-based targeted metabolomics. *Journal Chromatogr B* **871**, 236 (2008).

69 Dyson, N. Peak distortion, data sampling errors and the integrator in the measurement of very narrow chromatographic peaks. *Journal Chromatogr A* **842**, 321 (1999).

70 Cech, N. B. & Enke, C. G. Practical implications of some recent studies in electrospray ionization fundamentals. *Mass Spectrom Rev* **20**, 362 (2002).

71 Lawson, A. M. The scope of mass spectrometry in clinical chemistry. *Clin Chem* **21**, 803 (1975).

72 Rittenberg, D. F., G.L. A new procedure for quantitative analysis by isotope dilution, with application to the determination of amino acids and fatty acids. *J Biol Chem* **133**, 737 (1940).

73 Samuelsson, B., Hamberg, M. & Sweeley, C. C. Quantitative gas chromatography of prostaglandin E1 at the nanogram level: Use of deuterated carrier and multiple-ion analyzer. *Anal Biochem* **38**, 301 (1970).

74 Pigini, D., Cialdella, A. M., Faranda, P. & Tranfo, G. Comparison between external and internal standard calibration in the validation of an analytical method for 1-hydroxypyrene in human urine by high-performance liquid chromatography/tandem mass spectrometry. *Rapid Commun Mass Sp* **20**, 1013 (2006).

75 Rychlik, M. & Asam, S. Stable isotope dilution assays in mycotoxin analysis. *Anal Bioanal Chem* **390**, 617 (2008).

76 Henneberg, D. Eine Kombination von Graschromatograph und Massenspektrometer zur Analyse organischer Stoffgemische. *Fresenius' Zeitschrift für analytische Chemie* **183**, 12 (1961).

77 Sweeley, C. C., Elliott, W. H., Fries, I. & Ryhage, R. Mass spectrometric determination of unresolved components in gas chromatographic effluents. *Anal Chem* **38**, 1549 (1966).

78 U.S. Department of Health and Human Services - Food and Drug Administration. Bioanalytical method validation guidance for industry. (2018).

79 Gibson, K. M., Ten Brink, H. J., Schor, D. S. M., Kok, R. M., Bootsma, A. H., Hoffmann, G. F. *et al.* Stable-isotope dilution analysis of D- and L-2-hydroxyglutaric acid: application to the detection and prenatal diagnosis of D- and L-2-hydroxyglutaric acidemias. *Pediatr Res* **34**, 277 (1993).

80 Struys, E. A., Jansen, E. E. W., Verhoeven, N. M. & Jakobs, C. Measurement of urinary D- and L-2-hydroxyglutarate enantiomers by stable-isotope-dilution liquid chromatography–tandem mass spectrometry after derivatization with diacetyl-L-tartaric anhydride. *Clin Chem* **50**, 1391 (2004).

81 Kamerling, J. P., Duran, M., Gerwig, G. J., Ketting, D., Bruinvis, L., Vliegenthart, J. F. *et al.* Determination of the absolute configuration of some biologically important urinary 2-hydroxydicarboxylic acids by capillary gas-liquid chromatography. *J Chromatogr* **222**, 276 (1981).

82 Janin, M., Mylonas, E., Saada, V., Micol, J.-B., Renneville, A., Quivoron, C. *et al.* Serum 2-hydroxyglutarate production in IDH1- and IDH2-mutated de novo acute myeloid leukemia: A study by the acute leukemia french association group. *J Clin Oncol* **32**, 297 (2014).

83 Poinsignon, V., Mercier, L., Nakabayashi, K., David, M. D., Lalli, A., Penard-Lacronique, V. *et al.* Quantitation of isocitrate dehydrogenase (IDH)-induced D and L enantiomers of 2-hydroxyglutaric acid in biological fluids by a fully validated liquid tandem mass spectrometry method, suitable for clinical applications. *Journal Chromatogr B* **1022**, 290 (2016).

84 Delahousse, J., Verlingue, L., Broutin, S., Legoupil, C., Touat, M., Doucet, L. *et al.* Circulating oncometabolite D-2-hydroxyglutarate enantiomer is a surrogate marker of isocitrate dehydrogenase–mutated intrahepatic cholangiocarcinomas. *Eur J Cancer* **90**, 83 (2018).

85 Juratli, T. A., Peitzsch, M., Geiger, K., Schackert, G., Eisenhofer, G. & Krex, D. Accumulation of 2-hydroxyglutarate is not a biomarker for malignant progression in IDH-mutated low-grade gliomas. *Neuro Oncol* **15**, 682 (2013).

86 Navis, A. C., Niclou, S. P., Fack, F., Stieber, D., van Lith, S., Verrijp, K. *et al.* Increased mitochondrial activity in a novel IDH1-R132H mutant human oligodendroglioma xenograft model: in situ detection of 2-HG and α-KG. *Acta Neuropathol Commun* **1**, 18 (2013).

87 Borger, D. R., Goyal, L., Yau, T., Poon, R. T., Ancukiewicz, M., Deshpande, V. *et al.* Circulating oncometabolite 2-hydroxyglutarate is a potential surrogate biomarker in

patients with isocitrate dehydrogenase-mutant intrahepatic cholangiocarcinoma. *Clin Cancer Res* **20**, 1884 (2014).

88 Alpert, A. J. Hydrophilic-interaction chromatography for the separation of peptides, nucleic acids and other polar compounds. *Journal Chromatogr A* **499**, 177 (1990).

89 Gelman, S. J., Mahieu, N. G., Cho, K., Llufrio, E. M., Wencewicz, T. A. & Patti, G. J. Evidence that 2-hydroxyglutarate is not readily metabolized in colorectal carcinoma cells. *Cancer Metab* **3**, 13 (2015).

90 Becker-Kettern, J., Paczia, N., Conrotte, J. F., Kay, D. P., Guignard, C., Jung, P. P. *et al.* Saccharomyces cerevisiae forms D-2-hydroxyglutarate and couples its degradation to D-lactate formation via a cytosolic transhydrogenase. *J Biol Chem* **291**, 6036 (2016).

91 Bal, D. & Gryff-Keller, A. 1H and 13C NMR study of 2-hydroxyglutaric acid and its lactone. *Magn Reson Chem* **40**, 533 (2002).

92 Voelxen, N. F., Walenta, S., Proescholdt, M., Dettmer, K., Pusch, S. & Mueller-Klieser, W. Quantitative imaging of D-2-hydroxyglutarate in selected histological tissue areas by a novel bioluminescence technique. *Front Oncol* **6**, 46 (2016).

93 Longuespée, R., Wefers, A. K., De Vita, E., Miller, A. K., Reuss, D. E., Wick, W. *et al.* Rapid detection of 2-hydroxyglutarate in frozen sections of IDH mutant tumors by MALDI-TOF mass spectrometry. *Acta Neuropathol Commun* **6**, 21 (2018).

94 Stephanopoulos, G. Metabolic fluxes and metabolic engineering. *Metab Eng* **1**, 1 (1999).

95 Leighty, R. W. & Antoniewicz, M. R. Dynamic metabolic flux analysis (DMFA): a framework for determining fluxes at metabolic non-steady state. *Metab Eng* **13**, 745 (2011).

96 Wiechert, W. 13C metabolic flux analysis. *Metab Eng* **3**, 195 (2001).

97 Buescher, J. M., Antoniewicz, M. R., Boros, L. G., Burgess, S. C., Brunengraber, H., Clish, C. B. *et al.* A roadmap for interpreting (13)C metabolite labeling patterns from cells. *Curr Opin Biotechnol* **34**, 189 (2015).

98 Ahn, W. S. & Antoniewicz, M. R. Metabolic flux analysis of CHO cells at growth and non-growth phases using isotopic tracers and mass spectrometry. *Metab Eng* **13**, 598 (2011).

99 Wittmann, C. & Heinzle, E. Mass spectrometry for metabolic flux analysis. *Biotechnol Bioeng* **62**, 739 (2000).

100 Nanchen, A., Fuhrer, T. & Sauer, U. in *Metabolomics: Methods and Protocols* (ed Wolfram Weckwerth) 177 Humana Press (2007).

101 Kamphorst, J. J., Chung, M. K., Fan, J. & Rabinowitz, J. D. Quantitative analysis of acetyl-CoA production in hypoxic cancer cells reveals substantial contribution from acetate. *Cancer Metab* **2**, 23 (2014).

102 Lee, W. N., Boros, L. G., Puigjaner, J., Bassilian, S., Lim, S. & Cascante, M. Mass isotopomer study of the nonoxidative pathways of the pentose cycle with [1,2-13C2]glucose. *Am J Physiol* **274**, E843 (1998).

103 Chokkathukalam, A., Kim, D.-H., Barrett, M. P., Breitling, R. & Creek, D. J. Stable isotope-labeling studies in metabolomics: new insights into structure and dynamics of metabolic networks. *Bioanalysis* **6**, 511 (2014).

104 Lewis, C. A., Parker, S. J., Fiske, B. P., McCloskey, D., Gui, D. Y., Green, C. R. *et al.* Tracing compartmentalized NADPH metabolism in the cytosol and mitochondria of mammalian cells. *Mol Cell* **55**, 253 (2014).

105 Letisse, F., Portais, J.-C., Millard, P. & Sokol, S. IsoCor: correcting MS data in isotope labeling experiments. *Bioinformatics* **28**, 1294 (2012).

106 Heinrich, P., Kohler, C., Ellmann, L., Kuerner, P., Spang, R., Oefner, P. J. *et al.* Correcting for natural isotope abundance and tracer impurity in MS-, MS/MS- and high-resolution-multiple-tracer-data from stable isotope labeling experiments with IsoCorrectoR. *Sci Rep* **8**, 17910 (2018).

107 Dietl, K., Renner, K., Dettmer, K., Timischl, B., Eberhart, K., Dorn, C. *et al.* Lactic acid and acidification inhibit TNF secretion and glycolysis of human monocytes. *J Immunol* **184**, 1200 (2010).

108 van der Goot, A. T., Zhu, W., Vázquez-Manrique, R. P., Seinstra, R. I., Dettmer, K., Michels, H. *et al.* Delaying aging and the aging-associated decline in protein homeostasis by inhibition of tryptophan degradation. *P Natl Acad Sci USA* **109**, 14912 (2012).

109 Berger, R. S., Ellmann, L., Reinders, J., Kreutz, M., Stempfl, T., Oefner, P. J. *et al.* Degradation of D-2-hydroxyglutarate in the presence of isocitrate dehydrogenase mutations. *Sci Rep* **9**, 7436 (2019).

110 Achouri, Y., Noel, G., Vertommen, D., Rider, M. H., Veiga-Da-Cunha, M. & Van Schaftingen, E. Identification of a dehydrogenase acting on D-2-hydroxyglutarate. *Biochem J* **381**, 35 (2004).

111 Wickenhagen, W. V., Salomons, G. S., Gibson, K. M., Jakobs, C. & Struys, E. A. Measurement of d-2-hydroxyglutarate dehydrogenase activity in cell homogenates derived from d-2-hydroxyglutaric aciduria patients. *J Inherit Metab Dis* **32**, 264 (2009).

112 Han, J., Jackson, D., Holm, J., Turner, K., Ashcraft, P., Wang, X. *et al.* Elevated D-2-hydroxyglutarate during colitis drives progression to colorectal cancer. *P Natl Acad Sci USA* **115**, 1057 (2018).

113 Kaunzinger, A., Rechner, A., Beck, T., Mosandl, A., Sewell, A. C. & Bohles, H. Chiral compounds as indicators of inherited metabolic disease. Simultaneous stereodifferentiation of lactic-, 2-hydroxyglutaric- and glyceric acid by enantioselective cGC. *Enantiomer* **1**, 177 (1996).

114 Weibel, D. B., Walker, T. R., Schroeder, F. C. & Meinwald, J. Chiral silylation reagents for the determination of absolute configuration by NMR spectroscopy. *Org Lett* **2**, 2381 (2000).

115 Ding, X., Lin, S., Weng, H. & Liang, J. Separation and determination of the enantiomers of lactic acid and 2-hydroxyglutaric acid by chiral derivatization combined with gas chromatography and mass spectrometry. *J Sep Sci* **41**, 2576 (2018).

116 Cheng, Q.-Y., Xiong, J., Huang, W., Ma, Q., Ci, W., Feng, Y.-Q. *et al.* Sensitive determination of onco-metabolites of D- and L-2-hydroxyglutarate enantiomers by

chiral derivatization combined with liquid chromatography/mass spectrometry analysis. *Sci Rep* **5**, 15217 (2015).

117 Tsutsui, H., Mochizuki, T., Maeda, T., Noge, I., Kitagawa, Y., Min, J. Z. *et al.* Simultaneous determination of DL-lactic acid and DL-3-hydroxybutyric acid enantiomers in saliva of diabetes mellitus patients by high-throughput LC-ESI-MS/MS. *Anal Bioanal Chem* **404**, 1925 (2012).

118 Rashed, M. S., AlAmoudi, M. & Aboul-Enein, H. Y. Chiral liquid chromatography tandem mass spectrometry in the determination of the configuration of 2-hydroxyglutaric acid in urine. *Biomed Chromatogr* **14**, 317 (2000).

119 Calderón, C., Horak, J. & Lämmerhofer, M. Chiral separation of 2-hydroxyglutaric acid on cinchonan carbamate based weak chiral anion exchangers by high-performance liquid chromatography. *Journal Chromatogr A* **1467**, 239 (2016).

120 Dwivedi, P., Wu, C., Matz, L. M., Clowers, B. H., Siems, W. F. & Hill, H. H., Jr. Gas-phase chiral separations by ion mobility spectrometry. *Anal Chem* **78**, 8200 (2006).

121 Simó, C., García-Cañas, V. & Cifuentes, A. Chiral CE-MS. *Electrophoresis* **31**, 1442 (2010).

122 Shamsi, S. A. Chiral capillary electrophoresis-mass spectrometry: Modes and applications. *Electrophoresis* **23**, 4036 (2002).

123 Pritchard, J. B. Intracellular alpha-ketoglutarate controls the efficacy of renal organic anion transport. *J Pharmacol Exp Ther* **274**, 1278 (1995).

124 Yang, H., Ye, D., Guan, K.-L. & Xiong, Y. IDH1 and IDH2 mutations in tumorigenesis: mechanistic insights and clinical perspectives. *Clin Cancer Res* **18**, 5562 (2012).

125 Cairns, R. A. & Mak, T. W. Oncogenic isocitrate dehydrogenase mutations: mechanisms, models, and clinical opportunities. *Cancer Discov* **3**, 730 (2013).

126 Owen, O. E., Kalhan, S. C. & Hanson, R. W. The key role of anaplerosis and cataplerosis for citric acid cycle function. *J Biol Chem* **277**, 30409 (2002).

127 Zhang, Z., Chen, L., Liu, L., Su, X. & Rabinowitz, J. D. Chemical basis for deuterium labeling of fat and NADPH. *J Am Chem Soc* **139**, 14368 (2017).

128 Brekke, E., Walls, A. B., Norfeldt, L., Schousboe, A., Waagepetersen, H. S. & Sonnewald, U. Direct measurement of backflux between oxaloacetate and fumarate following pyruvate carboxylation. *Glia* **60**, 147 (2012).

129 Magnusson, I., Schumann, W. C., Bartsch, G. E., Chandramouli, V., Kumaran, K., Wahren, J. *et al.* Noninvasive tracing of Krebs cycle metabolism in liver. *J Biol Chem* **266**, 6975 (1991).

130 Izquierdo-Garcia, J. L., Cai, L. M., Chaumeil, M. M., Eriksson, P., Robinson, A. E., Pieper, R. O. *et al.* Glioma cells with the IDH1 mutation modulate metabolic fractional flux through pyruvate carboxylase. *Plos One* **9**, e108289 (2014).

131 Groen, A. K., Sips, H. J., Vervoorn, R. C. & Tager, J. M. Intracellular compartmentation and control of alanine metabolism in rat liver parenchymal cells. *Eur J Biochem* **122**, 87 (1982).

132 Ohka, F., Ito, M., Ranjit, M., Senga, T., Motomura, A., Motomura, K. *et al.* Quantitative metabolome analysis profiles activation of glutaminolysis in glioma with IDH1 mutation. *Tumour Biol* **35**, 5911 (2014).

133 Grassian, A. R., Parker, S. J., Davidson, S. M., Divakaruni, A. S., Green, C. R., Zhang, X. *et al.* IDH1 mutations alter citric acid cycle metabolism and increase dependence on oxidative mitochondrial metabolism. *Cancer Res* **74**, 3317 (2014).

134 Seltzer, M. J., Bennett, B. D., Joshi, A. D., Gao, P., Thomas, A. G., Ferraris, D. V. *et al.* Inhibition of glutaminase preferentially slows growth of glioma cells with mutant IDH1. *Cancer Res* **70**, 8981 (2010).

135 Mustafa, D. A., Swagemakers, S. M., Buise, L., van der Spek, P. J. & Kros, J. M. Metabolic alterations due to IDH1 mutation in glioma: opening for therapeutic opportunities? *Acta Neuropathol Commun* **2**, 6 (2014).

136 Gelman, S. J., Naser, F., Mahieu, N. G., McKenzie, L. D., Dunn, G. P., Chheda, M. G. *et al.* Consumption of NADPH for 2-HG synthesis ncreases pentose phosphate pathway flux and sensitizes cells to oxidative stress. *Cell Rep* **22**, 512 (2018).

137 Badur, M. G., Muthusamy, T., Parker, S. J., Ma, S., McBrayer, S. K., Cordes, T. *et al.* Oncogenic R132 IDH1 mutations limit NADPH for de novo lipogenesis through D-2-hydroxyglutarate production in fibrosarcoma cells. *Cell Rep* **25**, 1018 (2018).

138 Molenaar, R. J., Botman, D., Smits, M. A., Hira, V. V., van Lith, S. A., Stap, J. *et al.* Radioprotection of IDH1-mutated cancer cells by the IDH1-mutant inhibitor AGI-5198. *Cancer Res* **75**, 4790 (2015).

139 Bleeker, F. E., Atai, N. A., Lamba, S., Jonker, A., Rijkeboer, D., Bosch, K. S. *et al.* The prognostic IDH1R132mutation is associated with reduced NADP+-dependent IDH activity in glioblastoma. *Acta Neuropathol* **119**, 487 (2010).

140 Molenaar, R. J., Radivoyevitch, T., Maciejewski, J. P., van Noorden, C. J. F. & Bleeker, F. E. The driver and passenger effects of isocitrate dehydrogenase 1 and 2 mutations in oncogenesis and survival prolongation. *BBA - Rev Cancer* **1846**, 326 (2014).

141 Hollinshead, K. E. R., Munford, H., Eales, K. L., Bardella, C., Li, C., Escribano-Gonzalez, C. *et al.* Oncogenic IDH1 mutations promote enhanced proline synthesis through PYCR1 to support the maintenance of mitochondrial redox homeostasis. *Cell Rep* **22**, 3107 (2018).

142 Fendt, S. M., Bell, E. L., Keibler, M. A., Olenchock, B. A., Mayers, J. R., Wasylenko, T. M. *et al.* Reductive glutamine metabolism is a function of the alpha-ketoglutarate to citrate ratio in cells. *Nat Commun* **4**, 2236 (2013).

143 Mullen, A. R., Wheaton, W. W., Jin, E. S., Chen, P. H., Sullivan, L. B., Cheng, T. *et al.* Reductive carboxylation supports growth in tumour cells with defective mitochondria. *Nature* **481**, 385 (2011).

144 Khurshed, M., Molenaar, R. J., Lenting, K., Leenders, W. P. & van Noorden, C. J. F. In silico gene expression analysis reveals glycolysis and acetate anaplerosis in IDH1 wild-type glioma and lactate and glutamate anaplerosis in IDH1-mutated glioma. *Oncotarget* **8**, 49165 (2017).

145 Chesnelong, C., Chaumeil, M. M., Blough, M. D., Al-Najjar, M., Stechishin, O. D., Chan, J. A. *et al.* Lactate dehydrogenase A silencing in IDH mutant gliomas. *Neuro Oncol* **16**, 686 (2014).

146 Viswanath, P., Najac, C., Izquierdo-Garcia, J. L., Pankov, A., Hong, C., Eriksson, P. *et al.* Mutant IDH1 expression is associated with down-regulation of monocarboxylate transporters. *Oncotarget* **7**, 34942 (2016).

147 DiNardo, C. D., Propert, K. J., Loren, A. W., Paietta, E., Sun, Z., Levine, R. L. *et al.* Serum 2-hydroxyglutarate levels predict isocitrate dehydrogenase mutations and clinical outcome in acute myeloid leukemia. *Blood* **121**, 4917 (2013).

148 Fathi, A. T., Sadrzadeh, H., Borger, D. R., Ballen, K. K., Amrein, P. C., Attar, E. C. *et al.* Prospective serial evaluation of 2-hydroxyglutarate, during treatment of newly diagnosed acute myeloid leukemia, to assess disease activity and therapeutic response. *Blood* **120**, 4649 (2012).

149 Pollyea, D. A., Kohrt, H. E., Zhang, B., Zehnder, J., Schenkein, D., Fantin, V. *et al.* 2-Hydroxyglutarate in IDH mutant acute myeloid leukemia: predicting patient responses, minimal residual disease and correlations with methylcytosine and hydroxymethylcytosine levels. *Leuk Lymphoma* **54**, 408 (2013).

150 Hagos, Y., Krick, W., Braulke, T., Muhlhausen, C., Burckhardt, G. & Burckhardt, B. C. Organic anion transporters OAT1 and OAT4 mediate the high affinity transport of glutarate derivatives accumulating in patients with glutaric acidurias. *Pflugers Arch* **457**, 223 (2008).

151 Mühlhausen, C., Burckhardt, B. C., Hagos, Y., Burckhardt, G., Keyser, B., Lukacs, Z. *et al.* Membrane translocation of glutaric acid and its derivatives. *J Inherit Metab Dis* **31**, 188 (2008).

152 Thing Mortensen, B., Østrup Jensen, P., Helledie, N., Ole Iversen, P., RalfkiÆR, E., Knud Larsen, J. *et al.* Changing bone marrow micro-environment during development of acute myeloid leukaemia in rats. *Br J Haematol* **102**, 458 (2001).

153 Ohkuma, S., Moriyama, Y. & Takano, T. Identification and characterization of a proton pump on lysosomes by fluorescein-isothiocyanate-dextran fluorescence. *P Natl Acad Sci USA* **79**, 2758 (1982).

154 Havelaar, A. C., Beerens, C. E. M. T., Mancini, G. M. S. & Verheijen, F. W. Transport of organic anions by the lysosomal sialic acid transporter: a functional approach towards the gene for sialic acid storage disease. *FEBS Lett* **446**, 65 (1999).

155 Verheijen, F. W., Verbeek, E., Aula, N., Beerens, C. E. M. T., Havelaar, A. C., Joosse, M. *et al.* A new gene, encoding an anion transporter, is mutated in sialic acid storage diseases. *Nat Genetics* **23**, 462 (1999).

156 Mindell, J. A. Lysosomal acidification mechanisms. *Annu Rev Physiol* **74**, 69 (2012).

157 Sardiello, M., Palmieri, M., di Ronza, A., Medina, D. L., Valenza, M., Gennarino, V. A. *et al.* A gene network regulating lysosomal biogenesis and function. *Science* **325**, 473 (2009).

158 Linster, C. L. & Van Schaftingen, E. Vitamin C. *FEBS J* **274**, 1 (2006).

159 Mochizuki, K. Purification and characterization of a lactonase from Burkholderia sp. R-711, that hydrolyzes (R)-5-oxo-2-tetrahydrofurancarboxylic acid. *Arch Microbiol* **175**, 430 (2001).

160 Marchiq, I., Le Floch, R., Roux, D., Simon, M. P. & Pouyssegur, J. Genetic disruption of lactate/H+ symporters (MCTs) and their subunit CD147/BASIGIN sensitizes glycolytic tumor cells to phenformin. *Cancer Research* **75**, 171 (2015).

161 Jain, M., Nilsson, R., Sharma, S., Madhusudhan, N., Kitami, T., Souza, A. L. *et al.* Metabolite profiling identifies a key role for glycine in rapid cancer cell proliferation. *Science* **336**, 1040 (2012).

12 Supplement

12.1 Supplemental Figures

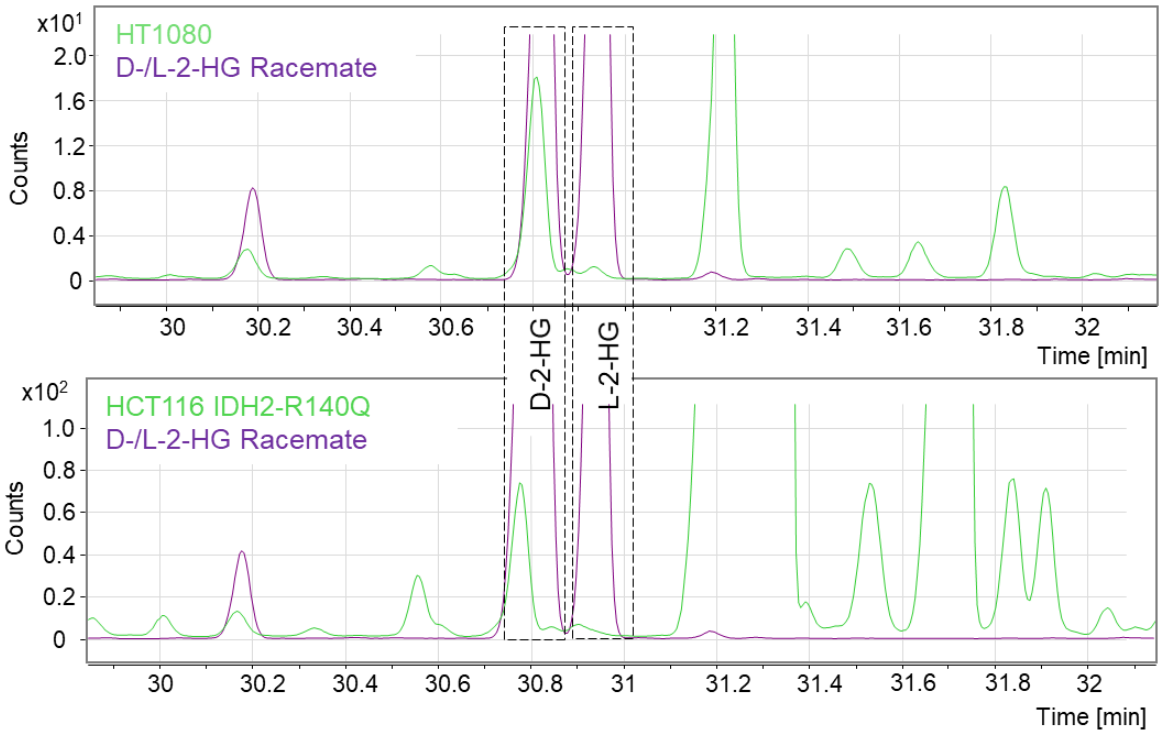

Supplemental Figure S 1. Chiral analysis of extracts of HT1080 and HCT116 IDH2-R140Q cells reveals that D-2-HG is the dominant enantiomer, while L-2-HG is present only at trace levels. Samples were derivatized as described in chapter 5.5.5. Purple lines represent standard samples, green line cell extracts.

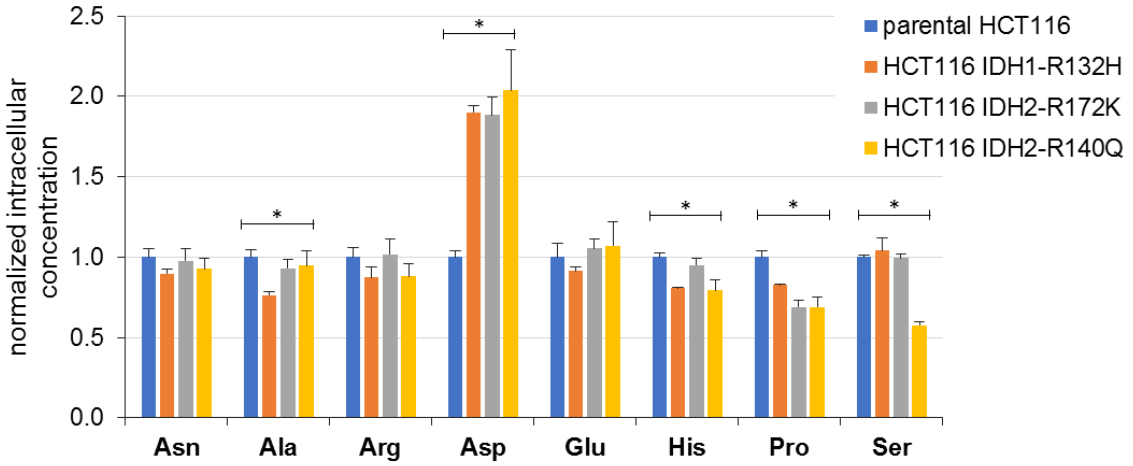

Supplemental Figure S 2. Intracellular levels of selected amino acids in the HCT116 panel (normalized to parental HCT116; n=2-3). Stars indicate significant p-values from ANOVA. Further statistics see Supplemental Table S 6).I

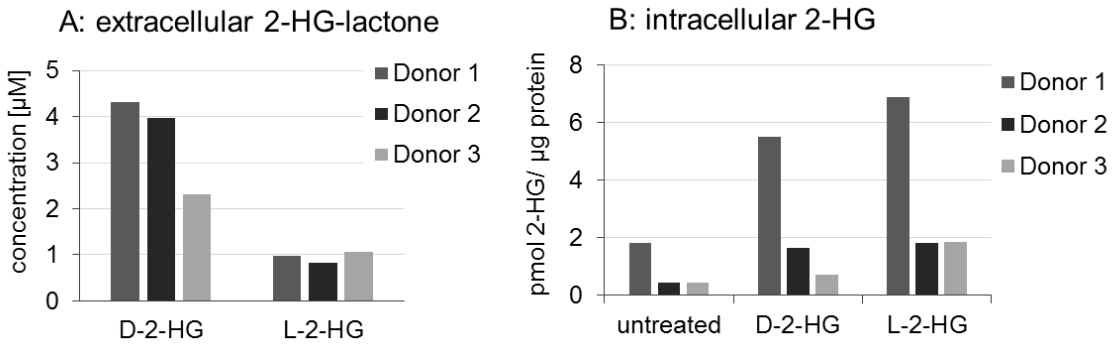

Supplemental Figure S 3. Primary macrophages of three different donors (bars represent n=1) were treated with 1 mM D- and L-2-HG, respectively. ***A)*** *Extracellular 2-HG-lactone levels were hardly detectable and equal to <0.5% of 1 mM 2-HG. In untreated cells 2-HG-lactone is below LLOQ.* ***B)*** *Intracellular 2-HG levels in treated cells tend to be higher compared to untreated, indicating uptake of D-/L-2-HG (paired t-test (treated vs untreated): $p_{D\text{-}2\text{-}HG}$ =0.1175, $p_{L\text{-}2\text{-}HG}$ =0.0825). 2-HG-lactone was not detected here.*

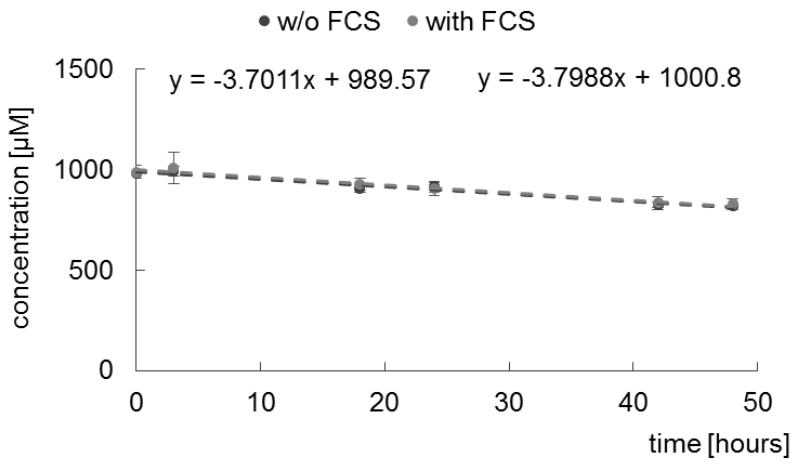

Supplemental Figure S 4. 1000 µM D-2-HG-lactone was spiked into RPMI medium with (heat-inactivated) and without FCS and incubated for 48 h. Shown here is the decrease in D-2-HG-lactone concentration, which is due to spontaneous hydrolysis. On the opposite, 2-HG concentrations increases in the same fashion (not shown). Hydrolysis by an serum esterase from FCS can be excluded, as medium with and without FCS do not differ in their hydrolysis rate. This figure was prepared on preliminary data, kindly provided by K. Dettmer.

12.2 Supplemental Tables

Supplemental Table S 1. Mean enrichment in intracellular TCA-intermediates and 2-HG/-lactone from $^{13}C_6$-glucose tracing in HCT116 cells. A one-way ANOVA was used to determine whether there are significant differences in mean enrichment between metabolites, while p_{adj} for pairwaise comparisons were computed using Tukey's HSD (n=3).

	Parental	IDH1-R132H	IDH2-R172K	IDH2-R140Q
Lactate ANOVA $p=2.15*10^{-3}$				
Parental		$1.80*10^{-3}$		
IDH1-R132H			$7.46*10^{-3}$	$3.48*10^{-2}$
IDH2-R172K				
IDH2-R140Q				
Citrate ANOVA $p=6.26*10^{-6}$				
Parental		$5.70*10^{-6}$	$8.84*10^{-5}$	$2.65*10^{-5}$
IDH1-R132H			$1.73*10^{-2}$	
IDH2-R172K				
IDH2-R140Q				
α-Ketoglutarate ANOVA $p=4.36*10^{-6}$				
Parental		$3.0*10^{-6}$	$4.45*10^{-5}$	$7.42*10^{-5}$
IDH1-R132H			$1.25*10^{-2}$	$5.37*10^{-3}$
IDH2-R172K				
IDH2-R140Q				
2-Hydroxyglutarate ANOVA p=0.034				
Parental				
IDH1-R132H				
IDH2-R172K				$3.15*10^{-2}$
IDH2-R140Q				
2-HG-lactone ANOVA p=0.056 ([1])				
Succinate ANOVA p=0.087				
Fumarate ANOVA $p=5.68*10^{-7}$				
Parental		$4.0*10^{-7}$	$1.03*10^{-5}$	$3.20*10^{-6}$
IDH1-R132H			$1.60*10^{-3}$	$1.95*10^{-2}$
IDH2-R172K				
IDH2-R140Q				
Malate ANOVA $p=4.29*10^{-7}$				
Parental		$3.0*10^{-7}$	$1.35*10^{-5}$	$2.10*10^{-6}$
IDH1-R132H			$5.56*10^{-4}$	$2.69*10^{-2}$
IDH2-R172K				$4.53*10^{-2}$
IDH2-R140Q				

([1]) Intracellular 2-HG-lactone concentrations are generally low abundant and mean isotopic enrichment from $^{13}C_6$-glucose into 2-HG as the precursor is already low. Therefore, signals for

2-HG-lactone isotopologues are rather close to the noise level and differences are not significant.

Supplemental Table S 2. Mean enrichment in intracellular TCA-intermediates and 2-HG/-lactone from $^{13}C_5$-glutamine tracing in HCT116 cells. A one-way ANOVA was used to determine whether there are significant differences in mean enrichment between metabolites, while p_{adj} for pairwaise comparisons were computed using Tukey's HSD (n=3).

	Parental	IDH1-R132H	IDH2-R172K	IDH2-R140Q
Citrate ANOVA $p=9.66*10^{-6}$				
Parental		$6.27*10^{-5}$	$7.35*10^{-5}$	
IDH1-R132H				$6.81*10^{-5}$
IDH2-R172K				$7.99*10^{-5}$
IDH2-R140Q				
α-Ketoglutarate ANOVA $p=6.33*10^{-5}$				
Parental		$5.12*10^{-4}$	$4.65*10^{-4}$	
IDH1-R132H				$3.92*10^{-4}$
IDH2-R172K				$3.57*10^{-4}$
IDH2-R140Q				
2-Hydroxyglutarate ANOVA $p=1.07*10^{-4}$				
Parental		$1.29*10^{-3}$	$1.63*10^{-2}$	
IDH1-R132H				$1.23*10^{-4}$
IDH2-R172K				$8.76*10^{-4}$
IDH2-R140Q				
2-HG-lactone ANOVA $p=4.08*10^{-6}$				
Parental		$2.59*10^{-5}$	$3.79*10^{-5}$	
IDH1-R132H				$2.52*10^{-5}$
IDH2-R172K				$3.67*10^{-5}$
IDH2-R140Q				
Succinate ANOVA $p=1.04*10^{-4}$				
Parental		$1.84*10^{-4}$	$1.47*10^{-3}$	
IDH1-R132H				$4.96*10^{-4}$
IDH2-R172K				$5.06*10^{-3}$
IDH2-R140Q				
Fumarate ANOVA $p=5.20*10^{-5}$				
Parental		$1.97*10^{-4}$	$6.77*10^{-4}$	
IDH1-R132H				$2.13*10^{-4}$
IDH2-R172K				$7.42*10^{-4}$
IDH2-R140Q				
Malate ANOVA $p=2.84*10^{-5}$				
Parental		$1.32*10^{-4}$	$3.35*10^{-4}$	
IDH1-R132H				$1.29*10^{-4}$
IDH2-R172K				$3.27*10^{-4}$
IDH2-R140Q				

Supplemental Table S 3. Mean isotopic enrichment in intracelluar amino acids from $^{13}C_6$-glucose tracing in HCT116 cells. A one-way ANOVA was used to determine whether there are significant differences in mean enrichment between metabolites, while p_{adj} for pairwaise comparisons were computed using Tukey's HSD (n=3).

	Parental	IDH1-R132H	IDH2-R172K	IDH2-R140Q
Alanine ANOVA $p=3.59*10^{-6}$				
Parental		$2.30*10^{-6}$	$2.24*10^{-3}$	$4.79*10^{-3}$
IDH1-R132H			$8.74*10^{-5}$	$5.26*10^{-5}$
IDH2-R172K				
IDH2-R140Q				
Serine ANOVA $p=1.91*10^{-3}$				
Parental		$2.15*10^{-3}$		
IDH1-R132H			$4.46*10^{-3}$	
IDH2-R172K				
IDH2-R140Q				
Aspartate ANOVA $p=5.4*10^{-6}$				
Parental		$4.60*10^{-6}$	$2.10*10^{-4}$	$2.44*10^{-5}$
IDH1-R132H			$2.96*10^{-3}$	
IDH2-R172K				
IDH2-R140Q				
Glutamate ANOVA $p=1.35*10^{-6}$				
Parental		$1.00*10^{-6}$		$1.05*10^{-5}$
IDH1-R132H			$2.54*10^{-3}$	$1.15*10^{-2}$
IDH2-R172K				$2.36*10^{-5}$
IDH2-R140Q				

Supplemental Table S 4. Mean isotopic enrichment in intracellular amino acids from $^{13}C_5$-glutamine tracing in HCT116 cells. A one-way ANOVA was used to determine whether there are significant differences in mean enrichment between metabolites, while p_{adj} for pairwaise comparisons were computed using Tukey's HSD (n=3).

	Parental	IDH1-R132H	IDH2-R172K	IDH2-R140Q
Alanine ANOVA $p=5.0*10^{-3}$				
Parental		$8.24*10^{-3}$		
IDH1-R132H			$7.37*10^{-3}$	$2.23*10^{-2}$
IDH2-R172K				
IDH2-R140Q				
Glutamate ANOVA $p=3.12*10^{-5}$				
Parental		$2.25*10^{-4}$	$2.41*10^{-4}$	
IDH1-R132H				$1.96*10^{-4}$
IDH2-R172K				$2.10*10^{-4}$
IDH2-R140Q				
Aspartate ANOVA $p=7.97*10^{-5}$				
Parental		$7.15*10^{-4}$	$5.50*10^{-4}$	
IDH1-R132H				$5.18*10^{-4}$
IDH2-R172K				$4.02*10^{-4}$
IDH2-R140Q				
Asparagine ANOVA $p=1.47*10^{-7}$				
Parental		$5.0*10^{-7}$		
IDH1-R132H			$2.0*10^{-7}$	$8.0*10^{-7}$
IDH2-R172K				
IDH2-R140Q				
Proline ANOVA $p=5.68*10^{-5}$				
Parental			$3.78*10^{-4}$	$8.03*10^{-4}$
IDH1-R132H			$2.06*10^{-4}$	$4.17*10^{-4}$
IDH2-R172K				
IDH2-R140Q				

Supplemental Table S 5. Significant differences in M+5 isotopologues from $^{13}C_5$-glutamine tracing for glutamate, 2-HG and α-KG. Differences in fractional abundance between metabolites were tested with one-way ANOVA, significant p_{adj} for pairwaise comparisons were computed using Tukey´s HSD (n=3).

	Parental	IDH1-R132H	IDH2-R172K	IDH2-R140Q
ANOVA	$2.07*10^{-2}$	0.054	0.332	0.860
Glu vs α-KG				
2-HG vs α-KG	$2.26*10^{-2}$			
2-HG vs Glu				

Supplemental Table S 6. Sigificant differences in intracellular amino acid concentrations: differences between cell lines were tested with ANOVA, significant p_{adj} for pairwaise comparisons are from Tukey´s HSD and Dunnett-test for aspartate for test vs. control=parental HCT116 (n=2-3).

	Parental	IDH1-R132H	IDH2-R172K	IDH2-R140Q
Alanine ANOVA $p=4.10*10^{-3}$				
Parental		$3.38*10^{-3}$		
IDH1-R132H			$2.10*10^{-2}$	$2.35*10^{-2}$
IDH2-R172K				
IDH2-R140Q				
Serine ANOVA $p=3.86*10^{-5}$				
Parental				$7.78*10^{-5}$
IDH1-R132H				$4.32*10^{-5}$
IDH2-R172K				$8.40*10^{-5}$
IDH2-R140Q				
Aspartate ANOVA $p=5.15*10^{-5}$				
Dunnett: Parental vs:		$2*10^{-4}$	$5.1*10^{-5}$	$4.2*10^{-5}$
Proline ANOVA $p=9.26*10^{-5}$				
Parental		$4.01*10^{-3}$	$1.11*10^{-4}$	$2.42*10^{-4}$
IDH1-R132H			$1.46*10^{-2}$	$2.78*10^{-2}$
IDH2-R172K				
IDH2-R140Q				
Histidine ANOVA $p=5.59*10^{-4}$				
Parental		$1.29*10^{-3}$		$1.67*10^{-3}$
IDH1-R132H			$6.91*10^{-3}$	
IDH2-R172K				$7.77*10^{-3}$
IDH2-R140Q				
Glutamate ANOVA p=0.201				
Arginine ANOVA p=0.117				
Asparagine ANOVA p=0.210				

Supplemental Table S 7. Significant differences in M+3 isotopologues from $^{13}C_6$-glucose tracing for alanine and serine. Differences in fractional abundance between metabolites were tested with ANOVA, significant p_{adj} for pairwaise comparisons are from Tukey´s HSD (n=3).

	Parental	IDH1-R132H	IDH2-R172K	IDH2-R140Q
Alanine ANOVA $p=3.80*10^{-6}$				
Parental		$2.50*10^{-6}$	$2.64*10^{-3}$	$5.91*10^{-3}$
IDH1-R132H			$8.71*10^{-5}$	$5.13*10^{-5}$
IDH2-R172K				
IDH2-R140Q				
Serine ANOVA $p=1.37*10^{-4}$				
Parental		$1.18*10^{-4}$		$1.80*10^{-2}$
IDH1-R132H			$5.55*10^{-4}$	$6.95*10^{-3}$
IDH2-R172K				
IDH2-R140Q				

Supplemental Table S 8. Significant differences in intracellular levels of α-KG, pyruvate and lactate in the HCT116 panel. A one-way ANOVA was used to determine whether there are significant differences in mean enrichment between metabolites, while p_{adj} for pairwaise comparisons were computed using Tukey's HSD (n=3).

	Parental	IDH1-R132H	IDH2-R172K	IDH2-R140Q
α-Ketoglutarate ANOVA $p=3.03*10^{-4}$				
Parental		$1.04*10^{-3}$		
IDH1-R132H				$6.67*10^{-4}$
IDH2-R172K				
IDH2-R140Q				
Pyruvate ANOVA $p=4.83*10^{-6}$				
Parental		$2.01*10^{-4}$	$1.22*10^{-3}$	$3.10*10^{-6}$
IDH1-R132H				
IDH2-R172K				$3.02*10^{-2}$
IDH2-R140Q				
Lactate ANOVA $p=7.62*10^{-6}$				
Parental		$1.60*10^{-5}$	$9.25*10^{-5}$	$1.18*10^{-5}$
IDH1-R132H				
IDH2-R172K				$9.09*10^{-3}$
IDH2-R140Q				

Supplemental Table S 9. Test for significant differences in mean isotopic enrichment of malate, fumarate and succinate from $^{13}C_6$-glucose tracing as an indicator of PC-activity. A one-way ANOVA was used to determine whether there are significant differences in mean enrichment between metabolites, while p_{adj} for pairwaise comparisons were computed using Tukey's HSD (n=3).

	Parental	IDH1-R132H	IDH2-R172K	IDH2-R140Q
ANOVA	$0.32*10^{-4}$	$6.67*10^{-3}$	$2.06*10^{-4}$	$2.11*10^{-3}$
Malate vs Fumarate	0.320	0.202	0.449	0.391
Fumarate vs Succinate	$7.76*10^{-4}$	$4.91*10^{-2}$	$5.94*10^{-4}$	$8.07*10^{-3}$
Malate vs Succinate	$2.64*10^{-4}$	$5.62*10^{-3}$	$2.52*10^{-4}$	$2.14*10^{-3}$

Supplemental Table S 10. Tests for significant differences in intracellular lacate levels in octyl-D-2-HG treated cells of the LS174T panel and untreated control cells. A one-way ANOVA was used to determine whether there are significant differences in mean enrichment between metabolites, while p_{adj} for pairwaise comparisons were computed using Tukey's HSD (n=3).

	WT	MCT1-/-	MCT4-/-	MCT1-/-MCT4-/-
untreated	ANOVA p= $2.69*10^{-7}$			
WT			$8.00*10^{-7}$	$1.30*10^{-6}$
MCT1-/-			$4.70*10^{-6}$	$9.30*10^{-6}$
MCT4-/-				
MCT1-/-MCT4-/-				
Octyl-D-2-HG	ANOVA p= $3.09*10^{-4}$			
WT				
MCT1-/-			$6.77*10^{-4}$	$4.48*10^{-4}$
MCT4-/-				
MCT1-/-MCT4-/-				

Supplemental Table S 11. Tests for significant differences in intracellular 2-HG & -lactone in octyl-D-2-HG treated cells of the LS174T panel and untreated control cells. Differences were tested with one-way ANOVA, significant p_{adj} for pairwaise comparisons are from Tukey´s HSD.

	WT	MCT1-/-	MCT4-/-	MCT1-/-MCT4-/-
untreated	ANOVA p= $6.66*10^{-6}$ / values below LLOQ			
WT		$2.49*10^{-3}$	$4.17*10^{-3)}$	$5.32*10^{-4}$
MCT1-/-			$2.55*10^{-5}$	$7.50*10^{-6}$
MCT4-/-				
MCT1-/- MCT4-/-				
Octyl-D-2-HG	ANOVA p= $1.46*10^{-4}$ / p= $1.27*10^{-9}$			
WT			$3.46*10^{-4}$	
MCT1-/-	$3.11*10^{-8}$		$1.74*10^{-4}$	
MCT4-/-		$6.37*10^{-8}$		$1.57*10^{-3}$
MCT1-/- MCT4-/-	$5.45*10^{-9}$	$5.71*10^{-5}$	$8.16*10^{-9}$	

Supplemental Table S 12. Tests for significant differences in extracellular 2-HG & -lactone in octyl-D-2-HG treated cells of the LS174T panel and untreated control cells. Differences were tested with one-way ANOVA, significant p_{adj} for pairwaise comparisons are from Tukey´s HSD.

	WT	MCT1-/-	MCT4-/-	MCT1-/-MCT4-/-
untreated	ANOVA p= $9.95*10^{-5}$/ p= 0.249			
WT		$2.15*10^{-4}$	$1.32*10^{-2}$	
MCT1-/-	$1.00*10^{-7}$		$2.34*10^{-2}$	$1.60*10^{-4}$
MCT4-/-		$2.00*10^{-7}$		$8.52*10^{-3}$
MCT1-/- MCT4-/-				
Octyl-D-2-HG	ANOVA p= 0.023 / p= $1.29*10^{-8}$			
WT			$3.46*10^{-4}$	
MCT1-/-			$1.74*10^{-4}$	
MCT4-/-	$2.69*10^{-2}$	$3.93*10^{-2}$		$1.57*10^{-3}$
MCT1-/- MCT4-/-	$3.88*10^{-8}$		$1.00*10^{-7}$	

13 Publications and Presentations

Peer-Reviewed Journal Articles

Böttcher, M., Renner, K., **Berger**, **R.**, Mentz, K., Thomas, S., Cadenas, E. Z., Dettmer, K., Oefner, P. J., Mackensen, A., Kreutz, M., Mougiakakos, D. 2018. D-2-hydroxyglutarate interferes with HIF-1α stability skewing T-cell metabolism towards oxidative phosphorylation and impairing Th17 polarization. ***Oncoimmunology*** 7(7): e1445454.

Berger, **R.S.**, Ellmann, L., Reinders, J., Kreutz, M., Stempfl, T., Oefner, P.J., Dettmer K. 2019. Degradation of D-2-hydroxyglutarate in the presence of isocitrate dehydrogenase mutations. ***Scientific Reports*** 9(1):7436.

Sun, X., Heinrich, P., **Berger**, **R.S.**, Oefner, P.J., Dettmer, K. 2019. Quantification and 13C-tracer analysis of total reduced glutathione by UHPLC-QTOFMS/MS. ***Analytica Chimica Acta***, in press.

Poster Presentations

Regensburg 2016 – 2nd Symposium of KFO262 “Tumor Metabolism meets Immunology”

Title: “Investigation of D-2-hydroxyglutarate degradation by D-2-HG dehydrogenase”

Prag 2017 – HPLC Symposium

Title: “D-2-Hydroxyglutarate Dehydrogenase Assay Reveals Regulation of D-2-Hydroxyglutarate Degradation.”

Oral Presentations

Hohenroda 2018 – Doktroandenseminar AK Separation Science (GDCh)

Title: “Origin and fate of the novel oncometabolite 2-HG-lactone”

Thessaloniki 2019 - 5th workshop on analytical metabolomics

Title: “Degradation of D-2-hydroxyglutarate in the presence of isocitrate dehydrogenase mutations”

14 Summary

This thesis investigated the impact and metabolism of the known oncometabolite D-2-hydroxyglutarate and its recently recognized lactone R-5-oxo-2-tetrahydro-furancarboxylic acid. Production and biological effects of 2-hydoxyglutarate are well described in the literature. However, accumulation of this metabolite as a result of insufficient degradation was studied for the first time in this thesis. Therefore, a cell-based enzyme assay was developed to measure D-2-hydoxyglutarate degradation by D-2-hydroxyglutarate dehydrogenase. Quantification of 2-hydroxyglutarate was accomplished by LC-MS/MS. Applying this assay, it was found that D-2-hydroxyglutarate dehydrogenase activity differs across cell lines but is not upregulated in response to elevated 2-hydroxyglutarate levels.

Moreover, in preliminary investigations on 2-hydroxyglutarate in serum of AML-patients with mutations in isocitrate dehydrogenase, 2-hydroxyglutarate-lactone was discovered. The HCT116 panel with *IDH1/2* mutation served as a model to learn more about the novel metabolite as both metabolites – 2-HG and 2-HG-lactone - can be detected in extracts of these cells. Thereby, 2-hydroxyglutarate was verified as the precursor by performing $^{13}C_5$-glutamine tracing experiments. However, 2-hydroxyglutarate lactonization does not take place whenever the precursor is abundant, as for some biological specimens with elevated 2-hydroxyglutarate the lactone was not detectable. Further experiments provided hints that 2-hydroxyglutarate-lactone is of enzymatic origin but did not lead to the identification of this enzyme.

In doing all these experiments, interconversion of 2-hydroxyglutarate and its lactone needed to be controlled and required development of new protocols using different approaches of hyphenated mass spectrometry. For instance, set up of an enantioselective analysis of 2-hydroxyglutarate and its lactone was an objective of this thesis but was not achieved with the possibilities at the institute. Finally, this thesis provided insights into origin, fate and impact of 2-HG and 2-HG-lactone in the context of tumor metabolism.

15 Zusammenfassung

Diese Arbeit untersuchte die Auswirkungen und den Stoffwechsel von Onko-Metaboliten am Beispiel von D-2-Hydroxyglutarat und seinem Lacton, R-5-Oxo-2-tetrahydrofurancarbonsäure mit Hilfe einiger bioanalytischer Methoden. Die Produktion und die biologischen Effekte von 2-Hydroxyglutarat sind in der Literatur gut beschrieben. Im Gegensatz dazu wurde in dieser Dissertation die Akkumulation dieses Metaboliten in Folgen seines ungenügenden Abbaus zum ersten Mal genauer untersucht. Um den Abbau von D-2-Hydroxyglutarat durch die D-2-Hydroxyglutarat-Dehydrogenase zu messen, wurde ein Zell-basierter Assay entwickelt. Die Quantifizierung von 2-Hydroxyglutarat erfolgte mittels einer LC-MS/MS-Methode. Die Anwendung des Enzym-Assays auf verschiedene Zelllinien zeigte unterschiedliche Aktivitäten für die D-2-Hydroxyglutarat-Dehydrogenase, die durch erhöhte 2-Hydroxyglutarat-Spiegel jedoch nicht wie erwartet hoch reguliert wurde.

Außerdem wurde bei (dieser Arbeit vorangegangener) Untersuchungen zu 2-Hydroxyglutarat in Serum von AML-Patienten mit Mutation der Isocitrat-Dehydrogenase das 2-Hydroxyglutarat-Lacton, der intramolekulare Ester des 2-Hydroxyglutarats, als endogener Metabolit identifiziert. Um mehr über den neuen Metaboliten zu erfahren, wurden einige Experimente durchgeführt. Dabei diente ein Set aus HCT116 Zelllinien, bestehend aus Zelllinien mit und ohne *IDH1/2*-Mutation als wichtiges Modell, da in Extrakten dieser Zellen sowohl 2-Hydoxyglutarat als auch das -Lacton nachgewiesen wurde. So zeigten Untersuchungen des Stoffwechsels in Zellen mit *IDH1/2*-Mutation durch Zugabe von $^{13}C_5$-Glutamin, dass das 2-Hydroxyglutarat-Lacton aus 2-Hydroxyglutarat gebildet wird. Weitere Daten dieses Versuchs zusammen mit Ergebnissen aus einem analogen Versuch, bei dem $^{13}C_6$-Glucose eingesetzt und dessen Verstoffwechselung nachverfolgt wurde, zeigten die Auswirkungen einer *IDH1/2*-Mutation auf den zellulären Stoffwechsel. So wurde z.B. klar, dass diese Zellen vorwiegend Glutamin nutzten, um den erhöhten Verbrauch von α-Ketoglutarat zur 2-Hydroxyglutarate-Synthese zu kompensieren. In Extrakten von einigen Seren oder Zellkultur-Proben mit erhöhtem 2-Hydroxyglutarat-Wert war das -Lacton nicht detektierbar. Daher scheint es, dass 2-Hydroxyglutarat in ausreichender Konzentration allein nicht ausreicht, um eine Laktonisierung beobachten zu können. In Zellkultur-Versuchen etwa wurde der 2-Hydroxyglutarat-Spiegel durch Zugabe des Zellmembran-permeablen 2-Hydroxyglutarate-Octyl-Esters

unabhängig von einer *IDH1/2*-Mutation erhöht und immer die Laktonisierung beobachtet. Weitere Experimente lieferten Hinweise, dass das 2-Hydroxyglutarat-Lacton enzymatischen Ursprungs ist, aber letztendlich konnte das verantwortliche Enzym nicht identifiziert werden.

Es wurden daneben auch Versuche zu Untersuchung der biologischen Effekte von 2-Hydroxyglutarat und -Lacton z.B. auf die Immunantwort von Makrophagen durchgeführt. Dabei wurde auch festgestellt, dass die Aufnahme-Raten von 2-Hydroxyglutarat und -Lacton (vermutlich bedingt durch verschieden Transporter) sich unterscheiden. Ebenso ist die intrazelluläre Hydrolyse-Rate des Lactons Zelltyp-spezifisch und erfolgt zumindest in Makrophagen enantioselektiv. Letztendlich war es schwer möglich, biologische Effekte eindeutig einem der beiden Metabolite, 2-Hydroxyglutarat und -Lacton, zuzuordnen.

Bei der Durchführung aller Versuche zu dieser Arbeit musste stets die mögliche, gegenseitige Umwandlung von 2-Hydroxyglutarat und -Lacton im Auge behalten werden. Daher wurde es auch notwendig, neue Methoden aus dem Bereich der gekoppelten Massenspektrometrie zu entwickeln. Beispielsweise wurde versucht eine enantioselektive Methode zur Quantifizierung von D-/L-2-Hydroxyglutarat und -Lacton zu etablieren. Hierzu wurden zwei verschiedene Ansätze getestet: zum einen die Verwendung enantioselektiver Chromatographie-Säulen, zum anderen eine Derivatisierung mit chiralen Reagenzien, wodurch Diasteromere entstehen. Jedoch war es mit den am Lehrstuhl verfügbaren Instrumenten und Mitteln nicht möglich eine valide, enantioselektive Methode für beide Analyten aufzusetzen. Die Ergebnisse dieser Arbeit basieren dementsprechend hauptsächlich auf Messungen mit einer (LC-MS/MS)-Methode, die Enantiomere nicht unterscheiden kann, bzw. auf Daten chiraler GC-MS-Analysen von 2-Hydroxyxglutarat. So konnten dennoch einige Erkenntnisse über den Ursprung, das Schicksal und den Einfluss von zwei Metaboliten im Kontext des Tumor-Stoffwechsels gewonnen werden.

Eidesstattliche Erklärung

Ich erkläre hiermit, dass ich die vorliegende Arbeit selbst verfasst und keine anderen als die angegebenen Quellen und Hilfsmittel verwendet habe.

---------- ----------

Ort, Datum Unterschrift